



Calhoun: The NPS Institutional Archive

Theses and Dissertations

Thesis Collection

1993-06

Detailed analysis case studies of trapped plasmas at
the earth's magnetic equator

Lantto, Eric S.

Monterey, California. Naval Postgraduate School

<http://hdl.handle.net/10945/39803>



Calhoun is a project of the Dudley Knox Library at NPS, furthering the precepts and goals of open government and government transparency. All information contained herein has been approved for release by the NPS Public Affairs Officer.

Dudley Knox Library / Naval Postgraduate School
411 Dyer Road / 1 University Circle
Monterey, California USA 93943

<http://www.nps.edu/library>

AD-A272 497

2



NAVAL POSTGRADUATE SCHOOL
Monterey, California



DTIC
SELECTE
NOV 05 1993
E D

THESIS

Detailed Analysis Case Studies of Trapped
Plasmas at the Earth's Magnetic Equator

by

Eric S. Lantto

June, 1993

Thesis Advisor:

R. C. Olsen

Approved for public release; distribution is unlimited.

93-27029



30

REPORT DOCUMENTATION PAGE

Form Approved
OMB No. 0704-0188

Public reporting burden for this collection of information is estimated to average 1 hour per response, including the time for reviewing instructions, searching existing data sources, gathering and maintaining the data needed, and completing and reviewing the collection of information. Send comments regarding this burden estimate or any other aspect of this collection of information, including suggestions for reducing this burden, to Washington Headquarters Services, Directorate for Information Operations and Reports, 1215 Jefferson Davis Highway, Suite 1204, Arlington, VA 22202-4302, and to the Office of Management and Budget, Paperwork Reduction Project (0704-0188), Washington, DC 20503

1. AGENCY USE ONLY (Leave blank)		2. REPORT DATE JUNE 1993	3. REPORT TYPE AND DATES COVERED Master's Thesis	
4. TITLE AND SUBTITLE Detailed Analysis Case Studies of Trapped Plasmas at the Earth's Magnetic Equator			5. FUNDING NUMBERS	
6. AUTHOR(S) Lantto, Eric S.				
7. PERFORMING ORGANIZATION NAME(S) AND ADDRESS(ES) Naval Postgraduate School Monterey, CA 93943-5000			8. PERFORMING ORGANIZATION REPORT NUMBER	
9. SPONSORING/MONITORING AGENCY NAME(S) AND ADDRESS(ES)			10. SPONSORING/MONITORING AGENCY REPORT NUMBER	
11. SUPPLEMENTARY NOTES The views expressed in this thesis are those of the author and do not reflect the official policy or position of the Department of Defense or the U.S. Government.				
12a. DISTRIBUTION / AVAILABILITY STATEMENT Approved for public release; distribution is unlimited.			12b. DISTRIBUTION CODE	
13. ABSTRACT (Maximum 200 words) <p>A previous statistical survey of data from the HPCE experiment on the AMPTE/CCE satellite established probability distributions for trapped ions and electrons. An extension of this survey for ions at 240 and 442 eV and for electrons at 340 and 770 eV confirmed these distributions. A further detailed analysis of the electron data from 13 individual data collection days also showed the trapped electron distribution to be concentrated in the dawn to noon region, centered at L=7. These trapped electron distributions can be described as a bi-Maxwellian distribution function and be characterized reasonably by the criteria that the flux has to exceed 5e6 per (sq. cm sec sr), the distribution has to be within 10 deg. of the magnetic equator, the ratio of the perpendicular temperature to the parallel temperature exceeds 3.0 and that the anisotropy exceeds 2.0 for 150 eV electrons and 4.4 for 340 eV electrons.</p>				
14. SUBJECT TERMS Equatorially Trapped Plasma, Plasmopause, AMPTE, Ion Distributions, Electron Distributions, Bi-Maxwellian			15. NUMBER OF PAGES 155	
			16. PRICE CODE	
17. SECURITY CLASSIFICATION OF REPORT UNCLASSIFIED	18. SECURITY CLASSIFICATION OF THIS PAGE UNCLASSIFIED	19. SECURITY CLASSIFICATION OF ABSTRACT UNCLASSIFIED	20. LIMITATION OF ABSTRACT UL	

Approved for public release; distribution is unlimited.

Detailed Analysis Case Studies of Trapped
Plasmas at the Earth's Magnetic Equator

by

Eric S. Lantto
Lieutenant Commander, United States Navy
B.S., University of Minnesota

Submitted in partial fulfillment
of the requirements for the degree of

MASTER OF SCIENCE IN PHYSICS

from the

NAVAL POSTGRADUATE SCHOOL

June 1993


Author:


Eric S. Lantto

Approved by:


R. C. Olsen, Thesis Advisor


S. Gnanalingham, Second Reader


K. E. Woehler, Chairman
Department of Physics

ABSTRACT

A previous statistical survey of data from the HPCE experiment on the AMPTE/CCE satellite established probability distributions for trapped ions and electrons. An extension of this survey for ions at 240 and 442 eV and for electrons at 340 and 770 eV confirmed these distributions. A further detailed analysis of the electron data from 13 individual data collection days also showed the trapped electron distributions to be concentrated in the dawn to noon region, centered at $L = 7$. These trapped electron distributions can be described as a bi-Maxwellian distribution function and be characterized reasonably by the criteria that the flux has to exceed $5 \times 10^6 \text{ (cm}^2 \text{ s sr)}^{-1}$, the distribution has to be within 10° of the magnetic equator, the ratio of the perpendicular temperature to the parallel temperature is greater than 3 and that the anisotropy is greater than 2.0 for 150 eV electrons and 4.4 for 340 eV electrons.

DTIC QUALITY INSPECTED 8

Accession For	
NTIS	<input checked="" type="checkbox"/>
CRA&I	<input type="checkbox"/>
DTIC	<input type="checkbox"/>
TAB	<input type="checkbox"/>
Unannounced <input type="checkbox"/>	
Justification	
By	
Distribution/	
Availability Codes	
Dist	Availability and/or Special
A-1	

TABLE OF CONTENTS

I. INTRODUCTION	1
II. BACKGROUND	4
A. THE PLASMASPHERE	4
B. THEORY	12
1. Plasma Definition	12
2. Debye Shielding	15
3. Plasma Parameter	16
4. Motion in a Uniform Magnetic Field	16
5. Magnetic Mirror	17
6. Statistical Distribution	21
C. PREVIOUS OBSERVATIONS	23
D. THE AMPTE/CCE SATELLITE	40
E. THE HOT PLASMA COMPOSITION EXPERIMENT (HPCE)	42
III. OBSERVATIONS	51
A. STATISTICAL SURVEY	51
1. Data Analysis	51
2. Local Time - McIlwain L Surveys	52
a. ION SURVEY	52
b. ELECTRON SURVEY	63
B. DETAILED ANALYSIS CASE STUDIES	69
1. Data Analysis	69

2. Day 84/336 Case Study Trapped Distributions	75
a. 150 eV	75
b. 340 eV	80
3. Day 85/002 Case Study Trapped Distributions	83
a. 150 eV	83
b. 340 eV	87
4. Detailed Analysis Trapped versus Non-Trapped Distributions	90
IV. DISCUSSION	96
A. STATISTICAL SURVEY	96
B. DETAILED ANALYSIS CASE STUDIES	97
V. CONCLUSIONS	107
A. STATISTICAL ANALYSIS	107
B. DETAILED ANALYSIS CASE STUDIES	108
APPENDIX (DETAILED ANALYSIS SPECTROGRAMS)	111
LIST OF REFERENCES	138
INITIAL DISTRIBUTION LIST	141

LIST OF FIGURES

Figure 1. The Earth's Magnetosphere	5
Figure 2. Plasma Density L Dependence	7
Figure 3. Plasmapause Magnetic Activity Dependence	8
Figure 4. Plasma Density L Dependence - Normalized	10
Figure 5. The Dusk Bulge	13
Figure 6. Magnetosphere's Electric and Magnetic Fields	14
Figure 7. Path of Mirroring Particle	19
Figure 8. Pitch Angle verses Mirror Latitude	22
Figure 9. Field Aligned and Pancake Trapped Ion Distributions	25
Figure 10. Trapped Ion Distribution With Relation to the Plasmapause	26
Figure 11. Ion Pitch Angle Distribution	27
Figure 12. Electron Pitch Angle Distribution	29
Figure 13. Energy Relations of Trapped Plasmas	30
Figure 14. Trapped Ion L verses Local Time Dependence	32
Figure 15. Flux - Spin Phase/Density Fits	33
Figure 16. Log of Flux verses Pitch Angle - 150 eV and 340 eV Electrons	39
Figure 17. The AMPTE/CCE Satellite	41
Figure 18. The AMPTE/CCE Payload	43
Figure 19. The HPCE Ion-Mass Spectrometer	44
Figure 20. The HPCE Electron Background Environment Monitor	46

Figure 21. Trapped Ions (240 eV) - Flux gt 10^5 , Anisotropy gt 1.5, Maglat gt 10°	53
Figure 22. Trapped Ions (240 eV) - Flux gt 10^5 , Anisotropy gt 1.5, Maglat gt 10° - Surface Plot	54
Figure 23. Trapped Ions (240 eV) - Flux gt 10^5 , Anisotropy gt 1.5, Maglat gt 5°	56
Figure 24. Trapped Ions (240 eV) - Flux gt 5×10^5 , Anisotropy gt 2.0, Maglat gt 5°	57
Figure 25. Trapped Ions (442 eV) - Flux gt 10^3 , Anisotropy gt 1.5, Maglat gt 5°	58
Figure 26. Trapped Ions (442 eV) - Flux gt 10^3 , Anisotropy gt 1.5, Maglat gt 5° - Surface Plot	59
Figure 27. Trapped Ions (30-150 eV) - Flux gt 10^6 , Anisotropy gt 1.5, Maglat gt 10°	61
Figure 28. Trapped Ions (30-150 eV) - Flux gt 10^6 , Anisotropy gt 1.5, Maglat gt 10° - Surface Plot . .	62
Figure 29. Trapped Electrons (340 eV) - Flux gt 5×10^6 , Anisotropy gt 1.5, Maglat gt 10°	64
Figure 30. Trapped Electrons (770 eV) - Flux gt 5×10^6 , Anisotropy gt 1.5, Maglat gt 10°	65
Figure 31. Trapped Electrons (770 eV) - Flux gt 5×10^6 , Anisotropy gt 1.5, Maglat gt 10° - Surface Plot . .	66
Figure 32. Trapped Electrons (150 eV) - Flux gt 5×10^6 , Anisotropy gt 1.5, Maglat gt 10°	67
Figure 33. Trapped Electrons (150 eV) - Flux gt 5×10^6 , Anisotropy gt 1.5, Maglat gt 10° - Surface Plot . .	68

Figure 34. Pitch Angle verses Time Spectrogram - Day 84/336, Energy 150 eV	71
Figure 35. Electron Pitch Angle Distribution	72
Figure 36. Fluxes verses Time - Day 84/336, Energy 150 eV	76
Figure 37. Anisotropies, Temperature Ratio and Temperatures verses Time - Day 84/336, Energy 150 eV	77
Figure 38. Average Anisotropy and Temperature Ratio verses Equator Anisotropy - Day 84/336, Energy 150 eV . .	79
Figure 39. Fluxes verses Time - Day 84/336, Energy 340 eV	81
Figure 40. Anisotropies, Temperature Ratio and Temperatures verses Time - Day 84/336, Energy 340 eV	82
Figure 41. Fluxes verses Time - Day 85/002, Energy 150 eV	85
Figure 42. Anisotropies, Temperature Ratio and Temperatures verses Time - Day 85/002, Energy 150 eV	86
Figure 43. Fluxes verses Time - Day 85/002, Energy 340 eV	88
Figure 44. Anisotropies, Temperature Ratio and Temperatures verses Time - Day 85/002, Energy 340 eV	89
Figure 45. Fluxes verses Time - Day 84/336, Energy 150 eV	

(Entire Orbit)	91
Figure 46. Anisotropies, Temperature Ratio and Temperatures verses Time - Day 84/336, Energy 150 eV (Entire Orbit)	92
Figure 47. Flux verses Pitch Angle - Various Days . . .	94
Figure 48. Detailed Analysis Orbital Coverage	98
Figure 49. Equatorially Trapped Electron Distributions - Energy 150 eV	99
Figure 50. Plasmapause Location	101
Figure 51. Equatorially Trapped Electron Distributions - Energy 340 eV	103
Figure 52. Temperature Ratio verses Equator Anisotropy - All 13 Detailed Analysis Case Study Days, Energy 150 eV	105
Figure 53. Pitch Angle verses Time Spectrogram - Day 84/266, Energy 150 eV	112
Figure 54. Pitch Angle verses Time Spectrogram - Day 84/283, Energy 150 eV	113
Figure 55. Pitch Angle verses Time Spectrogram - Day 84/296, Energy 150 eV	114
Figure 56. Pitch Angle verses Time Spectrogram - Day 84/315, Energy 150 eV	115
Figure 57. Pitch Angle verses Time Spectrogram - Day 85/002, Energy 150 eV	116
Figure 58. Pitch Angle verses Time Spectrogram - Day 85/039, Energy 150 eV	117

Figure 59. Pitch Angle verses Time Spectrogram - Day	
85/227, Energy 150 eV	118
Figure 60. Pitch Angle verses Time Spectrogram - Day	
85/238, Energy 150 eV	119
Figure 61. Pitch Angle verses Time Spectrogram - Day	
85/264, Energy 150 eV	120
Figure 62. Pitch Angle verses Time Spectrogram - Day	
85/301, Energy 150 eV	121
Figure 63. Pitch Angle verses Time Spectrogram - Day	
85/320, Energy 150 eV	122
Figure 64. Pitch Angle verses Time Spectrogram - Day	
85/337, Energy 150 eV	123
Figure 65. Pitch Angle verses Time Spectrogram - Day	
84/266, Energy 340 eV	124
Figure 66. Pitch Angle verses Time Spectrogram - Day	
84/283, Energy 340 eV	125
Figure 67. Pitch Angle verses Time Spectrogram - Day	
84/296, Energy 340 eV	126
Figure 68. Pitch Angle verses Time Spectrogram - Day	
84/315, Energy 340 eV	127
Figure 69. Pitch Angle verses Time Spectrogram - Day	
84/336, Energy 340 eV	128
Figure 70. Pitch Angle verses Time Spectrogram - Day	
85/002, Energy 340 eV	129
Figure 71. Pitch Angle verses Time Spectrogram - Day	
85/039, Energy 340 eV	130

Figure 72. Pitch Angle verses Time Spectrogram - Day	
85/227, Energy 340 eV	131
Figure 73. Pitch Angle verses Time Spectrogram - Day	
85/238, Energy 340 eV	132
Figure 74. Pitch Angle verses Time Spectrogram - Day	
85/264, Energy 340 eV	133
Figure 75. Pitch Angle verses Time Spectrogram - Day	
85/301, Energy 340 eV	134
Figure 76. Pitch Angle verses Time Spectrogram - Day	
85/320, Energy 340 eV	135
Figure 77. Pitch Angle verses Time Spectrogram - Day	
85/337, Energy 340 eV	136

LIST OF TABLES

TABLE I. ION ENERGY CHANNELS IN THE HPCE ON THE AMPTE/CCE	48
TABLE II. ELECTRON ENERGY CHANNELS IN THE HPCE ON THE AMPTE/CCE	49
Table III. DETAILED ANALYSIS DATA COLLECTION DAYS . .	69

I. INTRODUCTION

Equatorially trapped plasmas are ion and electron distributions trapped within a few degrees of the Earth's magnetic equator. Equatorially trapped plasmas can be described by a bi-Maxwellian distribution function. These trapped plasma distributions were defined by the initial observations by Olsen (1981). Ion and electron distributions with highly anisotropic pitch angle distributions, peaked at 90 degrees pitch angle, were observed at energies from a few eV to hundreds of eV, near geosynchronous orbit. These trapped distributions are of interest as indications of basic wave particle interactions, and as an intermediate process in plasmasphere filling.

The energy - pitch distribution indicates the wave particle interaction aspect of these plasma distributions. They are indicative of perpendicular acceleration ($T_{\text{perp}} > T_{\text{par}}$), and quasi-linear diffusion (flat diffusion at low energy). Though not yet proven, there are indications of a correspondence between equatorially trapped plasmas and Bernstein mode waves (equatorial noise) and electron cyclotron harmonics (Gurnett, 1976 and Kurth et al., 1979).

The plasmasphere filling role is indicated by the correspondence between the plasmopause region and the location of equatorially trapped ion distributions (Horwitz et al.,

1981). The variations in pitch angle structure with latitude also suggests the role (Olsen *et al.*, 1987).

There have been previous surveys of equatorially trapped plasmas. Olsen *et al.*, (1987) surveyed DE 1/RIMS (ion) data for 0 - 100 eV. Sagawa *et al.* (1987) surveyed the DE 1/EICS (ion) data for 0 - 1 keV. Both surveys of equatorially trapped plasmas were limited in altitude by the DE 1 orbit, which had apogee at $L = 4.7$. Both of these surveys also lacked complementary electron data.

Braccio (1991) surveyed AMPTE/CCE data for both ions (30 - 150 eV) and electrons (150 eV) out to 8.8 Earth radii. The first purpose of this thesis is to extend the survey done by Braccio by conducting a statistical survey of the next two higher energy channels for both the ions and electrons (i.e. 240 and 442 eV for the ions and 340 and 770 eV for the electrons.) The survey will be used to extend the findings in his paper and to attempt to answer questions he raised, such as whether the higher energy ions inhabit the region of decreased probability from 1200 to 1400 local time. The electron survey will ensure that the trapped distribution is not being under-evaluated and that the location and shape of the trapped distribution found by Braccio is accurate.

The second purpose of this thesis is to conduct a detailed analysis of 13 individual days to examine the nature of equatorially trapped distributions. The trapped distributions will be described as bi-Maxwellian distributions, in order to

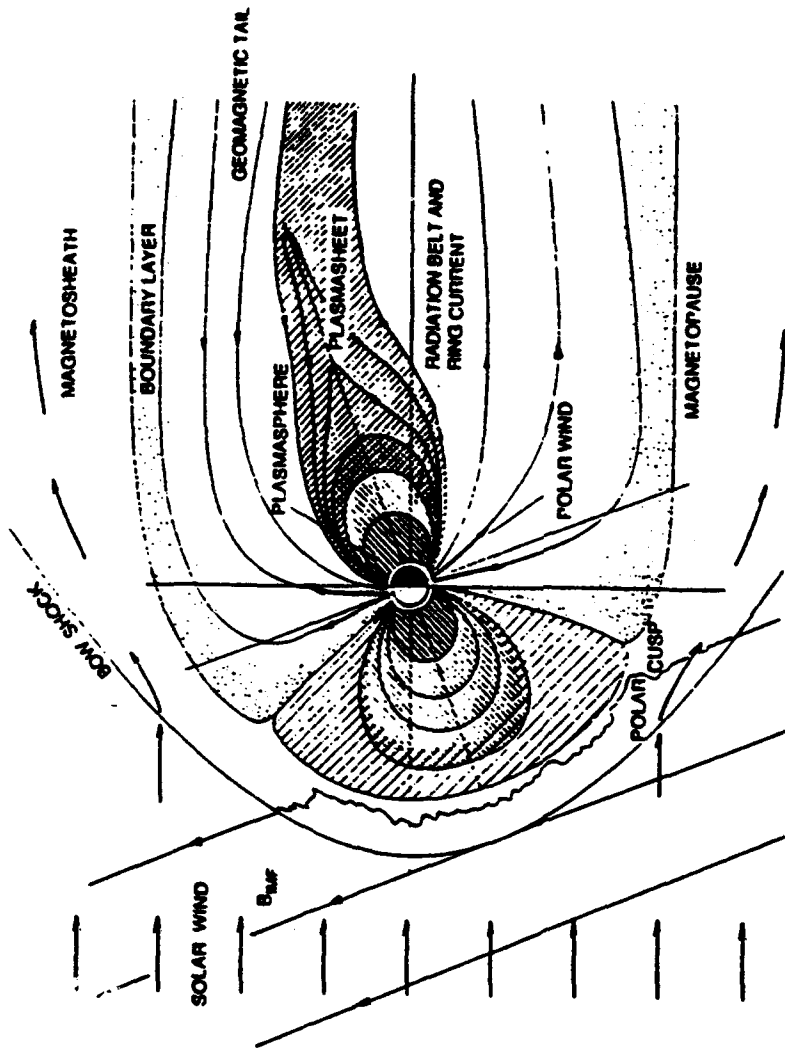
quantify a trapped distribution. In addition, this thesis will be used to better define the electron distributions, and the location of the trapped electron distributions.

II. BACKGROUND

A. THE PLASMASPHERE

A magnetosphere is the region around a magnetized planetary body in which that body's magnetic field plays the dominant role in defining the behavior of charged particles. It's outer boundary, the magnetopause, occurs where the solar wind, and the magnetic field in the solar wind, becomes dominant. This boundary occurs on the sunward side of the Earth at approximately 10 Earth radii (roughly 63,750 km). The location of this boundary is determined by a balance between the pressure exerted by the solar wind and the obstacle formed by the Earth's magnetic field. During active times, the magnetopause has been observed as close as 5 geocentric Earth radii (R_E). The inner boundary of the magnetosphere occurs at the top of the ionosphere. This boundary can be taken as occurring at an altitude of 1000 km or 1.16 R_E . (Parks, p.7)

As can be seen in Figure 1, the Earth's magnetosphere is highly asymmetric. While the sunward boundary is located at approximately 10 R_E , the Earth's magnetic tail has been seen to extend beyond 200 R_E on the nightside. The length and shape of the magnetic tail again depends on the interaction between the geomagnetic field and the solar wind. (Parks, pp. 7-8)



A schematic diagram of Earth's magnetosphere in the noon-midnight plane. The basic particle and magnetic field features are representative of other planetary magnetospheres although the details can be different.

Figure 1. The Earth's Magnetosphere

For our purposes, the major components of the magnetosphere are the plasmasphere, the plasmasheet, and the plasmopause. The plasmasphere is the region of the magnetosphere that is closest to the Earth. It begins just above the ionosphere, at low to mid-latitudes. The plasmasphere extends in altitude to between 3 and 5 R_E in the equatorial plane, and between $\pm 60^\circ$ magnetic latitude just above the ionosphere. The plasmasphere corotates with the Earth and particles in this region are affected by the Earth's corotational Electric field. (Parks, pp. 11 and 73)

This region contains plasma, ionized atoms and electrons, with densities of $10^2 - 10^4 \text{ cm}^{-3}$. Characteristic ion and electron energies are on the order of 1 eV at 4.5 R_E . The density of the plasmasphere decreases with altitude. In general, the density in this region experiences a gradual drop proportional to the fourth power of the McIlwain L parameter (a measure of altitude based on the magnetic field lines that will be discussed later). This is illustrated in Figure 2. (Chappell et al., 1970)

At approximately 3 to 5 Earth radii, again depending on the magnetic activity history, the plasmopause is encountered. This is a transition region for the plasma in which plasma energies sharply increase (Parks, pp. 231 and 502) and densities drop, generally very sharply, that is used to define the inner boundary of the plasmopause, Figure 3. (Harris et al., 1970).

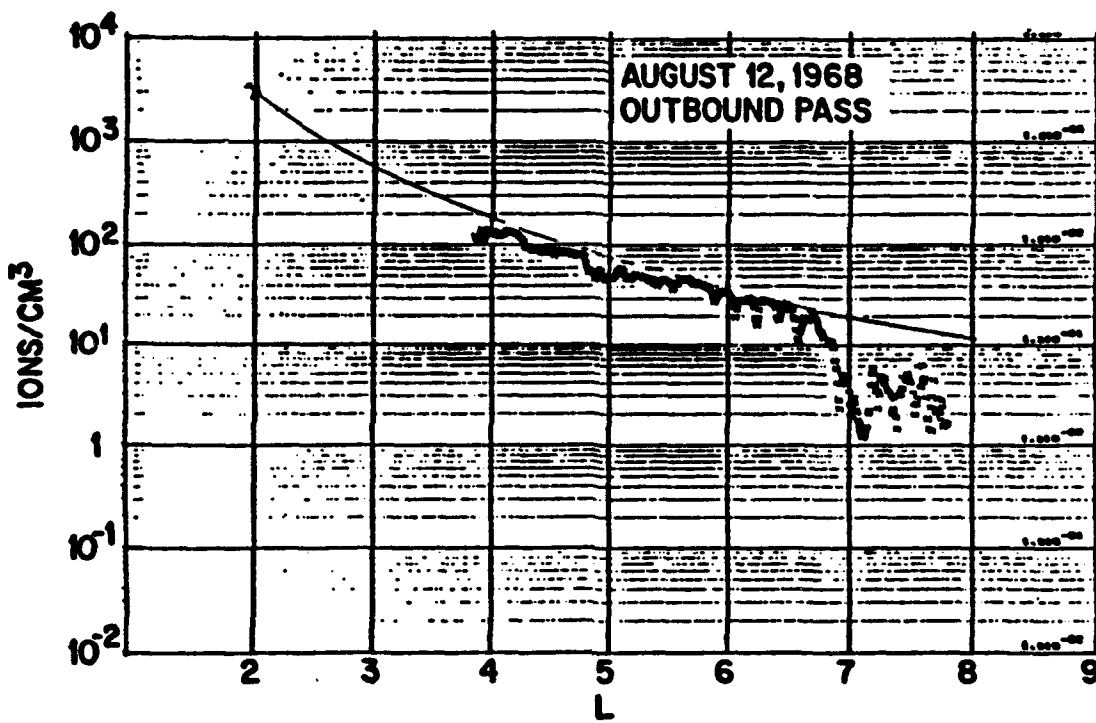
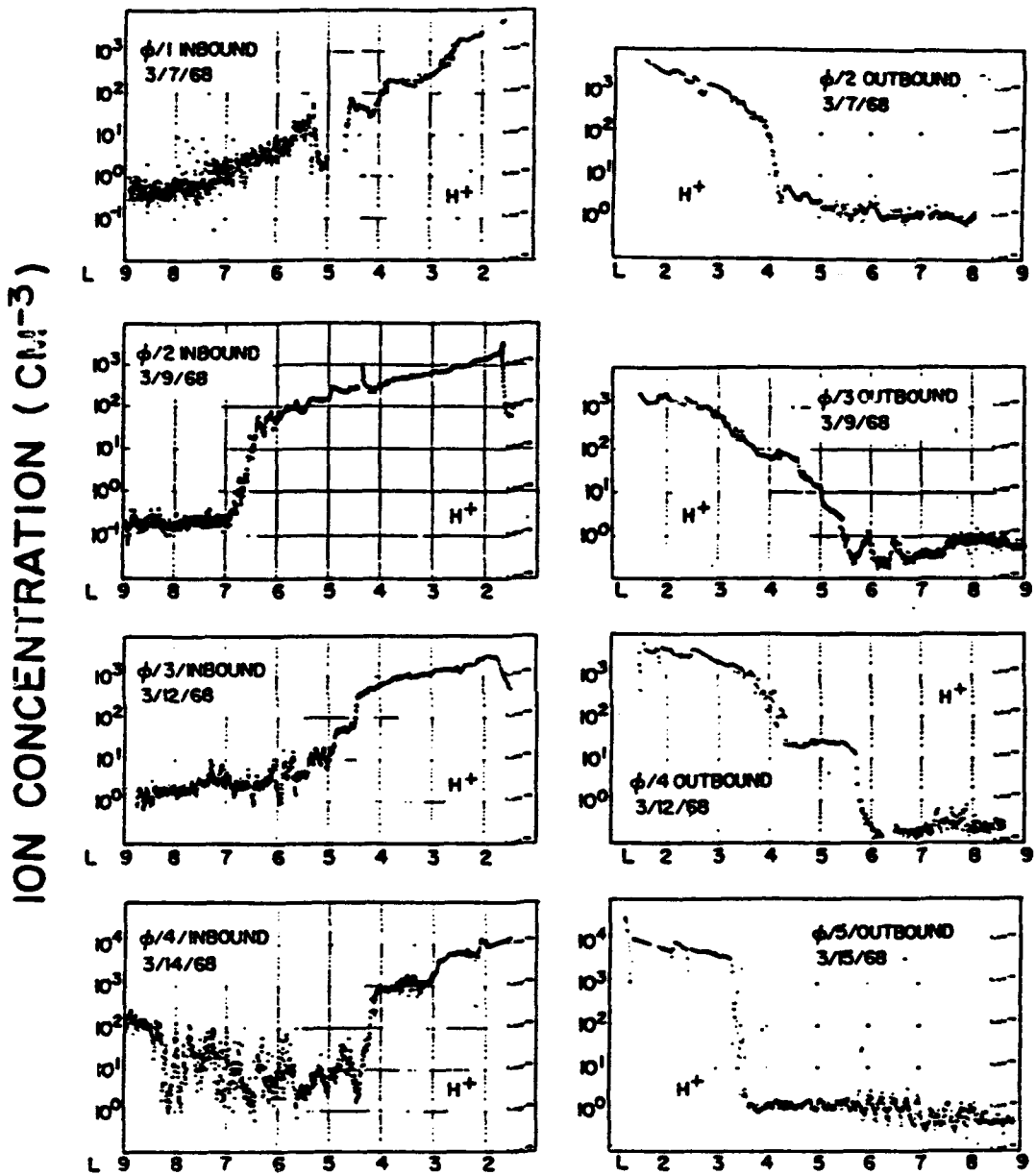


Figure 2. Plasma Density L Dependence



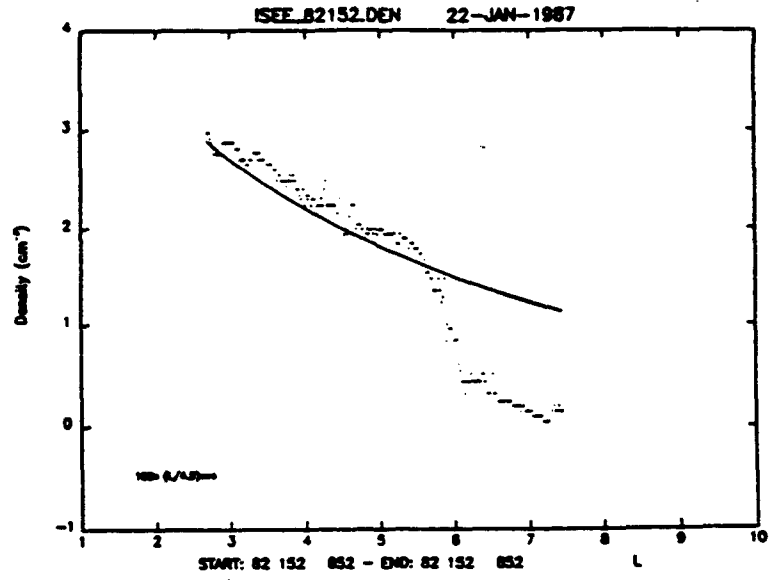
Composite of the first four H⁺ ion concentration profiles for the inbound and outbound passes of OGO 5.

Figure 3. Plasmapause Magnetic Activity Dependence

These aspects of the plasmasphere can be further illustrated using (relatively) more modern data from ISEE 1 total electron density measurements obtained from observations of plasma waves. Figure 4a shows density versus L, with a solid line at $100 \times (L/4.5)^{-4}$ superimposed. The plasmopause is at $L = 4.8$, 1700 local time. The plasma density outside the plasmopause continues to drop as L^{-4} . This characteristic of the plasma density profile can more easily be seen if the data are normalized by L^4 , as in Figure 4b. (Olsen, 1992)

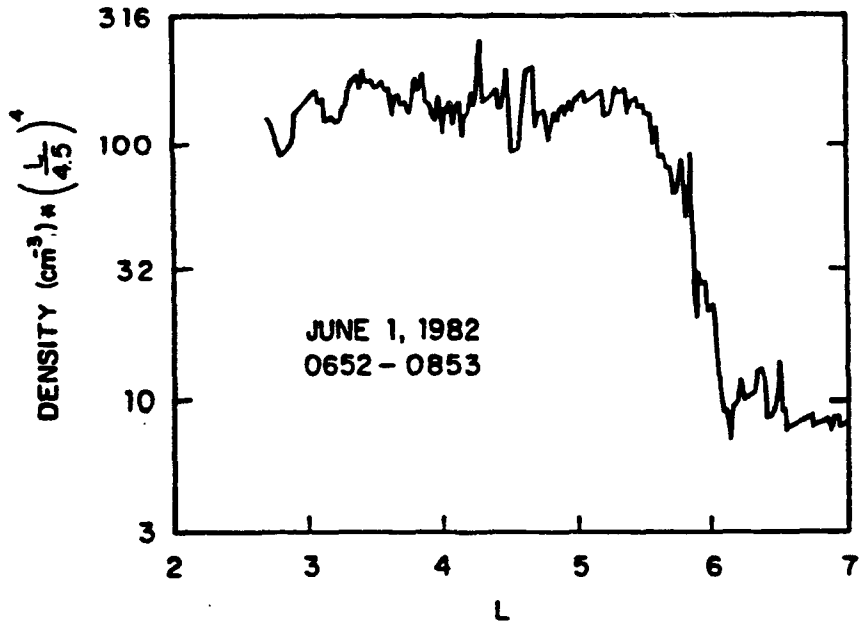
The plasmasphere density is dependent on the magnetic activity. A large magnetic storm can effectively push the plasmopause in to less than $3 R_E$. Figure 3 shows the effects of magnetic activity on the density and location of the plasmopause. Magnetic intensity increases from a low in the upper left panel in the figure to a maximum in the lower right hand panel. (Harris *et al.*, 1970)

The storm-time electric field strips away the plasma at higher altitudes, as the plasma is convected to the magnetopause. This region is then refilled from the ionosphere after the storm-time field relaxes. The process, termed polar wind, is driven by ambipolar diffusion after the electric field relaxes back to a steady state value of approximately 1 mV/m. This diffusion process calls for electrons to leave the upper ionosphere, probably driven by photoemission, and move along the geomagnetic field lines. The resulting ambipolar electric field, caused by the displacement between the



a.

ISEE-1



b.

Figure 4. Plasma Density L Dependence - Normalized

electrons and O^+ in the upper atmosphere, causes lighter ions, such as H^+ and He^+ , to be dragged up the field lines after the electrons. This 'polar wind' results in a refilling rate of 1 to 10 ions/cm³ per day. (Horwitz, 1983)

On the nightside the plasmasphere is bounded by the plasmashet, a region of low density, hot plasma (with densities on the order of 1 cm⁻³ and characteristic energies of 1-10 keV). The corresponding plasmopause for this region is very distinct and the transition from plasmopause to plasmashet takes place rather rapidly. This is not the case for the region that extends from just before dawn until just after dusk local time, on the dayside. (Parks, pp. 231 and 502)

On the sunward side of the Earth, the plasmopause is a region that can be as much as 1 R_E in width. Additionally, there is usually no sharp distinction corresponding to its inner and outer boundaries during this local time period (Parks, p.231). Therefore, it is usually a matter of judgement as to which region you are studying.

The region between the dayside plasmopause and the magnetopause is also ill defined. It is not clear whether the plasmashet encircles the Earth and occupies this region. While there is no known reason why this should not be the case, the plasma observed in this region does not display the characteristics of that which is found in the nightside plasmashet. This has led to questions concerning the plasma

filling mechanism for this region as well as to questions of where the plasma in this region comes from.

In the dusk region there is an additional asymmetry as seen in Figure 5. This dusk bulge is the result of interaction between the corotational electric field of the plasmasphere and the cross tail electric field induced by the solar wind. The corotational field is the result of the charged particles rotating with the Earth while trapped in its geomagnetic field and is directed radially inward toward the Earth. The cross tail electric field is induced by the solar wind's interaction with the Earth's magnetic field. This cross tail field is in the dawn-dusk direction in the equatorial plane of the magnetotail. The sum of these two electric fields results in a series of equipotential contours which mirror the dusk bulge, Figure 6. (Parks, pp. 231-236)

B. THEORY

1. Plasma Definition

A plasma is a collection of discrete ionized and neutral particles, which has overall electrical neutrality. The physical dimensions of the plasma must be large in comparison with a characteristic length λ_D , called the Debye

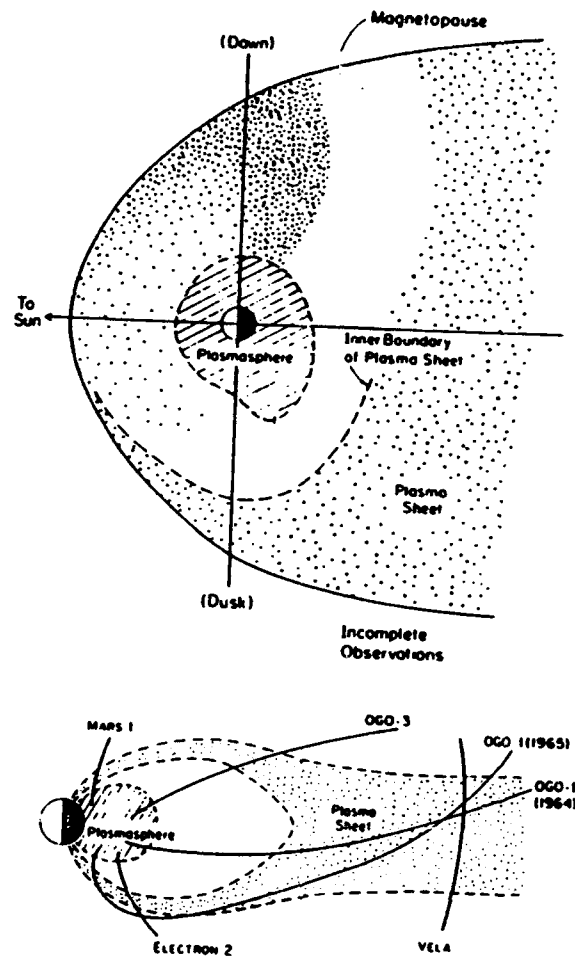
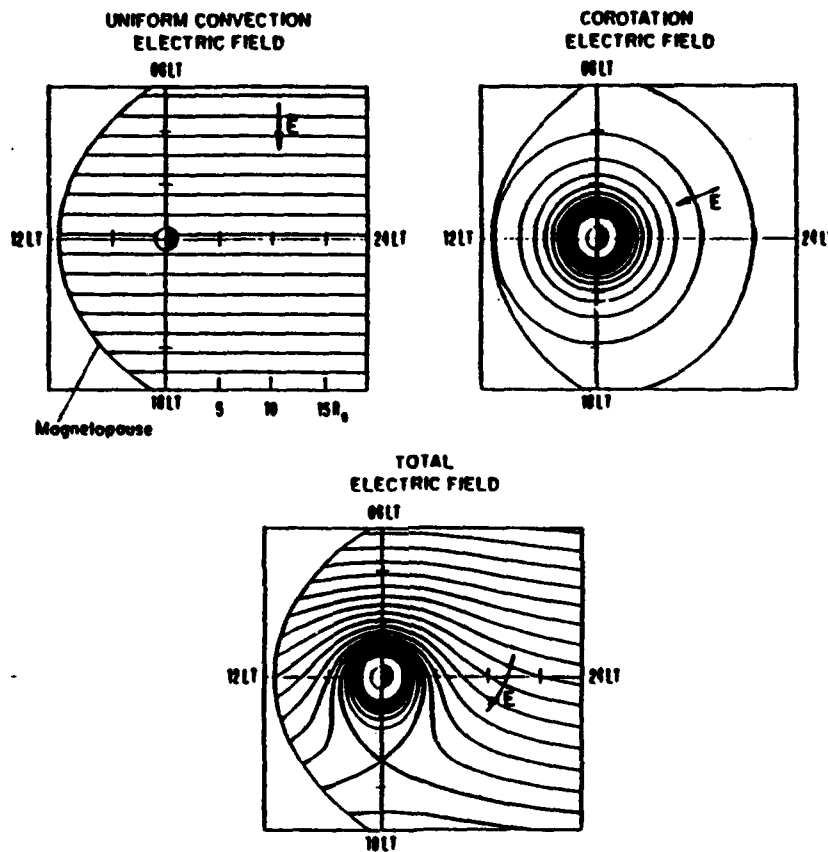


Figure 5. The Dusk Bulge



Equipotential contours for the magnetospheric electric field in the equatorial plane. Upper left: first-order approximation for the convection electric field E_c as uniform. The contours are spaced 3 kV apart for $E_c = 2.5 \times 10^{-4} \text{V m}^{-1}$. Upper right: the corotation electric field, contours spaced 3 kV apart. Lower: sum of convection and corotation electric fields. The heavy contour separates the closed and open convection regions. (From Lyons and Williams, 1984)

Figure 6. Magnetosphere's Electric and Magnetic Fields

length. The total number of charges in a sphere with a radius λ_D must be much greater than 1.

2. Debye Shielding

The electrostatic potential of a point charge q in a vacuum is given by:

$$(1) \quad \psi = \frac{q}{4\pi\epsilon_0 r} \text{ Volts}$$

where ψ is the electrostatic potential, ϵ_0 is the permittivity constant and r is the distance from the point charge (Halliday and Resnick, 1988). If the charge is immersed in a plasma, a positive charge will attract electrons while repelling ions, and similarly, a negative charge will attract ions and repel electrons. The potential then becomes:

$$(2) \quad \psi = \frac{q}{4\pi\epsilon_0 r} \exp^{-\frac{r}{\lambda_D}} \quad \lambda_D = \left(\frac{\epsilon_0 k T_e}{n e^2} \right)^{1/2}$$

where k is the Boltzman constant, T_e is the electron temperature, which is a measure of the average kinetic energy, n is the equilibrium density of the plasma, and e is the charge of the electrons. This has the effect of screening out electric potentials in a plasma. The electron temperature is used in the definition of λ_D because the electrons are more mobile than the ions and do most of the shielding by creating a surplus or deficit of negative charge. (Parks, 1991)

3. Plasma Parameter

In order for a collection of ionized particles to be considered a collisionless plasma, three conditions must be satisfied. The Debye length must be much less than the dimensions of the plasma. The number of particles in a Debye sphere defined as:

$$(3) \quad N_D = \frac{4\pi n \lambda_D^3}{3}$$

must be much greater than 1, that is, there must be a large enough number of particles for Debye shielding to be statistically valid. Finally the frequency of collisions of particles must be low. The plasma parameter g is defined as:

$$(4) \quad g = \frac{1}{N_D}$$

and for a collisionless plasma $g \ll 1$. (Parks, 1991 and Chen, 1983)

4. Motion in a Uniform Magnetic Field

A collisionless plasma will behave as a collection of individual particles. The individual charged particles will move in trajectories determined by the applied electric and magnetic fields. For space applications the fields resulting from the particle motion are often small and may be neglected. This is particularly true for the magnetic field, less so for the electric field. The force acting on a charged particle moving in a combined \underline{E} and \underline{B} field is given by the Lorentz equation:

$$(5) \quad \underline{F} = q(\underline{E} + \underline{v} \times \underline{B})$$

where \underline{F} is the Lorentz force, and \underline{v} is the particle velocity.

For the case where $\underline{E} = 0$, and the magnetic field is uniform, a charged particle will execute simple cyclotron gyration with a frequency:

$$(6) \quad \omega_c = \frac{|q|B}{m}$$

and radius:

$$(7) \quad r_L = \frac{v_{\text{perp}}}{\omega_c} = \frac{mv_{\text{perp}}}{|q|B} = \frac{mv \sin \alpha}{|q|B}$$

where m and v are the mass and velocity of the charged particle and the pitch angle α is the angle between the velocity vector of the charged particle and the magnetic field. The velocity parallel to the magnetic field line, $v_{\text{par}} = v \cos \alpha$, is not affected by the magnetic field. This motion describes a circular orbit about a guiding center which is travelling along the magnetic field line with velocity v_{par} . The trajectory of this particle is a helix with its axis parallel to the field line. (Chen, 1983)

5. Magnetic Mirror

The Earth's magnetic field lines converge at both the north and south magnetic poles, and the field strength increases with altitude. Because of this, there is an additional force that acts upon the charged particle. This force can be expressed as:

$$(8) \quad F = -\mu \nabla B \quad \mu = \frac{mv_{\perp}^2}{qB}$$

where μ is the magnetic moment. Because the gradient in the magnetic field is parallel to the direction of the field line it can be seen that this force is directed along the field line. Since the force is directed parallel to the particles parallel velocity component, it will obviously affect the particle's velocity. From Lenz's law, it can be shown that μ is invariant. (Parks, pp. 89-90)

Since μ is invariant, v_{perp} must increase as B is increased. For this to happen v_{par} must decrease since $v_{\text{perp}}^2 = v^2 - v_{\text{par}}^2$ (from conservation of energy). Therefore, given a large enough B, there will come a point where $v_{\text{par}} = 0$. At this point v_{perp} will equal v , and the particle will mirror back along the field line, Figure 7. (Gladstone, 1967). (Notice that the gyroradius also gets smaller as the particle approaches the mirror point as a result of its v_{perp} dependence.)

For a particle that mirrors, equation 8 then leads to:

$$(9) \quad \frac{mv_{\text{perp}o}^2}{qB_0} = \frac{mv_{\text{perp}m}^2}{qB_m}$$

where subscript o refers to values at the equator and m to

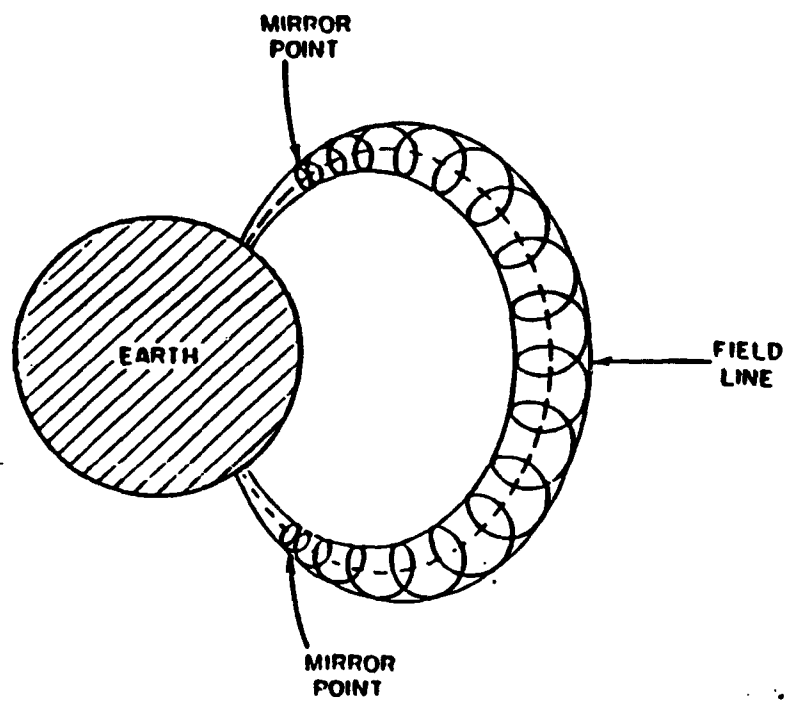


Figure 7. Path of Mirroring Particle

those at the mirror point. Rearranging equation 9 gives:

$$(10) \quad \frac{B_o}{B_m} = \frac{V_{perp o}^2}{V_{perp m}^2} = \frac{V_{perp o}^2}{V_o^2}$$

defining the pitch angle of a particle, α , to be the angle between velocity vector of the particle and the magnetic field line gives $v_{perp} = v \sin \alpha$. Plugging this into equation 10 gives:

$$(11) \quad \frac{B_o}{B_m} = \sin^2 \alpha_o$$

which states that all particles with a pitch angle α_o will mirror at the location defined by $B = B_m$. Particles with $\alpha > \alpha_o$ will mirror at lower altitudes. (Parks, pp. 111-112)

The magnitude of the Earth's magnetic field is given according to:

$$(12) \quad B = B_{os} \frac{\sqrt{4 - 3 \cos^2 \lambda}}{L^3 \cos^6 \lambda}$$

where B_{os} is the magnitude of the Earth's magnetic field on the Earth's surface at the magnetic equator, λ is the magnetic latitude, and L is the McIlwain L parameter (Parks, p. 54). The McIlwain L parameter is variable, given in units of Earth radii, used to label magnetic field lines with relation to where they cross the plane of the magnetic equator. Its value is given by:

$$(13) \quad L = \frac{r}{\cos^2 \lambda}$$

where r is the distance from the Earth center, in R_E , to the field line at the magnetic equator. (Parks, p. 115)

Substituting equation 12 into equation 11 gives:

$$(14) \quad \sin^2 \alpha_o = \frac{\cos^6 \lambda_m}{\sqrt{4 - 3 \cos^2 \lambda_m}}$$

Therefore, by defining an equatorially trapped plasma to mirror at a magnetic latitude of $\pm 10^\circ$ or less, this requires that a charged particle have a pitch angle greater than 69° , at the equator, in order to be equatorially trapped, Figure 8. It is these trapped particles that will be investigated in this paper.

6. Statistical Distribution

When dealing with a system which is composed of a very large number of individual particles it becomes impractical to solve the equations of motion for the system. Instead the particles may be treated statistically through the use of the distribution function. Classically the distribution function gives the probability distribution of the values of the coordinates and momenta of the particles. The density of particles in coordinate space is obtained by integrating the distribution function over the momentum or velocity space.

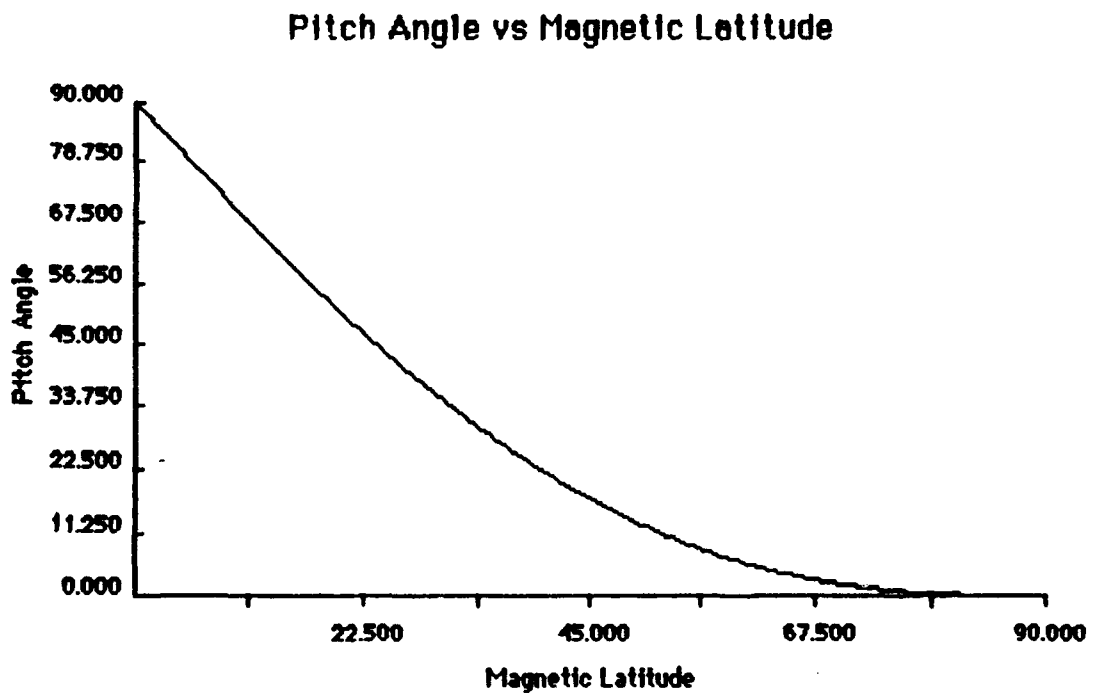


Figure 8. Pitch Angle verses Mirror Latitude

That is:

$$(15) \quad n = \int f(\mathbf{r}, \mathbf{v}) d^3\mathbf{v}$$

where n is the density, and $f(\mathbf{r}, \mathbf{v})$ is the distribution as a function of position and velocity integrated over three dimensional velocity space.

The two distribution functions of interest in this thesis are the bi-Maxwellian, and the Maxwellian or isotropic distribution function, given by:

$$(16) \quad f_{bi} = n \left[\frac{m}{2\pi kT_{perp}} \right] \left[\frac{m}{2\pi kT_{par}} \right]^{1/2} e^{-\frac{m}{2} \left[\frac{v_{perp}^2}{kT_{perp}} + \frac{v_{par}^2}{kT_{par}} \right]}$$

$$(17) \quad f_{\circ} = n \left[\frac{m}{2\pi kT} \right]^{3/2} e^{-\frac{mv^2}{2kT}}$$

where T_{perp} and T_{par} are the characteristic temperatures in the perpendicular and parallel directions with respect to the magnetic field line.

C. PREVIOUS OBSERVATIONS

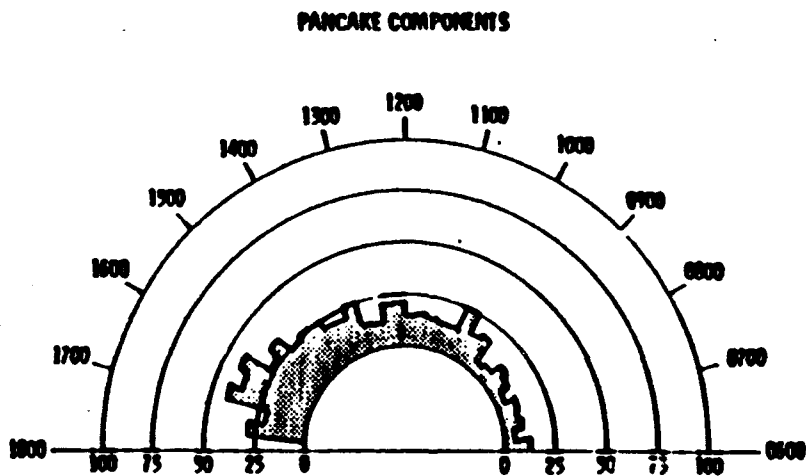
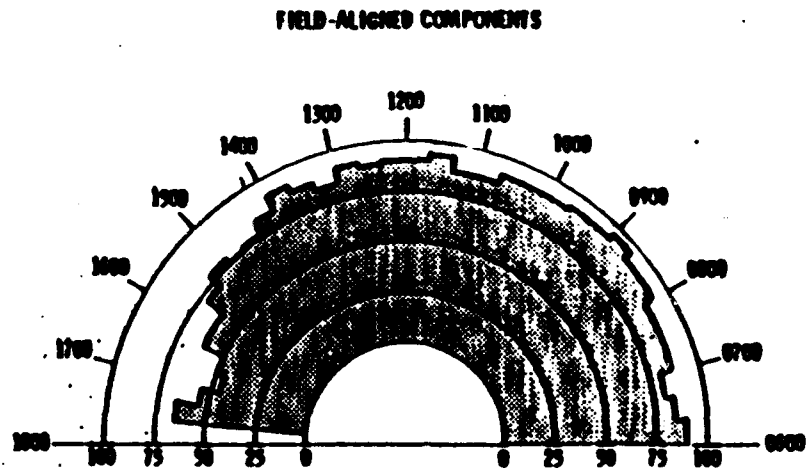
Thermal plasma pitch angle distributions seem to have been first studied by Horwitz and Chappell (1979) and Comfort and Horwitz (1980). These authors used electrostatic analyzer data to study ion pitch angle distributions at geosynchronous orbit, using ATS 6 data taken in 1974. The surveys dealt with data taken at 10.5° off the magnetic equator.

Comfort and Horwitz (1980) observed two important aspects of ion pancake distributions (peak flux near 90° pitch angle). The first was the occurrence probability for the pancake component of the ion distribution was local time and energy dependent. The highest probability of occurrence occurred in the lowest energy channel (20 - 40 eV) studied and for local times between 1400 and 1800. Pancake distributions were seen 42% of the time in this sector for ions of that energy.

The second was that Comfort and Horwitz observed that field aligned ions and ions with 90° pitch angle seem to be anti-correlated at 1700. Figure 9 shows that there is a decrease in the occurrence probability of field aligned ions when there is a peak in the pancake occurrence probability.

Horwitz *et al.* (1981) studied pancake distributions in low energy (≤ 100 eV) ion data obtained from the ISEE 1 mass spectrometer. The H^+ distributions were often found in the vicinity of the plasmopause, Figure 10, and usually just inside the plasmopause. Horwitz *et al.* also observed that the pancake distribution was often seen in the presence of colder, isotropic plasma.

Olsen (1981) observed a thermal plasma population, trapped within a few degrees of the magnetic equator, using electrostatic analyzer data from the SCATHA satellite. Figure 11 shows the ion count rate, for various ion energies, as a function of pitch angle. The data for this plot was taken at the equator at approximately 1000 local time and $5.5 R_E$. This



Total percent occurrence frequencies
for ion pitch angle distributions having
designated components, as functions of local
time.

Figure 9. Field Aligned and Pancake Trapped Ion Distributions

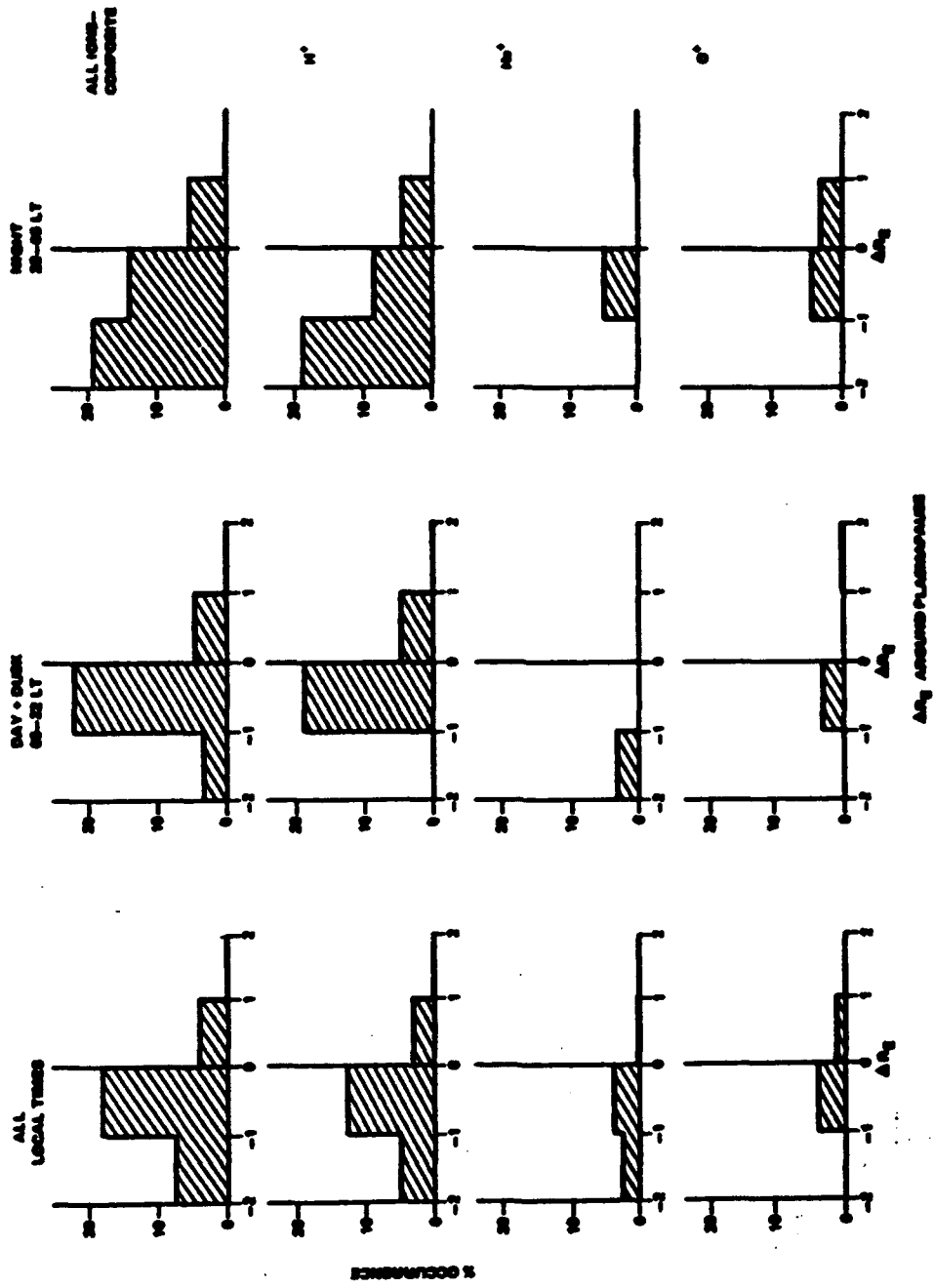
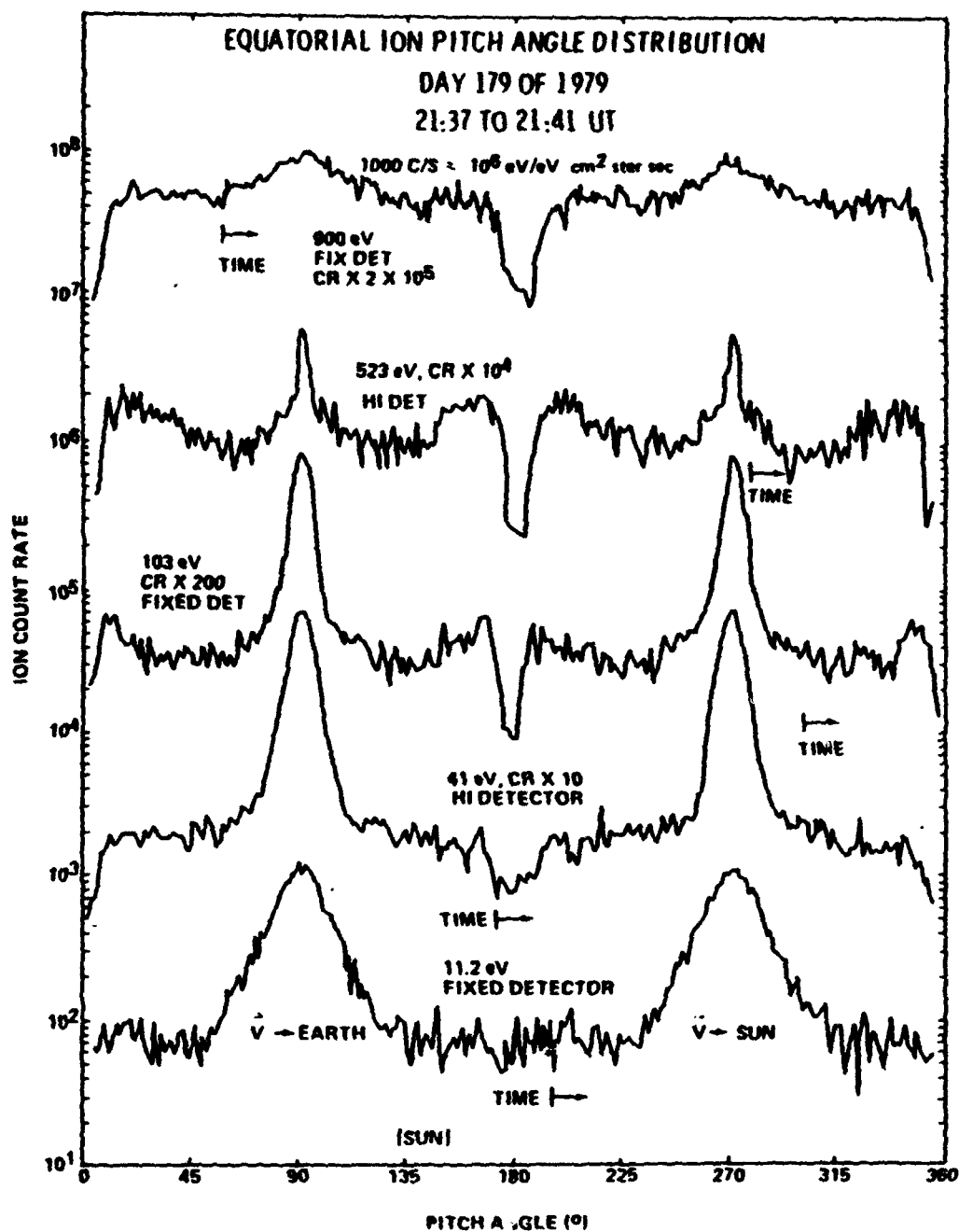


Fig. 11: Occurrence of sequences of pancake distributions for inside and outside 'sharp' plasmopause in 1 Rg bins around the sharp plasmopause position, based on time as a measure.

Figure 10. Trapped Ion Distribution With Relation to the Plasmopause

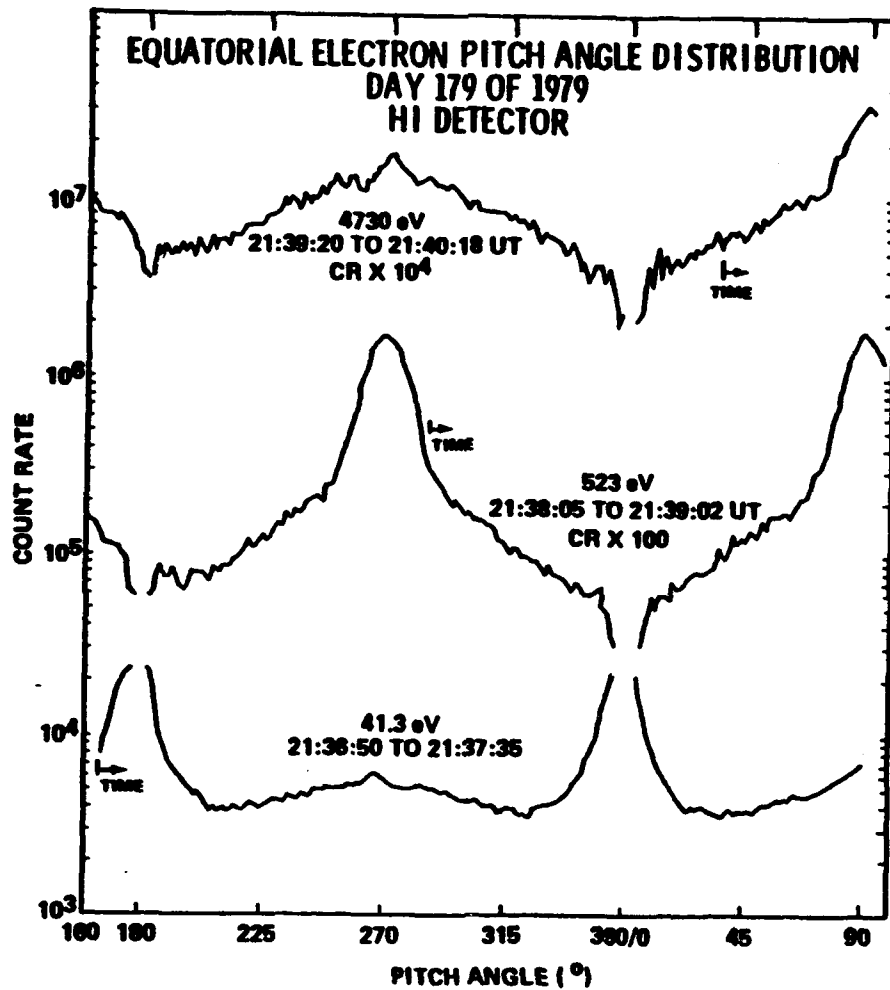


Ion pitch angle distributions at the equator for day 179 of 1979. Data are plotted from the FIX and HI detectors at 11, 41, 193, 523, and 900 eV. Fluxes are scaled by increasing factors to keep them from overlapping. Maximum values, with increasing energy are 1150 c/s, 7300 c/s, 4200 c/s, 550 c/s, and 540 c/s. The 0°-180° range corresponds to looking sunward, with 0° corresponding to looking south.

Figure 11. Ion Pitch Angle Distribution

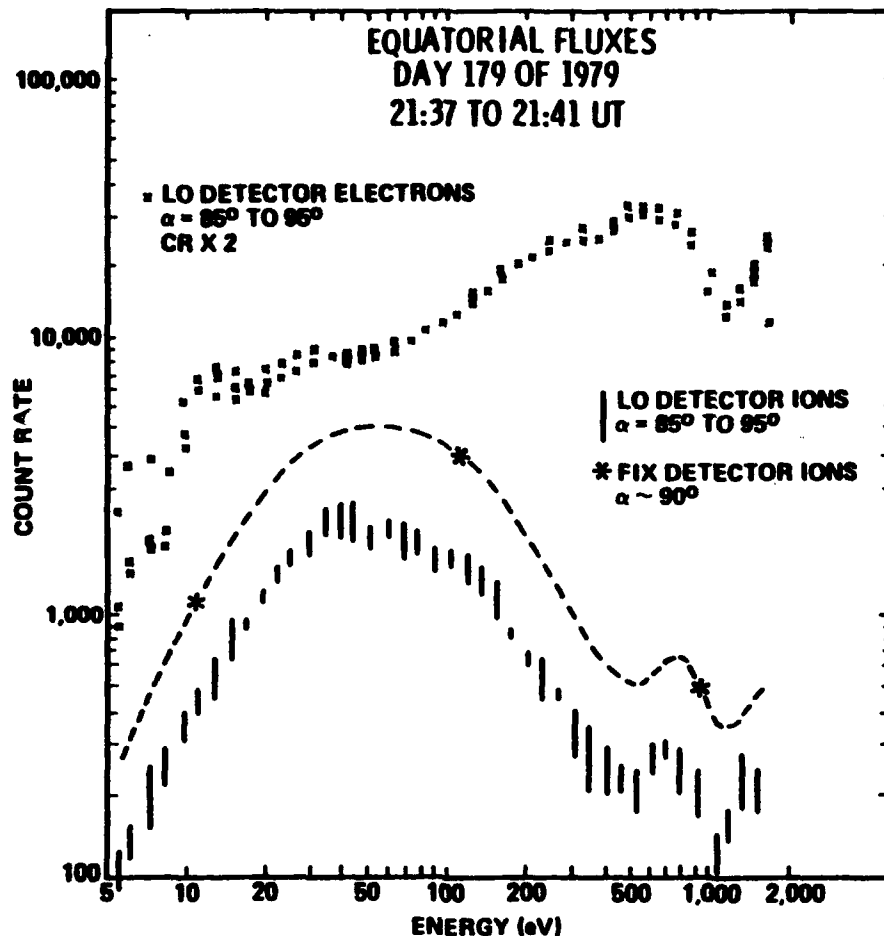
figure clearly shows a trapped distribution, centered at 90° and 270° pitch angle, for ions of energies 11 to 103 eV and, to a lesser extent, for those at 523 eV. The 900 eV ions do not show evidence of a trapped distribution. This figure also shows a well defined loss cone for the three highest energies.

Olsen observed a like distribution in the electron data, Figure 12. A source cone, centered at 0° and 180° pitch angles, was seen in the 41 eV electron flux concurrent with the trapped distribution at higher energies. This led to speculation that the field aligned particles were the (ionospheric) plasma source, and these particles were subsequently heated in the traverse direction. Note that the count rates in the last two figures are scaled differently for different energy levels in order to facilitate presentation of the data. Figure 13, from Scott (1991), shows a plot of count rate versus energy (in eV). The trapped electron distribution is seen to exist in the 50 to 1000 eV range, corresponding to temperatures of 100 - 200 eV and densities of $1 - 10 \text{ cm}^{-3}$. The trapped ions show a peak in the 20 to 200 eV range. This corresponds to temperatures of 20 to 50 eV and densities of $1 - 10 \text{ cm}^{-3}$. Sagawa *et al.* (1987) observed a local time dependence in the location of the trapped ions in data from the Dynamics Explorer (DE) 1 satellite. Sagawa *et al.* additionally saw that the trapped ions were composed primarily of H^+ ions and that these were in the lowest energy bin (0.01 - 1 keV) of the DE 1/EICS summary plots. They reported that



Electron pitch angle distributions at the equator for day 179 of 1979. Data are plotted from the HI detector at 41, 523, and 4730 eV. Pitch angle conventions are as in Figure 7.

Figure 12. Electron Pitch Angle Distribution



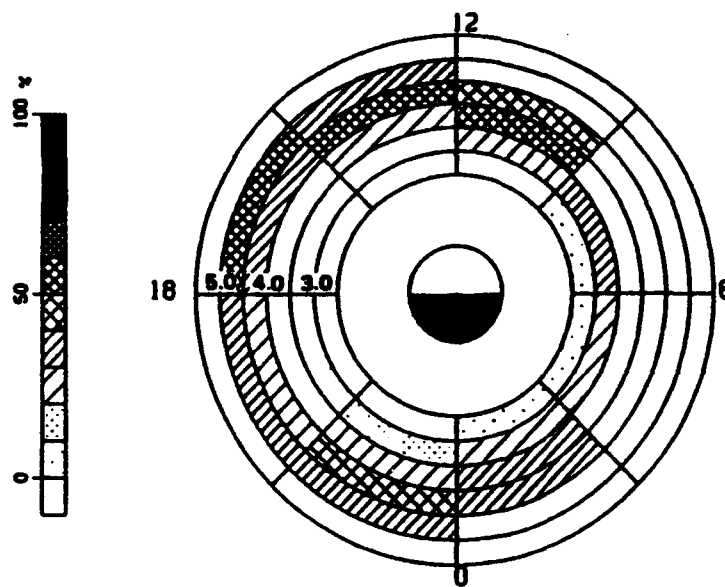
Ion and electron count rates as a function of energy from the LO detector near 90° pitch angle for day 179 of 1979. The electron count rate has been scaled by a factor of 2. The count rates from the FIX detector dwells were selected at their maxima (90° pitch angle). The difference between the LO and FIX ion data reflects degradation of the spiraltrons for the LO ion detector. The LO count rate curve has been traced and moved up to overlap the FIX detector data (about a factor of 2). The peak in ion count rate at 700 eV is a local maximum in the distribution function as well (see Figure 10).

Figure 13. Energy Relations of Trapped Plasmas

the McIlwain L value was higher, for the peak ion occurrence probability, in the local noon and dusk sectors than it was near local midnight, Figure 14. Olsen *et al.* (1987) also saw this in their statistical survey. Olsen *et al.* noted that the latitudinal extent of the high probability region is local time dependant, ranging from $\pm 30^\circ$ in the early afternoon region to $\pm 10^\circ$ in the early dawn region.

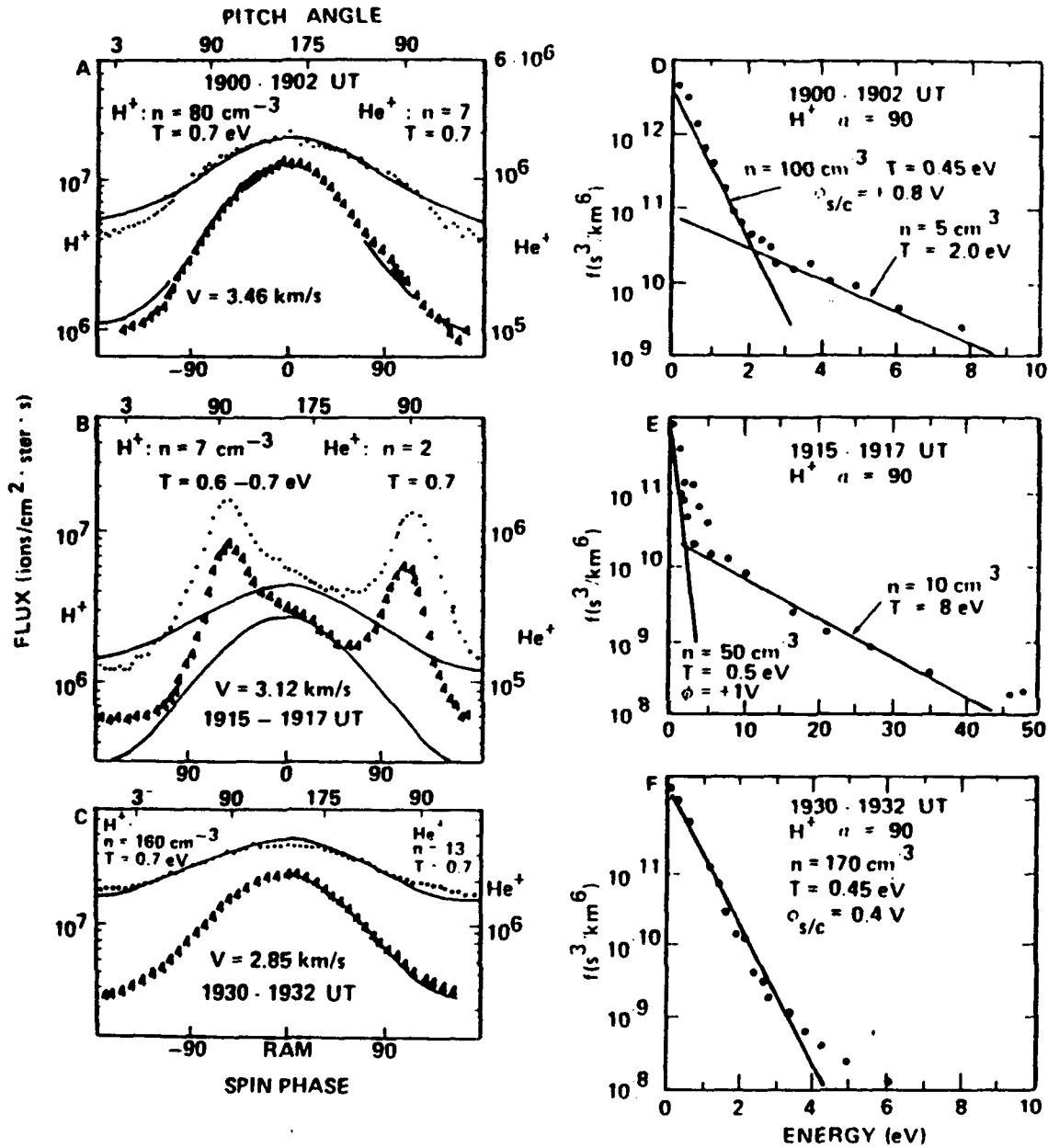
Olsen *et al.* (1987) observed, from data collected by DE 1, that the trapped ion distribution was composed primarily of H^+ , but that He^+ was seen to have a trapped component, having 10% the density of the trapped H^+ , approximately 40% of the time. In one case, trapped O^+ was seen with a relative density of 0.1% that of H^+ . Additionally, the trapped distribution was observed to be very localized about the equator. This is seen in the fact that the ions change from a field aligned distribution to a trapped distribution and then back very quickly as the satellite traverses the equatorial region. Figure 15 illustrates this aspect of the evolution in the pitch angle distributions.

Figures 15a, 15b, and 15c show plots of flux verses pitch angle for the magnetic latitudes of -7.9° , -1.9° (approximately), and 3.6° respectively. In this case, the He^+ ions mirror the H^+ ions, although at about 3.5% of its flux. Figures 15d, 15e, and 15f show the distribution functions for H^+ in these time periods. Notice the drop in density and the increase in temperature as the satellite enters the equatorial



Occurrence probability of low-energy (0.01-1 keV) H^+ pancake distribution with peak ion flux above $10^5 (\text{cm}^2 \text{s sr})^{-1}$, within 5° of the magnetic equator for active times ($K_p \geq 3-$) as a function of MLT and L shell. L shell bin size $\Delta L = 0.5$.

Figure 14. Trapped Ion L versus Local Time Dependence



(a) Spin curves for H^+ (circles) and He^+ (triangles) prior to the equator crossing, with fits. (b) Spin curves at the equator, with lines drawn for the same temperatures found in Figures 8a and 8c, at reduced densities. (c) Spin curves after the equator crossing. (d) H^+ distribution function for the period shown in Figure 8a. (e) H^+ distribution function for the period shown in Figure 8b. Note the change in energy scale as compared to Figures 8d and 8f. (f) H^+ distribution function for period shown in Figure 8c.

Figure 15. Flux - Spin Phase/Density Fits

region. (Olsen *et al.*, 1987)

Klumpar *et al.* (1987) found examples of equatorially trapped plasma in the data from the AMPTE/CCE satellite. The trapped ion distribution was found near the plasmapause interface. The temperature of these ions were found to be on the order of 30 - 50 eV. Like Olsen (1981), they also observed that the angular distributions of the trapped ion distribution became narrower for increasing ion energies.

Braccio (1991) extended the survey of the AMPTE/CCE data by surveying ions in the 30 - 150 eV energy channel and electrons in the 150 eV energy channel out to 8.8 Earth radii. In this survey Braccio concluded that the location of equatorially trapped plasmas is species dependant. The ions and electrons show a different local time dependance in the location of their occurrence probability peak. The following summarizes his conclusions:

Electrons

- display a uniform high probability distribution centered at 0900 local time and a L value of 6
- display a weak, if any, L dependence on local time
- trapped electrons begin to be seen at dawn leading to speculation that their existence is dependent on photoelectron emission from the Earth's ionosphere
- the shape of the distribution is basically conical, however, it drops off more rapidly than it decreases, with respect to local time

Ions

- distribution shows a strong L dependence on local time
- high trapped ion probability region begins at local dawn, for L approximately 4, and rises to a maximum at between 1400 and 1500 local time with an L value of 8
- the distribution drops off quickly in altitude after peaking as local time increases there is a region of decreased probability in the afternoon sector for his data that he suggested may be inhabited by higher energy ions. Part of this thesis will investigate this.
- the overall shape of the high trapped ion probability region mirrors that of the location of the plasmopause
- trapped electrons seem to be excluded from regions of high trapped ion probabilities and vice versa.

This thesis will further extend the look at the AMPTE data by conducting a statistical survey of ions in the 240 eV and 442 eV energy channels and electrons in the 340 eV and 770 eV energy channels.

There is not always a clear criteria used to define an equatorially trapped plasma. Intuitively, the definition seems to be that the bulk of the plasma is confined to (mirror within) 10° of the magnetic equator. One aspect of the development which follows is an attempt to quantify this concept, and relate the various definitions, tests, and survey techniques. Braccio (1991) defined, for the purpose of his study, an equatorially trapped plasma as having a minimum (threshold) flux in the 80° to 90° pitch angle bin of 10^6 ($\text{cm}^2 \text{ s sr}^{-1}$) for ions and 5×10^6 ($\text{cm}^2 \text{ s sr}^{-1}$) for electrons with an anisotropy greater than 1.5 (The anisotropy is defined as the

ratio of the fluxes in the 80° to 90° pitch angle bin to those in the 60° to 70° pitch angle bin.) in the same period. His survey generally was restricted to data taken within 10° of the magnetic equator. For the purpose of the statistical survey in this paper, the anisotropy criterion of 1.5 remains the same for both ions and electrons and the minimum flux criterion for an equatorially trapped plasma will be as follows:

Ions

- 240 eV: $10^5 \text{ (cm}^2 \text{ s sr)}^{-1}$
- 442 eV: $10^3 \text{ (cm}^2 \text{ s sr)}^{-1}$

Electrons

- 340 eV and 770: $5 \times 10^6 \text{ (cm}^2 \text{ s sr)}^{-1}$

The lower flux values for the ions partly accounts for the lower flux of ions at the higher energy channels.

Another criterion which could be used to characterize a trapped distribution is the ratio of the plasma's characteristic temperatures in the perpendicular and parallel directions with respect to the magnetic field line; T_{perp} and T_{parl} . An equatorially trapped distribution may be described by a bi-Maxwellian distribution function with these characteristic temperatures (Scott 1991). For the purpose of the case studies of this thesis a ratio of T_{perp} to T_{parl} equal to three will be used as a lower threshold required for an

equatorially trapped distribution to occur. The relationship between the above two definitions; flux ratios and temperature ratios, is considered next.

Applying the threshold of a temperature ratio of three determines the anisotropy in flux that must be met for an electron distribution to be considered trapped. Figure 16 shows plots of the log of the flux versus pitch angle for 150 eV and 340 eV. In each the perpendicular temperature was set to 75 eV and the parallel to 25 eV; a temperature ratio of three. These temperatures were selected as representative of values seen in the data analyzed. Scott (1991) got slightly larger ratios. The density was set arbitrarily to 1.2 cm^{-3} as a reasonable value. The density does not affect the illustration.

In both Figure 16a and 16b there are shown two curves. The uppermost is the plot of the bi-Maxwellian distribution function with the above T_{perp} and T_{parl} values at the magnetic equator. The lower of the two curves is a plot of the same function with the same temperatures, but mapped to a magnetic latitude of 10° . The peak flux of this curve is equal to the magnitude of the flux at the magnetic equator at a pitch angle of 69° . This is because a pitch angle of 69° at the equator maps to a pitch angle of 90° at a magnetic latitude of 10° . With our previous criterion for a trapped distribution being one that is limited to within 10° of the magnetic equator this establishes a lower limit on the pitch angles analyzed at the

equator at 69° and a relevant pitch angle range of 69° to 90° for the analysis of a bi-Maxwellian distribution.

Taking the ratio of the top curve to the bottom curve in Figures 16a and 16b a differential anisotropy was derived. The results of this calculation was 1.67 for 150 eV and 3.2 for 340 eV. The survey work done here, and those by Braccio (1991) use an integral anisotropy calculated by taking the ratios of the flux in the 80° to 90° pitch angle bin to the flux in the 60° to 70° pitch angle bin. Note that the survey files were divided into pitch angle bins of 10° in size. Using this definition for the anisotropy we take the ratio of the integral of the distribution function over pitch angles 80° to 90° to the integral of the distribution function over pitch angles 60° to 70° . The results of this is an anisotropy of 1.953 for 150 eV and 4.421 for 340 eV. For the purposes of the detailed analysis case studies in this thesis the rounded values of 2.0 and 4.4 will be used for 150 eV and 340 eV, respectively, as applied to a definition of being bi-Maxwellian and hence an equatorially trapped electron distribution. This will allow for comparison between this work and previous survey techniques. Note that the integral ratio calculated here is higher than that used in the initial survey.

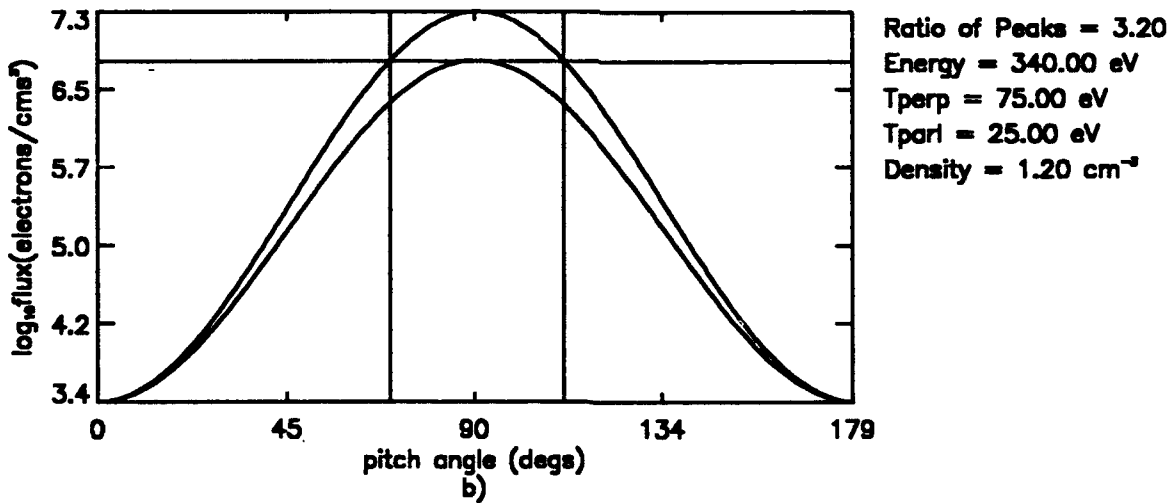
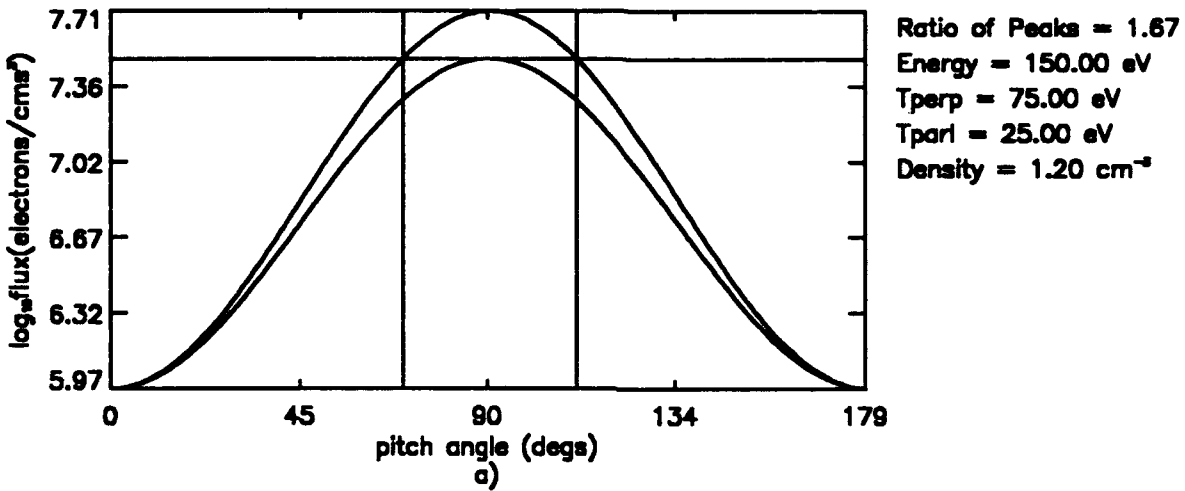


Figure 16. Log of Flux verses Pitch Angle - 150 eV and 340 eV
Electrons

D. THE AMPTE/CCE SATELLITE

The Active Magnetospheric Particle Tracer Explorers (AMPTE) mission consists of three satellites that were launched on August 16, 1984. The purpose of this mission (Acuña *et al.*, 1985) was to:

1. investigate the transfer of mass and energy from the solar wind to the magnetosphere and to study its further transport and energization within the magnetosphere.
2. to study the interaction between artificially injected and natural space plasma.
3. to establish the elemental and charge composition and dynamics of the charged population in the magnetosphere over a broad energy range.

Two of the satellites, the Ion Release Module (IRM) and the United Kingdom Sub-satellite (UKS), were concerned primarily with the introduction of artificially injected ions into the magnetosphere and will not be discussed further. The third satellite was the Charged Composition Explorer (CCE), Figure 17. The purpose of this satellite was to measure the particle distribution of the naturally occurring plasma, with respect to species, energy, and pitch angle, as well as to measure the artificially released ions from IRM. (Dassoulas *et al.*, 1985) The CCE was placed in an elliptical orbit around the Earth with a period of 15.66 hours and an inclination to the Earth's equatorial plane of 4.8° . It had an altitude at perigee of 1108 km and at apogee of 49,684 km (roughly 1.2 and $8.8 R_E$ respectively). It was spin stabilized with a spin rate

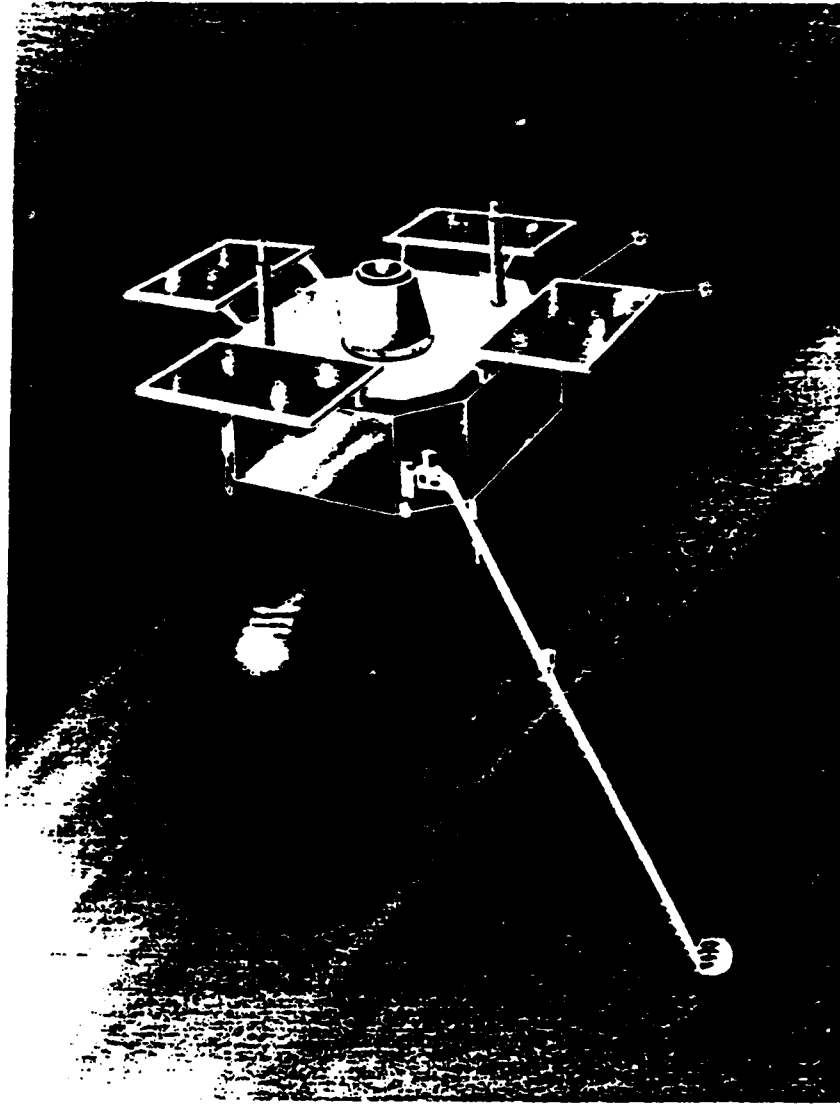


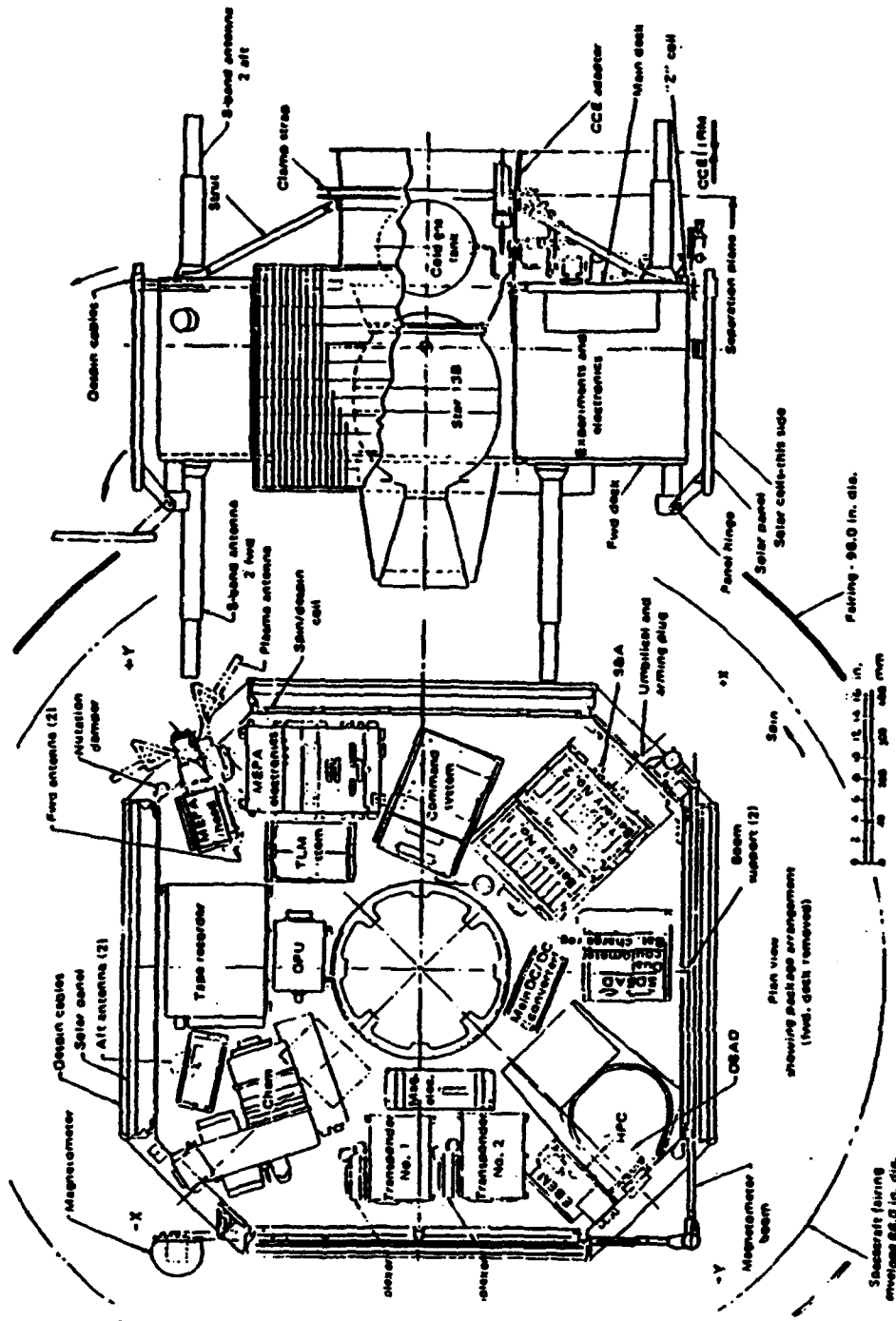
Figure 17. The AMPTE/CCE Satellite

of 10.25 rev/min (Dassoulas et al., 1985). Data began to be collected by this satellite on August 26, 1984.

The payload of the CCE, Figure 18, consisted of five experiments; 1) the Hot Plasma Composition Experiment (HPCE), 2) the Charge Energy Mass Spectrometer (CHEM), 3) the Medium Energy Particle Analyzer, 4) the Magnetometer, and 5) the Plasma Wave Experiment (Dassoulas et al., 1985). This paper concerns itself with data from the HPCE (and, indirectly, the Magnetometer).

E. THE HOT PLASMA COMPOSITION EXPERIMENT (HPCE)

The HPCE consists of the Ion-Mass Spectrometer and the Electron Background Environment Monitor (EBEM). The ion-mass spectrometer, Figure 19, provides mass per charge ion-composition measurements from very low energies (corresponding to the spacecraft potential) to approximately 17 keV. The ions enter the detector through a collimator which limits both azimuthal and elevation angles of acceptance. The azimuthal limits are at $\pm 5.5^\circ$ while the elevation acceptance angle ranges from approximately $\pm 25^\circ$ for ions at the spacecraft potential to $\pm 7.5^\circ$ for those at 17 keV. The ions are sent through a retarding potential analyzer (RPA) and then accelerated through a -2960 V potential. (Shelley et al., 1985)



Package arrangement of the AMPTE CCE as seen from the top (left) and from the side (right).

Figure 18. The AMPTE/CCE Payload

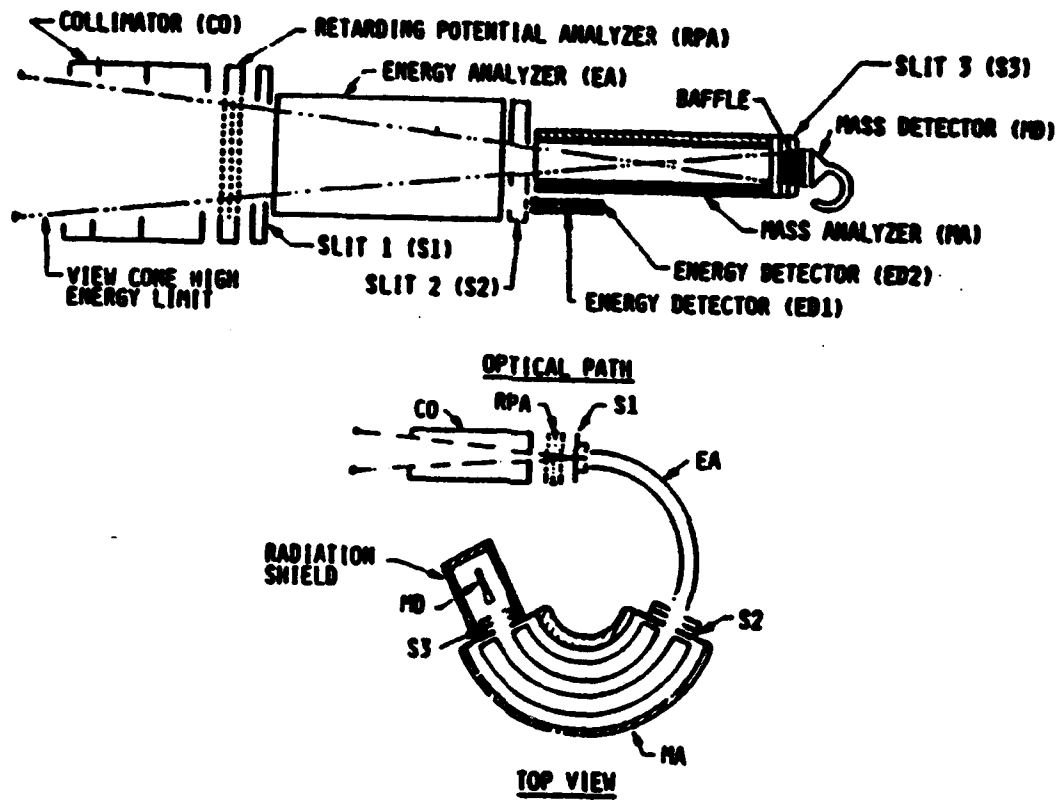


Figure 19. The HPCE Ion-Mass Spectrometer

The ions then pass through the object slit and into the cylindrical electrostatic energy analyzer. The electrostatic energy analyzer is programmable in 32 energy per charge steps from 3 to 20 keV/e. The central portion of the ion flux then enters the mass analyzer through a second slit, with a portion of the spectrum measured by "energy detectors" (ED1 and ED2). The mass analyzer consists of a second cylindrical electrostatic deflection system suspended in a 978 G magnetic field. The ions that exit this region, through the image slit, are detected by a high-current electron multiplier (Shelley *et al.*, 1985). This instrument was active from August 26, 1984 until it failed on April 4, 1985.

The EBEM consisted of eight independent 180° permanent magnet electron spectrometers. Electrons entered the EBEM through a 5° full angle collimator and were then deflected through 180° by a permanent magnet, Figure 20. They were then focused onto an exit aperture, that defined the allowed momentum range, and were then detected by a channel electron multiplier. (Shelley *et al.*, 1985)

Both the ion and electron data for the AMPTE/CCE HPCE were processed into pool files. These were the data files used for survey. These pool files consist of data arranged in 6.5 minute bins from 0000 to 2400 universal time. There is a separate data file for each day's data and each file contains both electron and ion data for that day. (Shelley *et al.*, 1985)

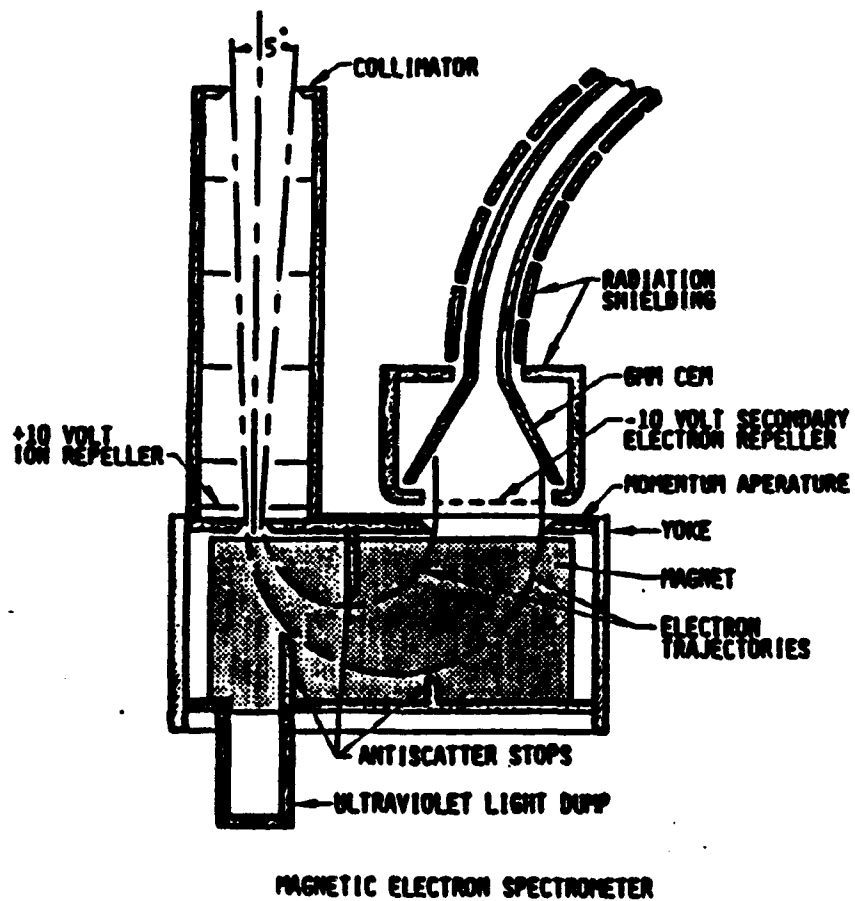


Figure 20. The HPCE Electron Background Environment Monitor

For this work, the ion flux measurements from the energy detectors (ED) are used, since we were not interested in differentiating between H^+ and He^+ for this survey. The pool data are sorted, by time, into 18 logarithmically spaced energy bins. The lowest four channels use the "RPA" mode data. The bulk of the data which are available in the pool file have only the fourth RPA channel, which provides an integral measurement from approximately 30 to 150 eV, with a weighted center at 50 to 65 eV. The remaining channels extend up to 17keV/e. The ion flux is also sorted by time verses pitch angle, with pitch angle bins from 0° to 90° in increments of 10° . (Shelley et al., 1985)

The electron data is likewise sorted into 8 energy bins from 50 eV to 25 keV and by pitch angle from 0° to 90° in 10° increments, each also verses time. The energy channels for the ion electrostatic energy analyzer and for the EBEM are given in TABLE I and II. Data was also collected for ions species verses time verses energy and for ion species verses time verses pitch angle (Shelley et al., 1985). This aspect of the data was not used in this paper.

TABLE I. ION ENERGY CHANNELS IN THE HPCE ON THE AMPTE/CCE

Energy Channel	Energy of Channel Center (keV/e)	Full Energy Width (keV/e)
1	0.0014	0.0028
2	0.0067	0.0076
3	0.020	0.020
4	0.050	0.125 RPA1
	0.052	0.122 RPA2
	0.055	0.115 RPA3
	0.065	0.095 RPA4
5	0.240	0.216
6	0.442	0.209
7	0.657	0.222
8	0.885	0.235
9	1.127	0.338
10	1.660	0.567
11	2.261	0.641
12	2.941	0.724
13	3.709	1.056
14	5.058	1.480
15	6.668	2.143
16	9.339	3.041
17	12.75	3.884
18	17.11	2.600

TABLE II. ELECTRON ENERGY CHANNELS IN THE HPCE ON THE AMPTE/CCE

Electron Detector	Energy Channel Center (keV/e)	Full Energy Width (keV/e)
CMEA	0.067	0.051
CMEB	0.150	0.126
CMEC	0.340	0.284
CMED	0.770	0.643
CMEE	1.74	1.45
CMEF	3.94	3.28
CMEG	8.89	7.41
CMEH	20.1	11.7

III. OBSERVATIONS

A. STATISTICAL SURVEY

1. Data Analysis

Data collected from August 26, 1984 until December 6, 1985 were processed and analyzed. However, ion data were only available through April 4, 1985. This was due to the failure of the ion-mass spectrometer on that day. The stop date for the analysis was chosen because the satellite completed one precession around the Earth, starting from August 26, 1984 and ending on December 6, 1985.

For each day of data, two different types of spectrograms were produced for both the ions and electron data. The first type was an energy channel-time spectrogram, for pitch angles in the 80-90 degree range. The second was a pitch angle-time spectrogram. The energy channels used were the ion fifth and sixth channels (240 and 442 eV) and the electron third and fourth channels (340 and 770 eV).

These spectrograms were examined for periods when the satellite encountered the magnetopause. The spectrograms were also inspected to find periods of very "choppy" data and periods when the instrument was undergoing diagnostic testing. Data in these periods were then removed from the data file to ensure that the analysis would not be contaminated by such artifacts.

These edited data files were then surveyed to produce local time vs McIlwain L probability distribution plots. The results for ions and electrons were plotted separately then compared.

2. Local Time - McIlwain L Surveys

a. ION SURVEY

Figure 21 shows a plot of the probability distribution for equatorially trapped ions using the lowest criteria from the previous chapter, namely the ion flux in the 80° - 90° pitch angle bin, at 240 eV, be greater than 10^5 ions/($\text{cm}^2 \text{ s sr}$), that the anisotropy be greater than 1.5, and that the ions be observed within 10° latitude from the magnetic equator.

The grey scale for the results runs from 0% to 60% with zero being white and 60% being black. The coverage plot's grey scale ranges from 0 to 200 counts and from white to black respectively. The scales are allowed to saturate (peak coverage was approximately 600 samples at apogee). Note that the 1800 to 2400 local time sector's zero occurrence probability is due to lack of coverage.

The contents of Figure 21 are alternately presented as a surface plot in Figure 22. This plot has x and y axes of local time and L. The z axis is probability of occurrence, from 0 to 100%. A contour plot is also displayed as part of this figure to facilitate the reading of the surface plot. Again, the 1800 to 2400 local time sector was not sampled.

AMPTe SURVEY
 IONS FROM ESA 240 eV
 Anisotropy gt 1.5 Flux gt 1.00E+05 MagLat lt 10.0

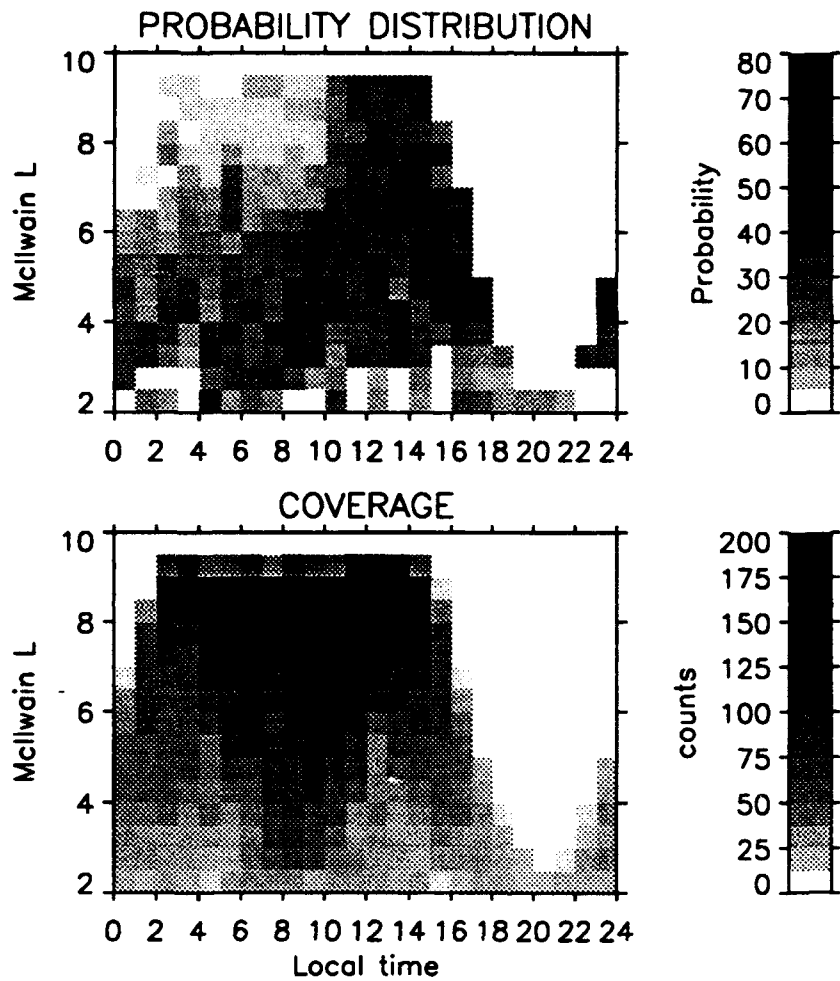


Figure 21. Trapped Ions (240 eV) - Flux gt 10^5 , Anisotropy gt 1.5, Maglat gt 10°

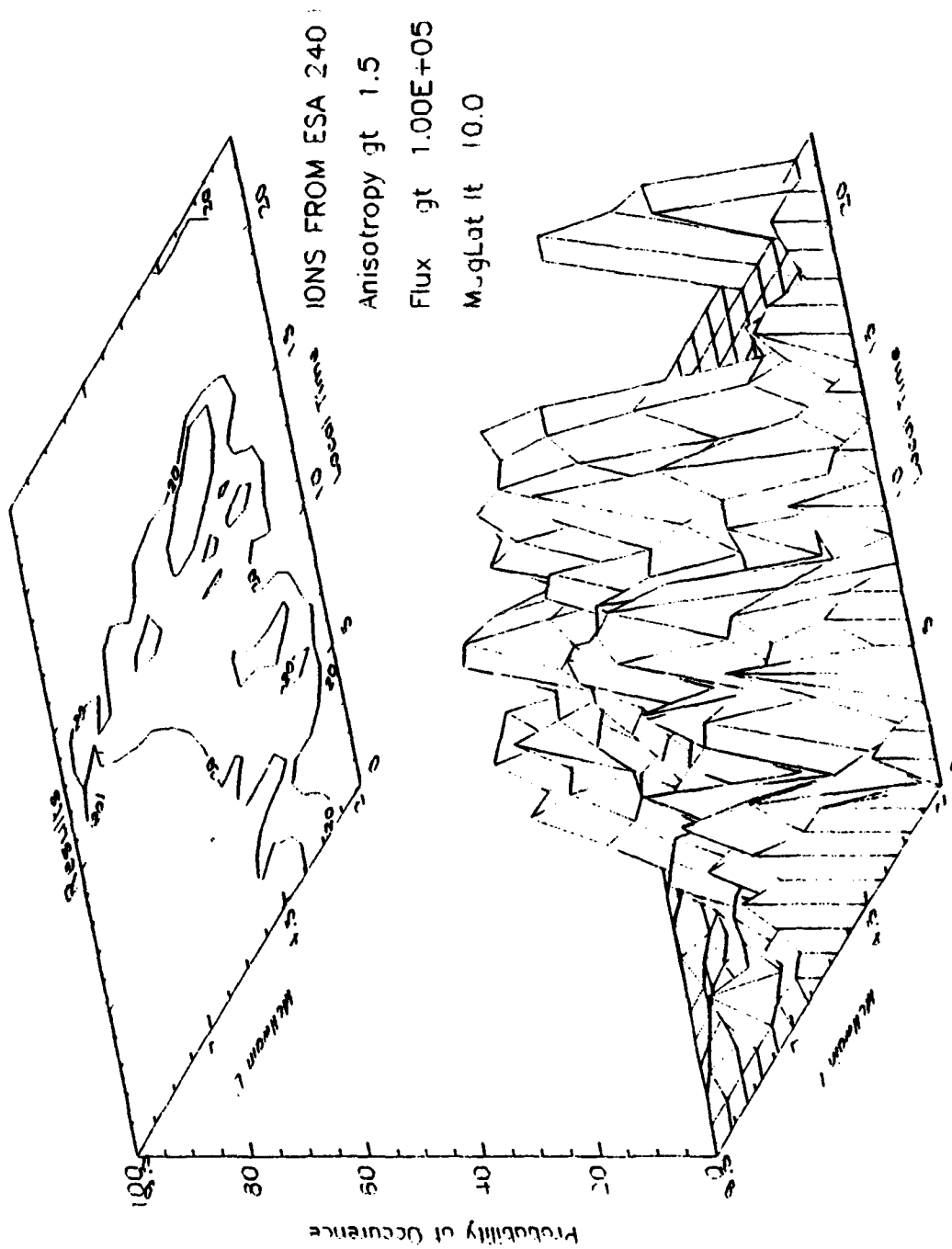


Figure 22. Trapped Ions (240 eV) - Flux gt 10^5 , Anisotropy gt 1.5, Maglat gt 10° - Surface Plot

The high probability (greater than 30%) region these ions starts at 0500 local time at an L of 3.5. As local time increases so does the L value of the peak probability. At 1400 local time the maximum L value, 8, is reached. At this point the probability appears to drop off sharply in L as local time moves toward dusk. This, however, may be an artifact brought about by the low coverage after 1800 local time.

In Figures 23 and 24 the results of raising the selection criteria for a trapped ion distribution are shown. In Figure 23 the selection criteria are flux greater than 10^5 , anisotropy greater than 1.5, and measurements within 5° of the magnetic equator. In Figure 24 the selection criteria are flux greater than 5×10^5 , anisotropy greater than 2.0, and measurements within 5° of the magnetic equator. The local time dependence is similar in these three figures.

Figure 25 shows a plot of the probability distribution for equatorially trapped ions for the sixth energy channel (i.e. 442 eV). Here the selection criteria is a flux greater than 10^3 ions/($\text{cm}^2 \text{ s sr}$), an anisotropy greater than 1.5, and a magnetic latitude between within 5° of the magnetic equator. The grey scales are the same as in the previous two figures. Figure 26 is a surface plot of the same data.

The high probability (greater than 30%) region for these ions starts at 0500 local time at an L of 3.5. Again, as

AMPTE SURVEY
IONS FROM ESA 240 EV
Anisotropy gt 1.5 Flux gt 1.00E+05 MagLat It 5.0

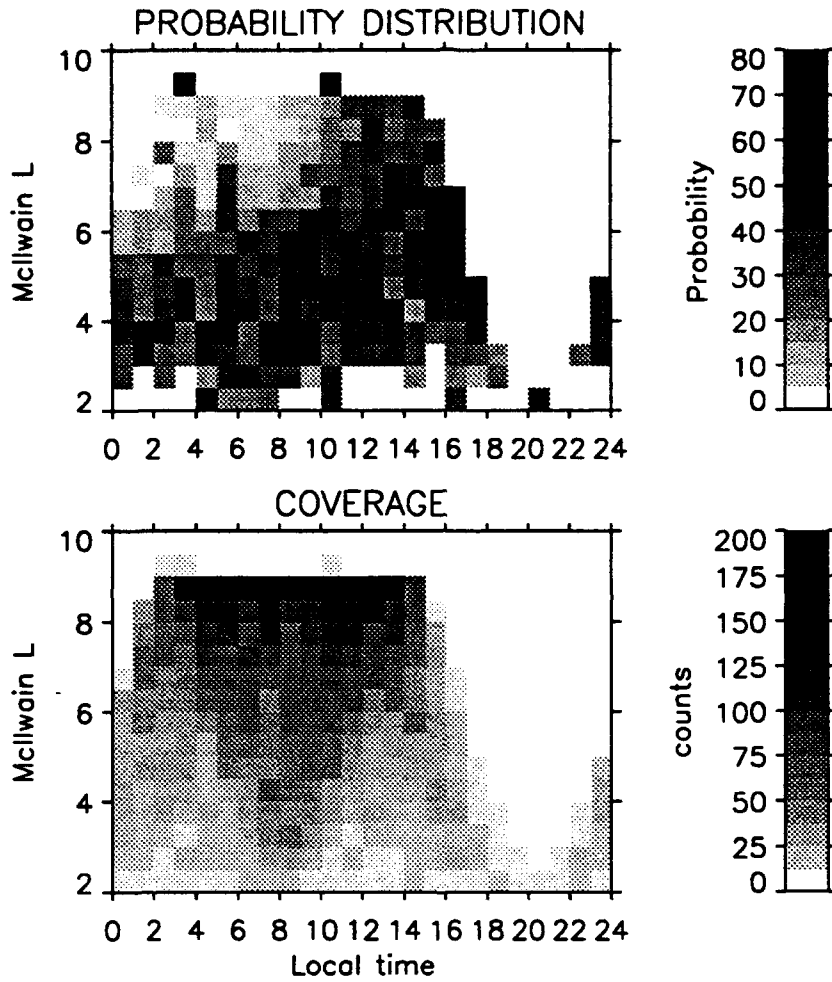


Figure 23. Trapped Ions (240 eV) - Flux gt 10^5 , Anisotropy gt 1.5, Maglat gt 5°

AMPTTE SURVEY
IONS FROM ESA 240 EV
Anisotropy gt 2.0 Flux gt 5.00E+05 MagLat lt 5.0

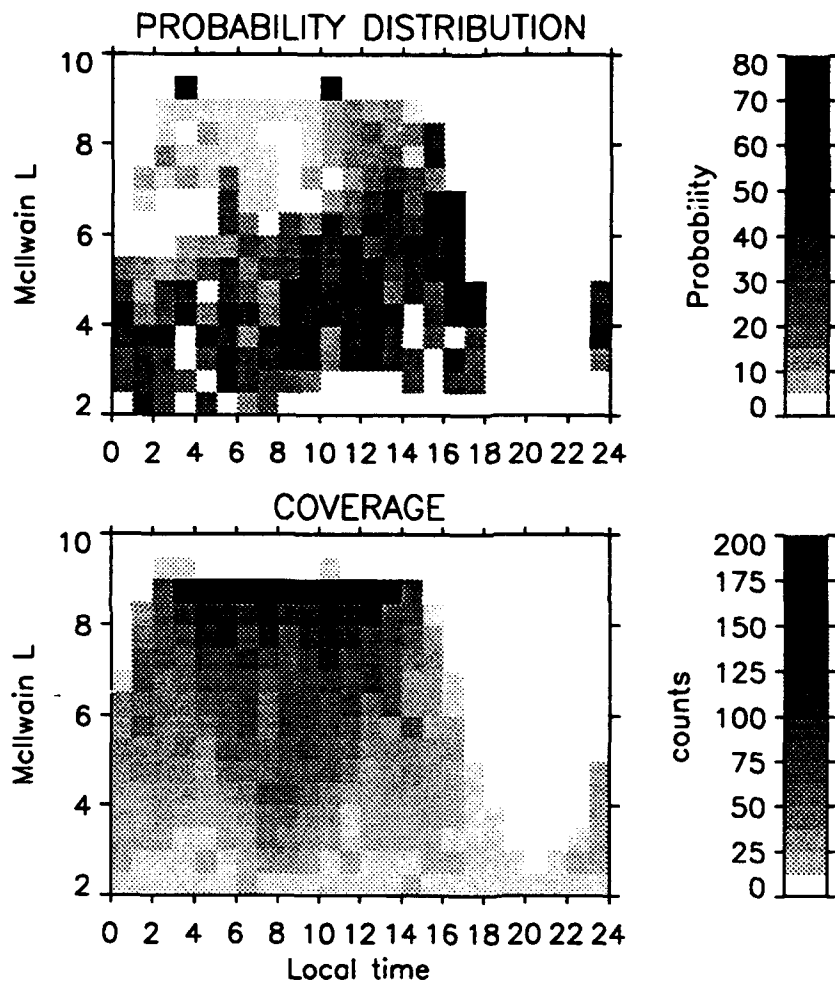


Figure 24. Trapped Ions (240 eV) - Flux gt 5×10^5 , Anisotropy gt 2.0, Maglat gt 5°

AMPTe SURVEY
IONS FROM ESA 442 eV
Anisotropy gt 1.5 Flux gt 1.00E+03 MagLat lt 5.0

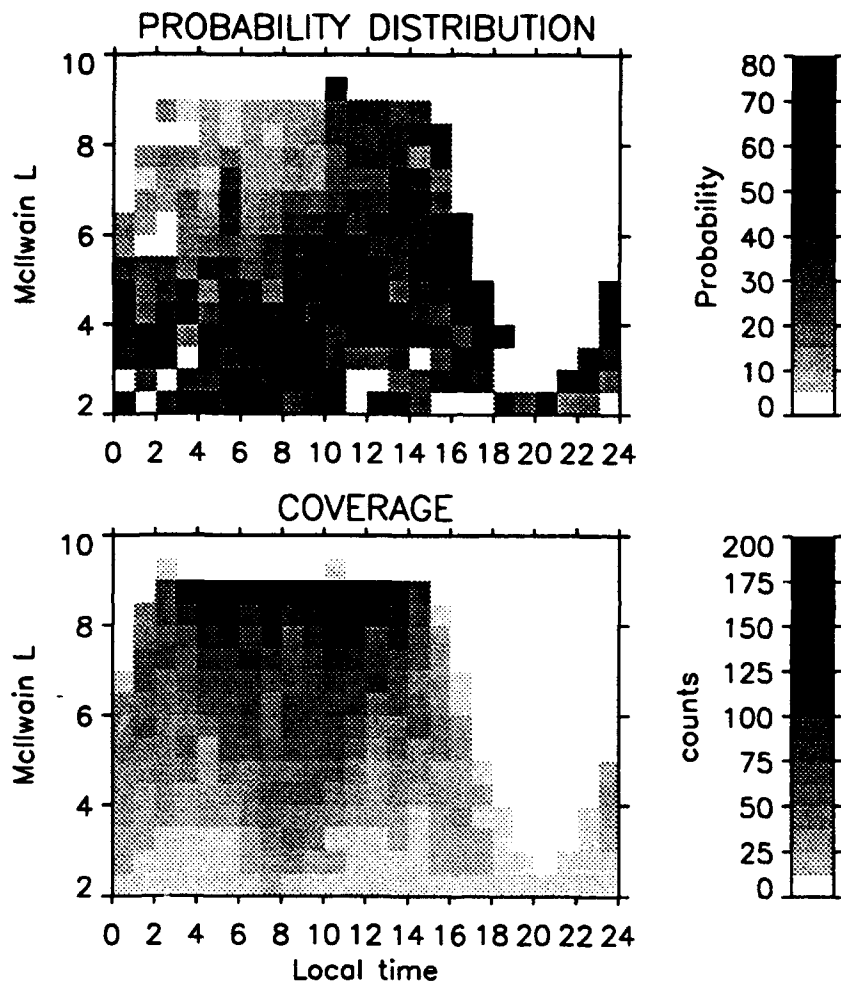


Figure 25. Trapped Ions (442 eV) - Flux gt 10^3 , Anisotropy gt 1.5, Maglat gt 5°

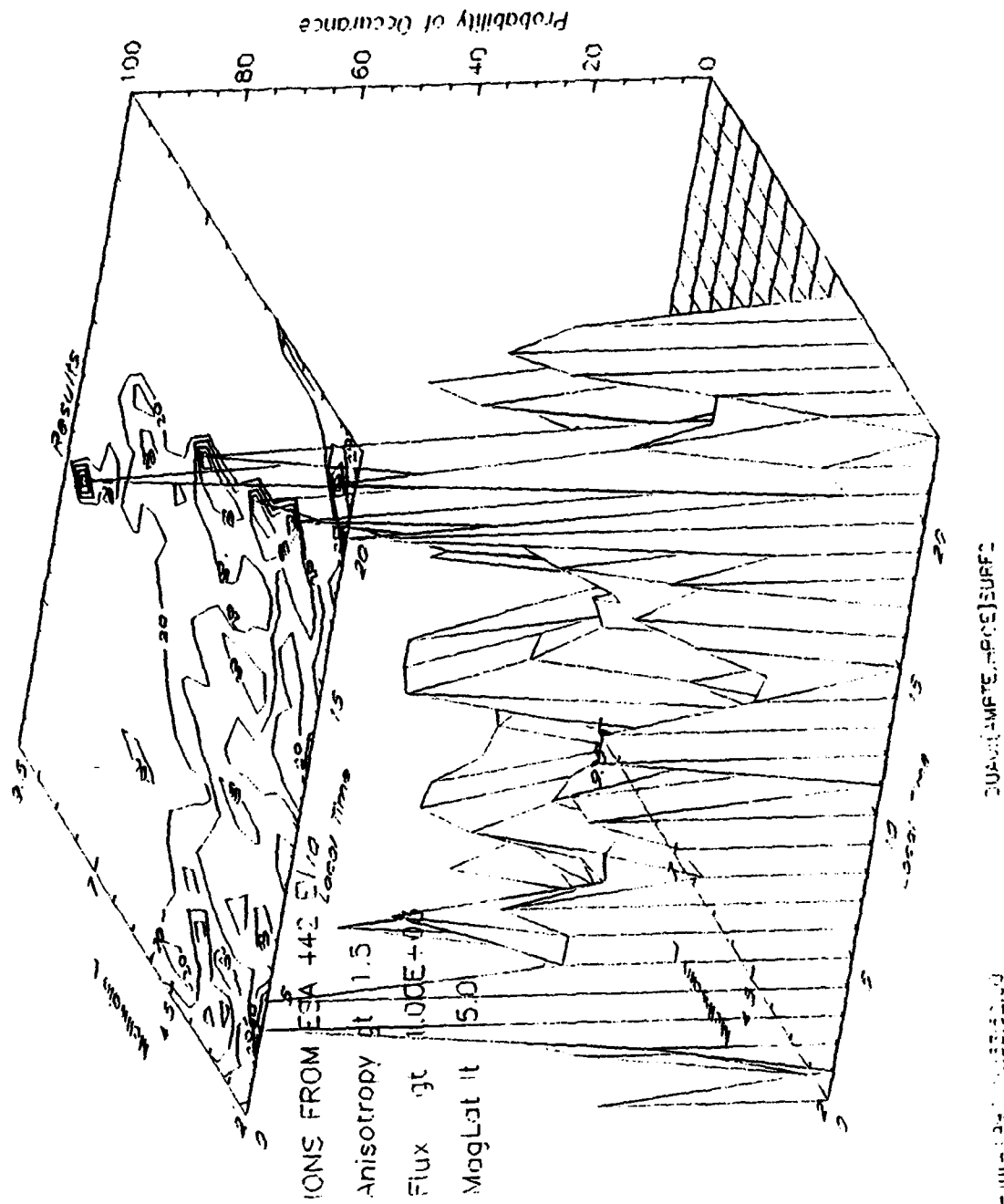


Figure 26. Trapped Ions (442 eV) - Flux gt 10^3 , Anisotropy gt 1.5, Maglat gt 5° - Surface Plot

as local time increases so does the L value of the peak probability. At 1400 local time the maximum L value, 8, is reached and then the probability drops off sharply, probably due to the lack of data after 1800.

The survey of the additional energy channels for the ions did not dramatically change the results found by Braccio. Figures 27 and 28 are the probability distribution plot and surface plot from Braccio (1991) for ions in the fourth RPA energy channel (30 - 150 eV) with the criteria of flux in the 80°-90° pitch angle bin be greater than 10⁶ ions/(cm² s sr), that the anisotropy be greater than 1.5, and that the measurements be within 10° latitude of the magnetic equator. It is found that the high probability region (greater than 45%) for the ions started at 0500 local time and in the area of L = 3.5. His maximum L value is on average about 8.0 and occurs generally around 1400 local time. At the maximum the probability appears to drop off sharply in L as local time moves toward dusk, similar to the results above.

The apparent decrease in probability of occurrence for ions in the region of 1200 to 1400 local time found by Braccio is readily evident in both energy channels surveyed, which seems to dampen Braccio's hypothesis that the higher energy ions inhabited this region.

AMPTe SURVEY

Ions:

Anisotropy gt 1.5 Flux gt 1.00E+06 MagLat lt 10.0

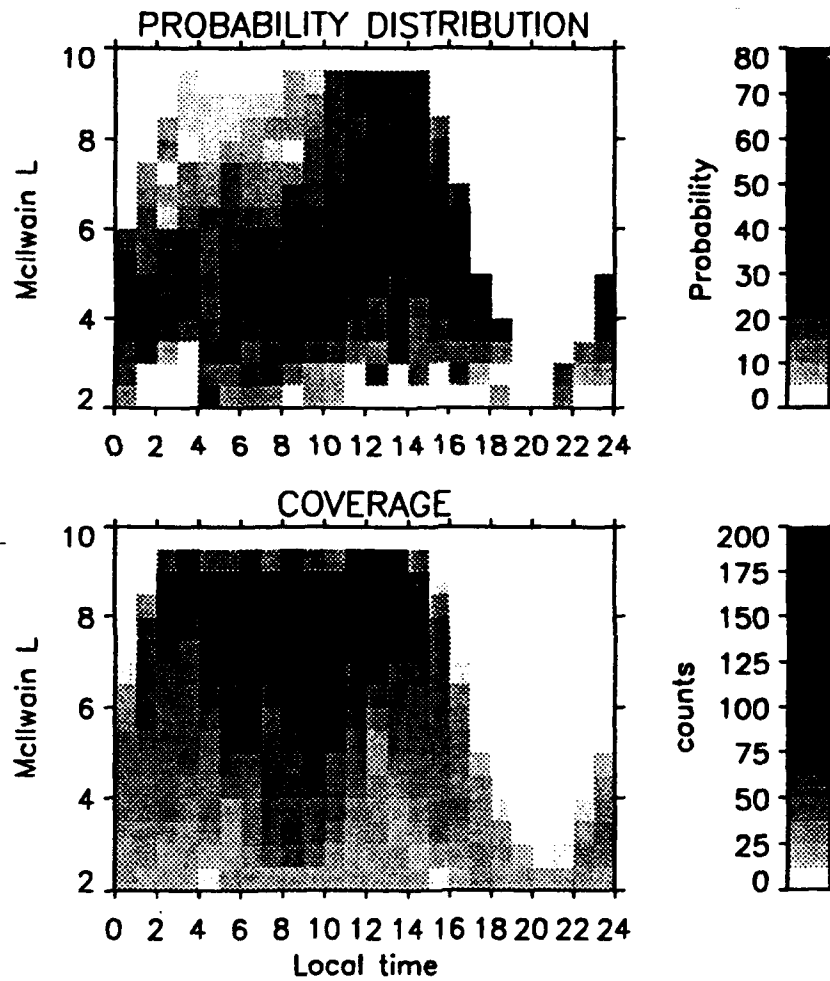


Figure 27. Trapped Ions (30-150 eV) - Flux gt 10^6 , Anisotropy gt 1.5, Maglat gt 10°

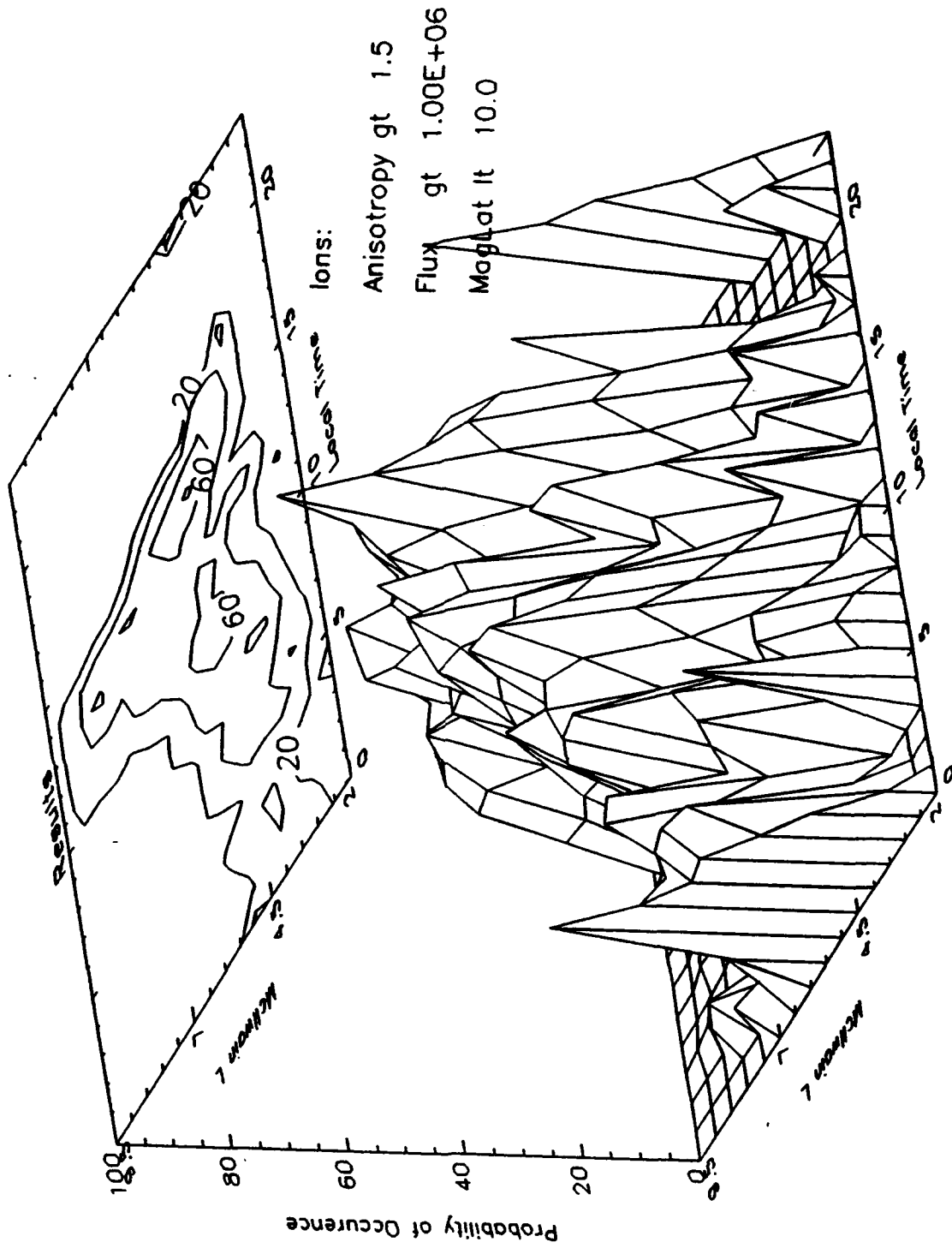


Figure 28. Trapped Ions (30-150 eV) - Flux gt 10^6 , Anisotropy gt 1.5, Maglat gt 10° - Surface Plot

b. ELECTRON SURVEY

Figure 29 shows the probability distribution for trapped electrons with an energy of 340 eV meeting the criteria of flux greater than 5×10^6 electrons/(cm² s sr), anisotropy greater than 1.5, and measurements within 10° of the magnetic equator. Figure 30 shows the same type of plot for 770 eV electrons meeting the same criteria. Figure 31 presents this 770 eV data as a surface plot. It is readily apparent that the electron distribution is vastly different from that of the ions. There is no obvious L versus local time trend for the electron probability distribution, similar to the results found by Braccio, who also found the electron probability distribution to be conical in shape with the region of highest probability being between 1000 and 1100 local time and for L values around 6.5 - 7.0, as shown in the probability and surface plots, Figures 32 and 33, taken from Braccio (1991). Here, the criteria is flux greater than 5×10^6 electrons/(cm² s sr), anisotropy greater than 1.5, and measurements within 10° of the magnetic equator.

The cone is not completely symmetrical. The probability of occurrence increases to its peak value more gradually, as a function of local time, than it decreases. This characteristic does not seem to alter even when changing the selection criteria or energy channels and is the same as that found by Braccio. The statistical analysis of the

AMPTe SURVEY
ELECTRONS AT 340 eV
Anisotropy gt 1.5 Flux gt 5.00E+06 MagLat lt 10.0

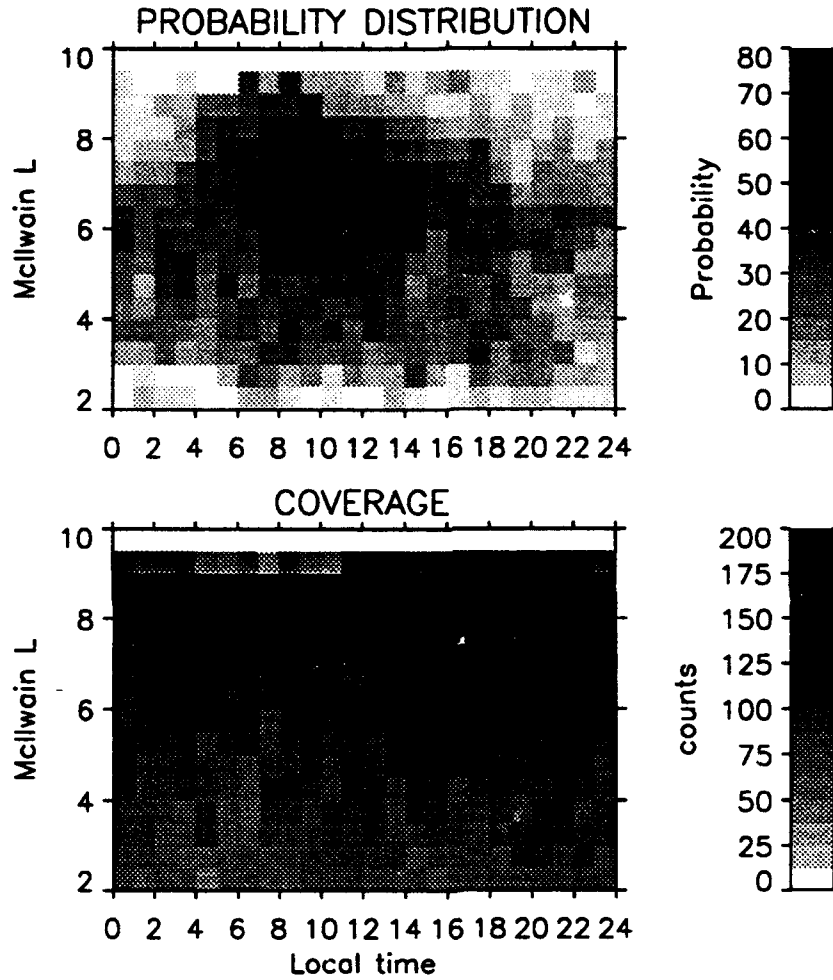


Figure 29. Trapped Electrons (340 eV) - Flux gt 5×10^6 ,
Anisotropy gt 1.5, Maglat gt 10°

AMPTe SURVEY ELECTRONS AT 770eV

Anisotropy gt 1.5 Flux gt 5.00E+06 MagLat lt 10.0

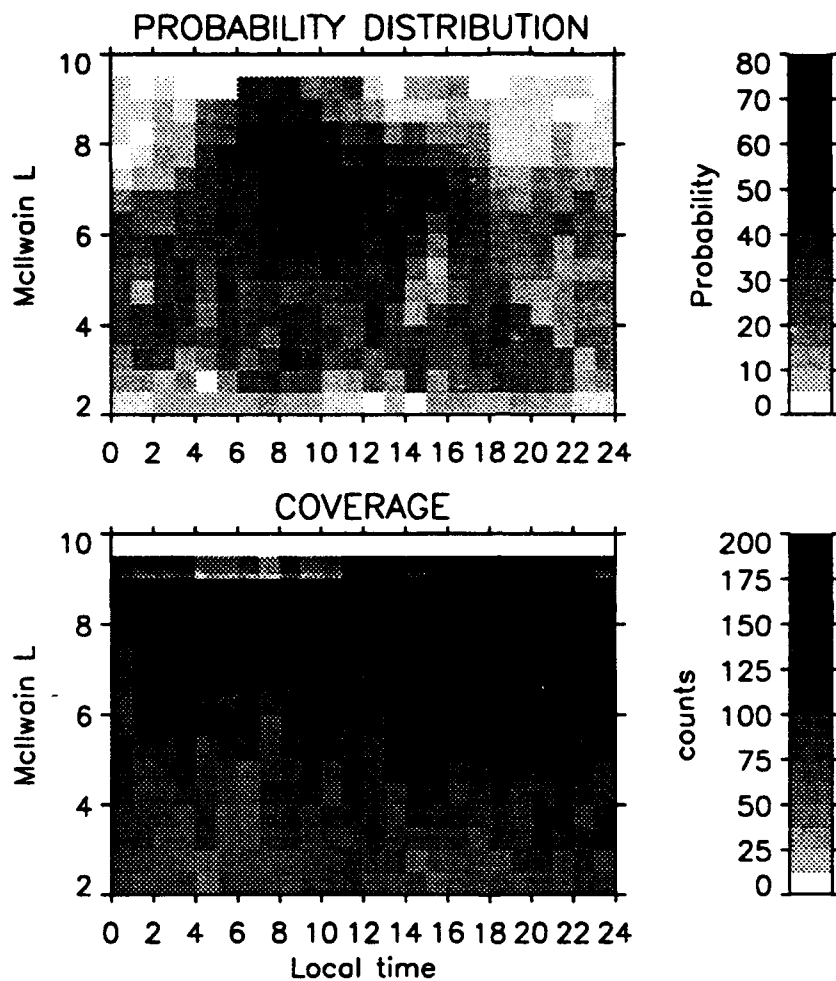


Figure 30. Trapped Electrons (770 eV) - Flux gt 5×10^6 ,
Anisotropy gt 1.5, Maglat gt 10°

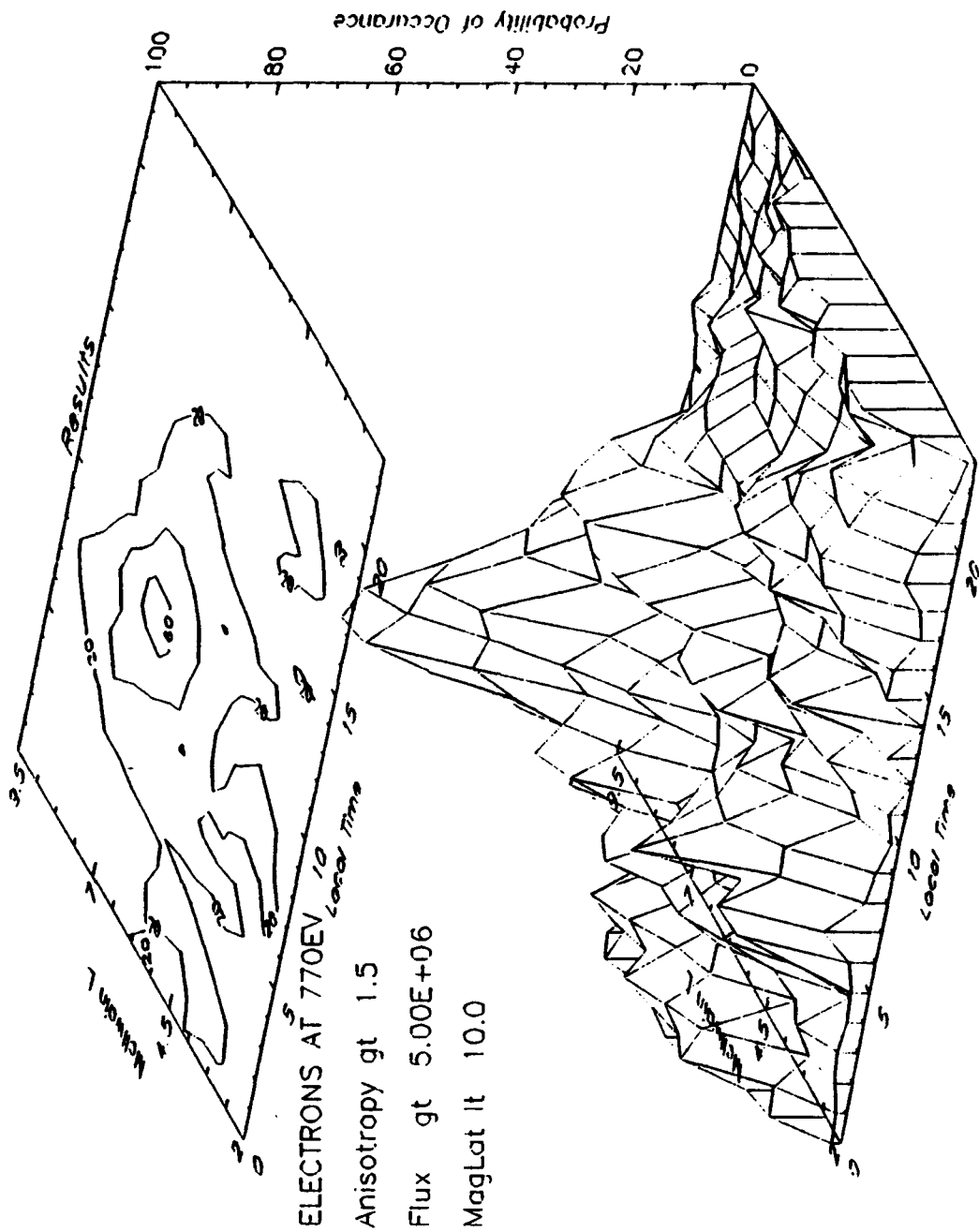


Figure 31. Trapped Electrons (770 eV) - Flux gt 5×10^6 ,
 Anisotropy gt 1.5, Maglat gt 10° - Surface Plot

AMPTE SURVEY

Electrons:

Anisotropy gt 1.5 Flux gt 5.00E+06 MagLat lt 10.0

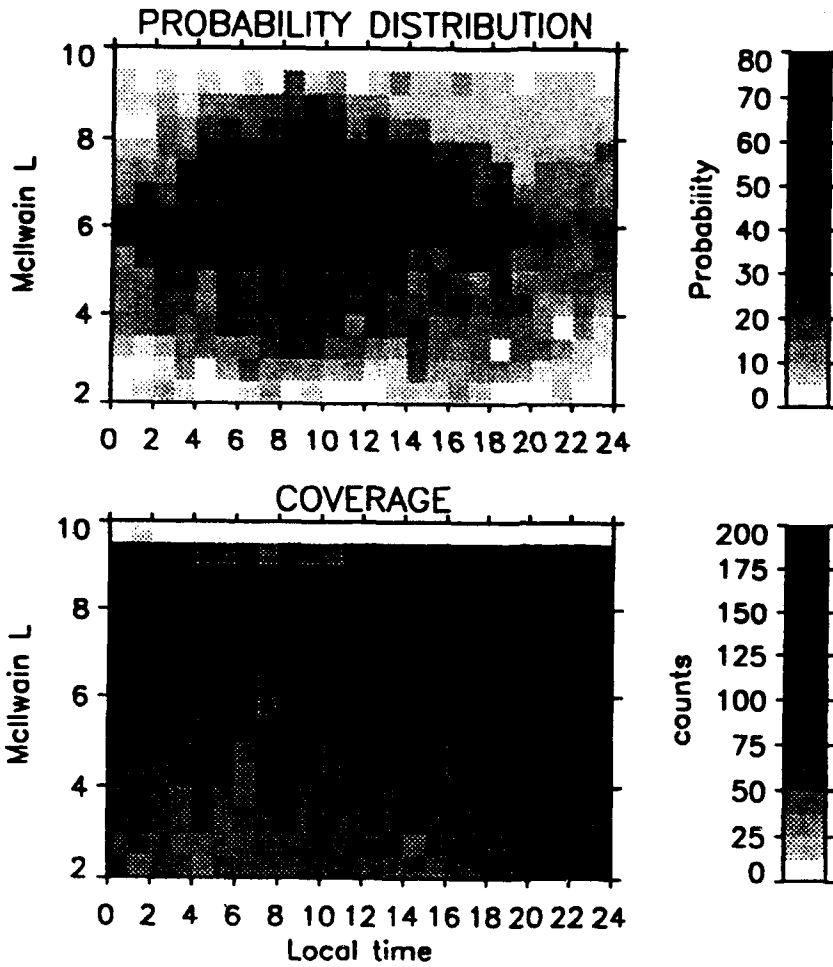


Figure 32. Trapped Electrons (150 eV) - Flux gt 5×10^6 , Anisotropy gt 1.5, Maglat gt 10°

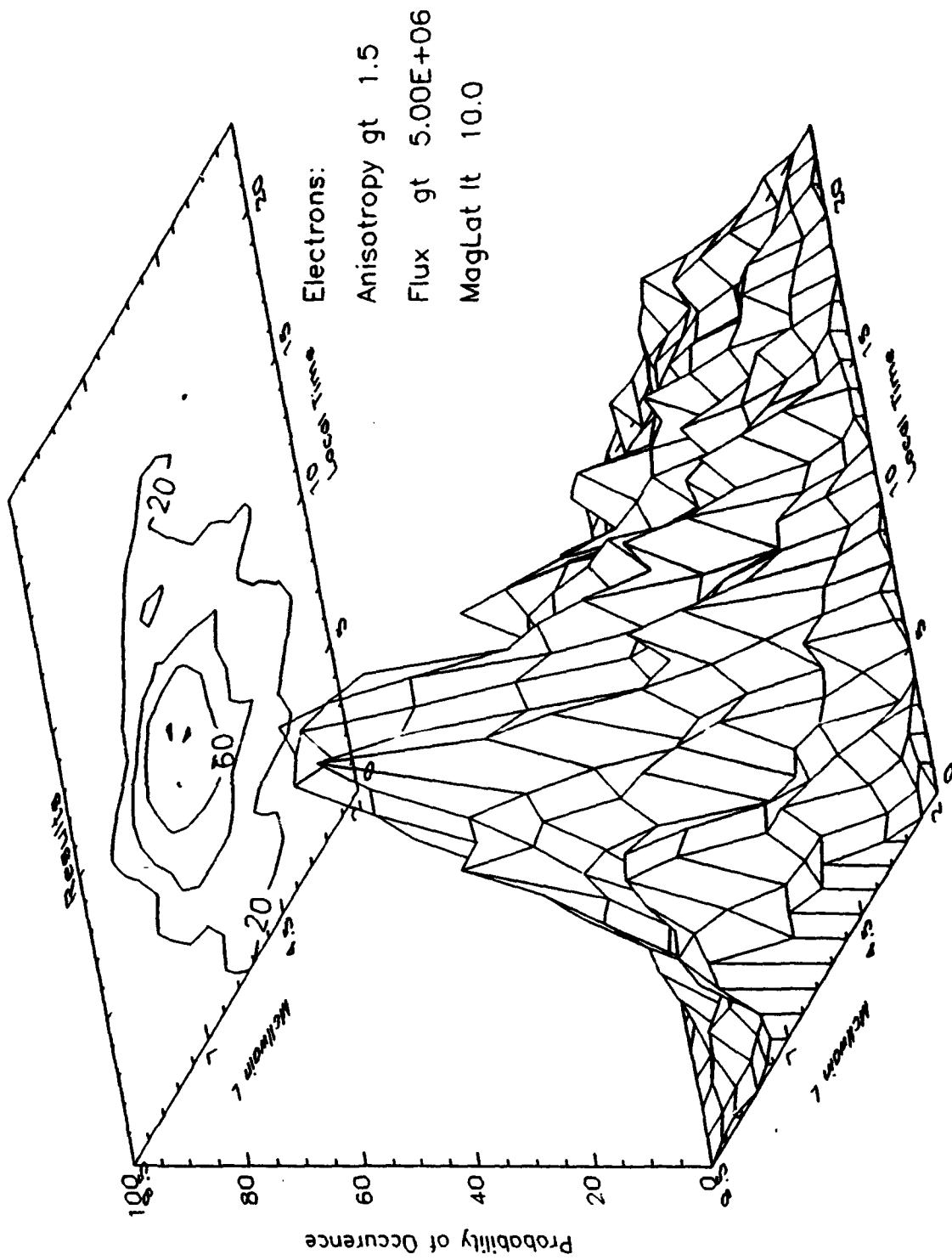


Figure 33. Trapped Electrons (150 eV) - Flux gt 5×10^6 , Anisotropy gt 1.5, Maglat gt 10° - Surface Plot

coarsely gridded survey files is now extended using more detailed looks at the raw data files.

B. DETAILED ANALYSIS CASE STUDIES

1. Data Analysis

Detailed analysis of the electron data was conducted, using data at 150 eV and 340 eV. Ion data were not readily available. Data were collected for the days in TABLE III. Only days 84/336 and 85/002 will be presented in the thesis. The days listed in TABLE III were selected from the set of days where "large" electron events occurred, as found in Braccio

Table III. DETAILED ANALYSIS DATA COLLECTION DAYS

Day	Local Time Range	ΣK_p	D_{st}
84/266	0941-1634	26	-21
84/283	0510-1538	26	-24
84/296	0755-1420	39	-55
84/315	0655-1349	23	-11
84/336	0533-1249	22	-24
85/002	0359-1418	24	-3.2
85/039	0129-0834	28	-24
85/227	1440-1938	20	-21
85/238	1330-2330	22	-10
85/264	2002-2156	29	-19
85/301	1618-2049	7	-17
85/320	1116-1837	19	-18
85/337	1021-1742	17	-31

(1991) and extended here, to obtain reasonably complete local time coverage. Special emphasis was given to the morning sector (0600 to 1200 local time). Each segment of data considered covered the period between plasmopause encounters, roughly 15 hours of data per day. Also, listed with the days and times in TABLE III are the magnetic activity indices, ΣK_p and D_{st} , for the respective time period.

Data were initially considered in one hour increments. For each hour and each of the energy channels surveyed, 150 and 340 eV, a pitch angle vs UT time spectrogram was generated. Figure 34 is a compilation of the one hour pitch angle vs time spectrograms in reduced form for 150 eV electrons on day 84/336. The 150 eV spectrograms for the additional days surveyed can be found in the Appendix. The grey scale for the spectrogram runs from 7.2 to 9.0 on a log scale of the flux. Pitch angle runs from $0^\circ - 180^\circ$ and UT from 0000 to 1400. Also, plotted on the x-axis is the corresponding local time (LT), McIlwain L value and magnetic latitude. Note the high flux at 90 degrees from 1000 to 1400 UT. Note how the equatorially trapped distribution fades as the satellite approaches perigee (the plasmopause at $L \sim 3.9$.) This characteristic can be seen in a number of the survey spectrograms as shown in Appendix. The data were analyzed by considering the log of distribution function as a function of $\cos^2 \alpha$, Figure 35. This functional form should produce straight line segments, if the data are well represented as a

AMPTE 84336 150 eV Electrons

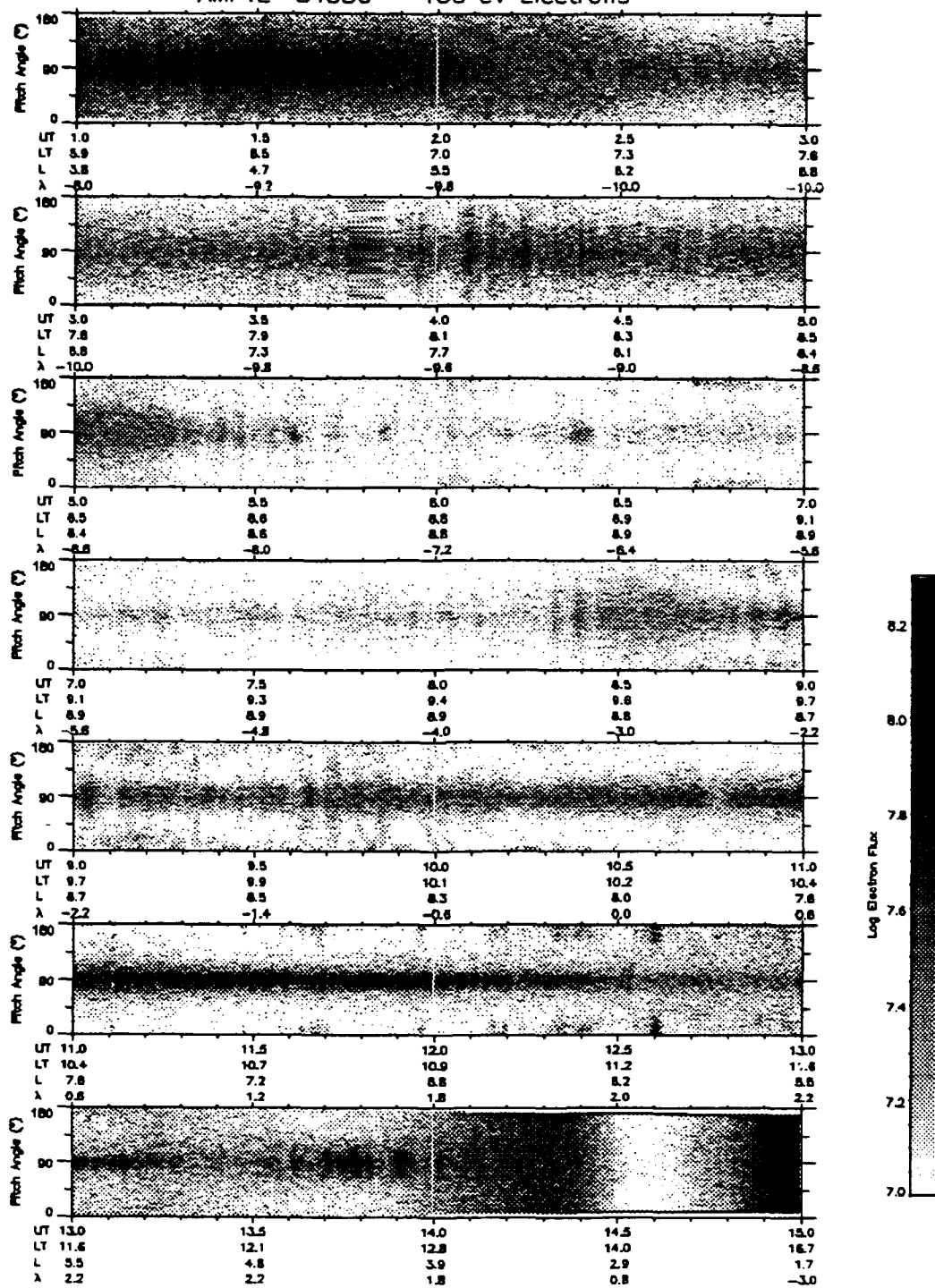


Figure 34. Pitch Angle versus Time Spectrogram - Day 84/336, Energy 150 eV

AMPTE Survey - 84/336

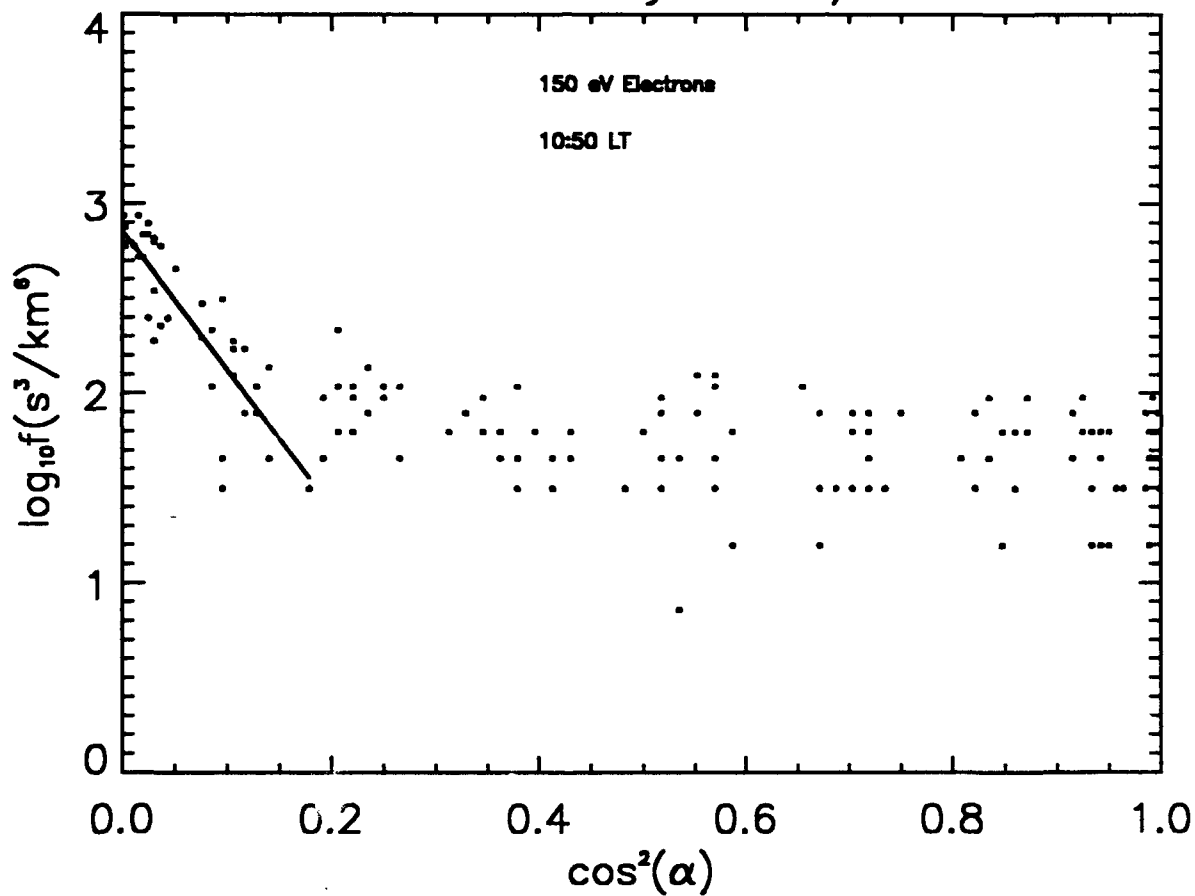


Figure 35. Electron Pitch Angle Distribution

bi-Maxwellian (Scott, 1991.) From these segments values for T_{perp} and T_{parl} can be estimated, and various flux ratios obtained. Much of this work is based on consideration of how the data ($\log f$) vary with pitch angle ($\cos^2\alpha$).

From this figure a distinct break in the vicinity of 60 degrees can be seen. At lower pitch angles the isotropic background dominates the pitch angle distribution. Because of this effect the data analysis range was limited to between 60° and 90°, a restriction that more accurately considers the phenomenon of interest. This restriction, however, has the effect of limiting the data set which can be analyzed. These equatorial pitch angles (60° to 90°) do not map far from the equator. A restriction of $\pm 6^\circ$ magnetic latitude was chosen, which allows a suitable range of (equatorial) pitch angles, and allows a reasonable range of events.

Fluxes were obtained in three ways:

1. Average Flux (60° - 70°): the flux in the 60° to 70° pitch angle bin at the location of the satellite.
2. Average Flux (80° - 90°): the flux in the 80° to 90° pitch angle bin at the location of the satellite.
3. Fitted Flux (60° - 90°): the fitted flux was derived by taking a least squares fit of the data at pitch angles between 60° and 90° on a plot of the log of the distribution function versus $\cos^2\alpha$. This fit was used to project the values which would have been obtained at the magnetic equator, effectively assuming a bi-Maxwellian form.

Two different anisotropies were calculated and are defined as follows:

1. Average Anisotropy: the ratio of the average fluxes in the 80° to 90° pitch angle bin to those in the 60° to 70° pitch angle bin.
2. Equator Anisotropy: the fluxes at the latitude of measurement mapped to the equator and a ratio taken for the flux at 90° versus the flux at 69°.

Two temperatures were calculated for each energy channel:

1. T_{perp} : the characteristic temperature in the perpendicular direction, with respect to the magnetic field line, of a bi-Maxwellian distribution. Calculated from the difference in the log of the distribution functions for 150 eV and 340 eV at a pitch angle of 0°. The calculated value is the same for both energy channels.
2. T_{parl} : the characteristic temperature in the parallel direction, with respect to the magnetic field line, of a bi-Maxwellian distribution. This is based on the calculated T_{perp} and the slope of the pitch angle distribution at the respective energy. The calculated value is different for each energy channel, reflecting the non-Maxwellian element of the energy distribution.

Both temperatures and the density were calculated from a bi-Maxwellian form for the distribution function. This produces valid and well behaved results if the distribution can be characterized as a bi-Maxwellian. If it is not well described as a bi-Maxwellian the results will be invalid and not well behaved.

The ratio of T_{perp} to T_{parl} was also calculated for the data. This ratio was used to further characterize a trapped distribution. For the purposes of this paper the ratio had to

exceed three for a distribution to be characterized as equatorially trapped. This corresponds to a density decrease factor of 20% at 10° magnetic latitude in the absence of parallel electric fields. (Scott, 1991)

2. Day 84/336 Case Study Trapped Distributions

a. 150 eV

Figure 36 shows the plots of the previously defined fluxes vs UT time at 150 eV. The solid horizontal line plotted with the fluxes in the bottom two plots is for the flux value of $5 \times 10^6 \text{ (cm}^2 \text{ s sr)}^{-1}$, the minimum threshold established in the last chapter. Also, plotted on the x-axis are the local time, McIlwain L and the magnetic latitude.

Figure 37 shows the plots of the previously defined anisotropies versus time at 150 eV. The solid horizontal line plotted on each is the anisotropy threshold of 2.0, defined in the previous chapter as the minimum anisotropy allowed to characterize a trapped distribution. Note the periods that the anisotropies exceed the threshold correspond to the periods of increased flux. Also, shown in Figure 37 is the plots of T_{perp} vs time, T_{parl} vs time, and the ratio T_{perp} to T_{parl} vs time. The solid horizontal line plotted on the plots for temperature ratios vs time is the ratio threshold level of three defined in the last chapter. At the time the temperature ratio exceeds three perpendicular temperature is on average 70 eV while the parallel temperature drops from values of 20 eV to 10 eV. The peak of the ratio has a value of 6.0. For this day a

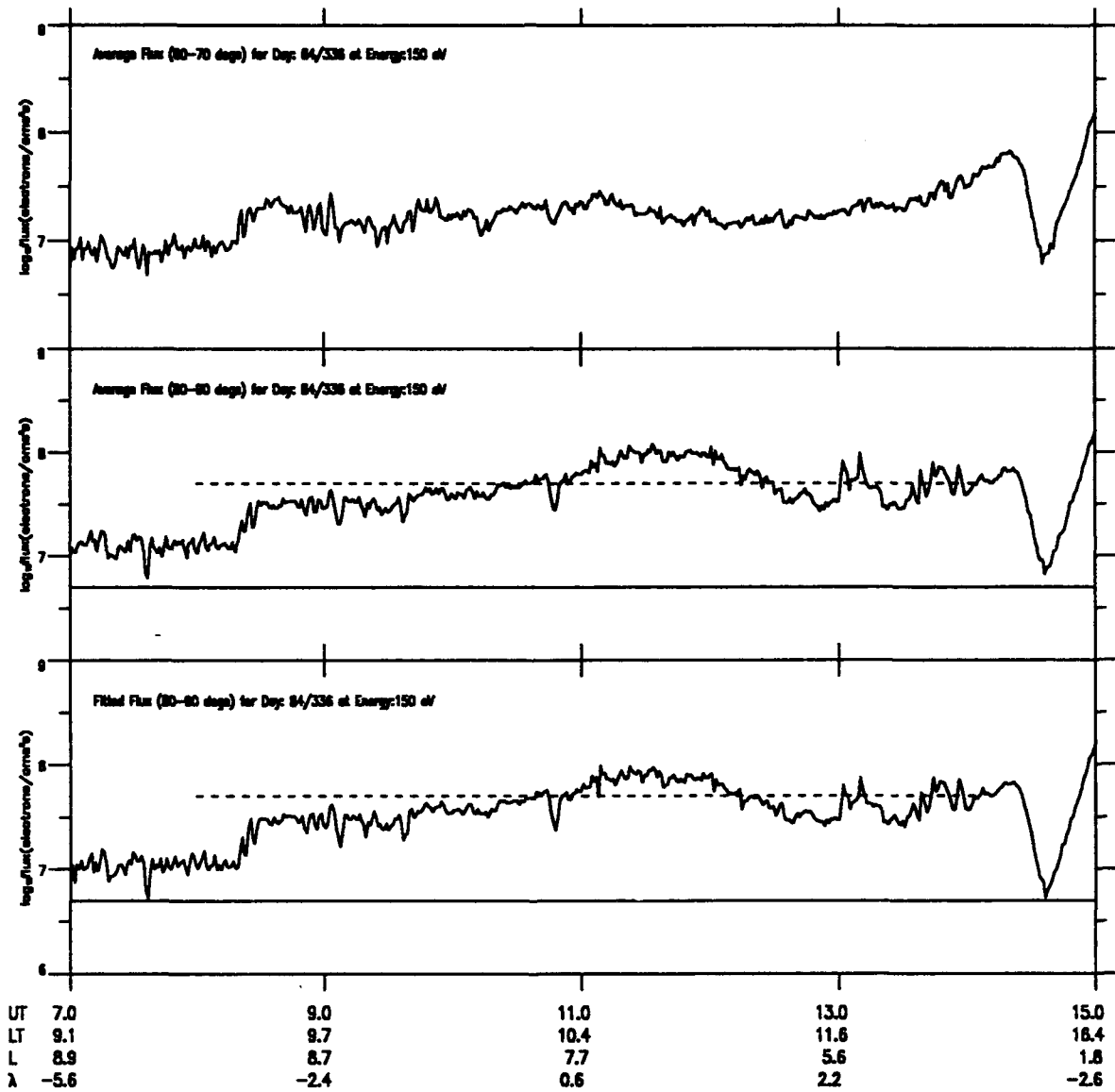


Figure 36. Fluxes versus Time - Day 84/336, Energy 150 eV

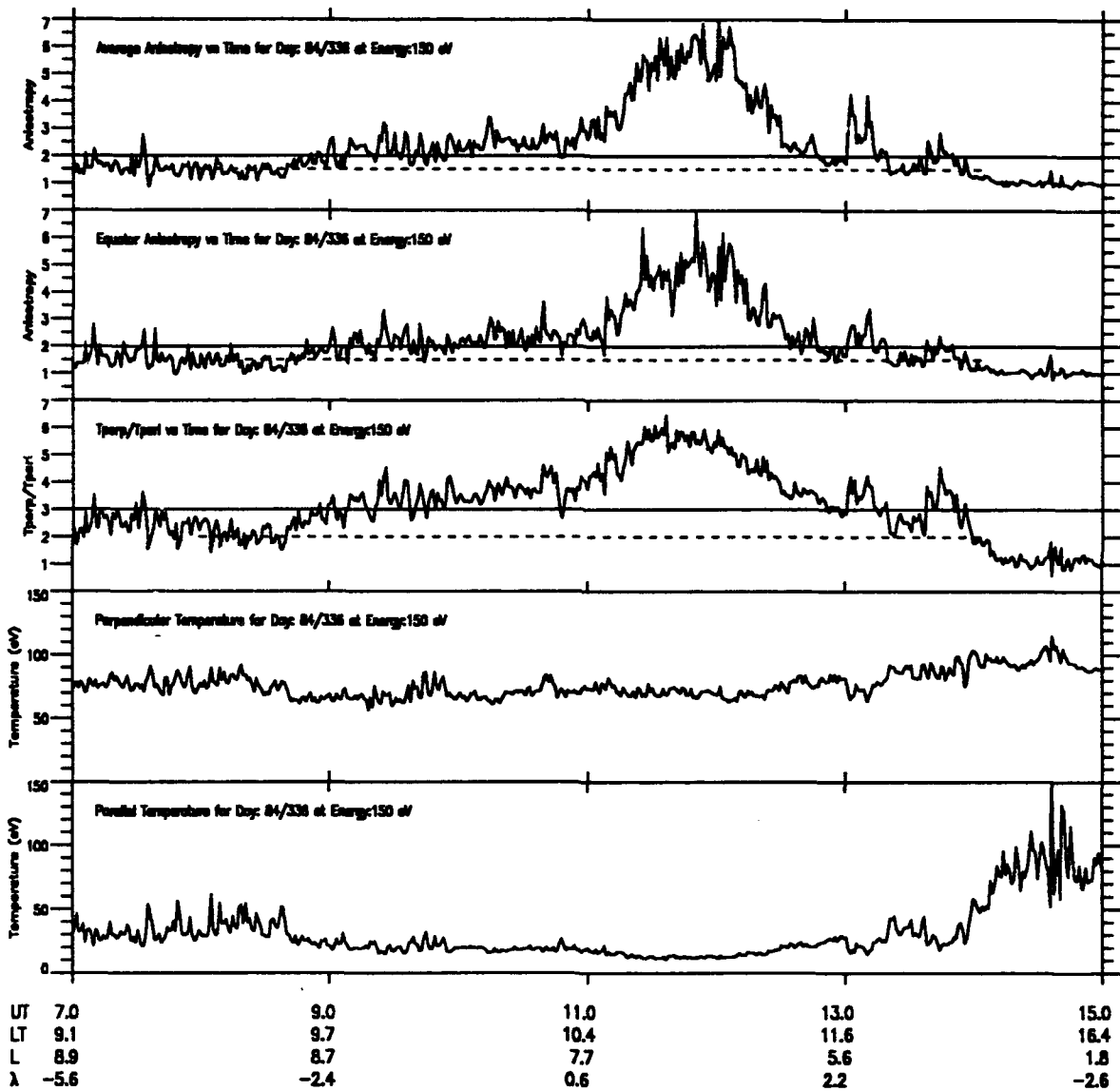


Figure 37. Anisotropies, Temperature Ratio and Temperatures versus Time - Day 84/336, Energy 150 eV

equatorially trapped electron distribution appears to occur for a McIlwain L value of about 6 to 7.5. Note that the lower anisotropy, 1.5 (the dashed line in Figure 37), used in the statistical survey would give a wider L extent, from L = 3 to 9. With this lower anisotropy and the corresponding L range as a boundary, for where equatorially trapped electron distributions exist, a flux value of 5×10^7 and a temperature ratio of two can be interpreted as new criterion thresholds for equatorially trapped electrons, as seen by the dashed lines in the flux and temperature ratio plots of Figures 36 and 37.

Figure 38 shows the plot of the average anisotropy versus the equator anisotropy and the plot of temperature ratio versus equator anisotropy. The average anisotropy is slightly higher than the fitted equatorial anisotropy as can be seen when compared to a line of slope one (the line on the plot.) In the plot of temperature ratio vs equator anisotropy the data starts to exceed the ratio criterion threshold of three at an equator anisotropy of about 2.0, if the high end of the data points is taken. This tends to support our definition for an equatorially trapped electron distribution using flux ratios, and shows that a bi-Maxwellian description gives comparable results.

Using the criteria for equatorially trapped electron distributions defined in the previous chapter of a minimum flux for 150 eV electrons of 5×10^6 ($\text{cm}^2 \text{ s sr}^{-1}$), an

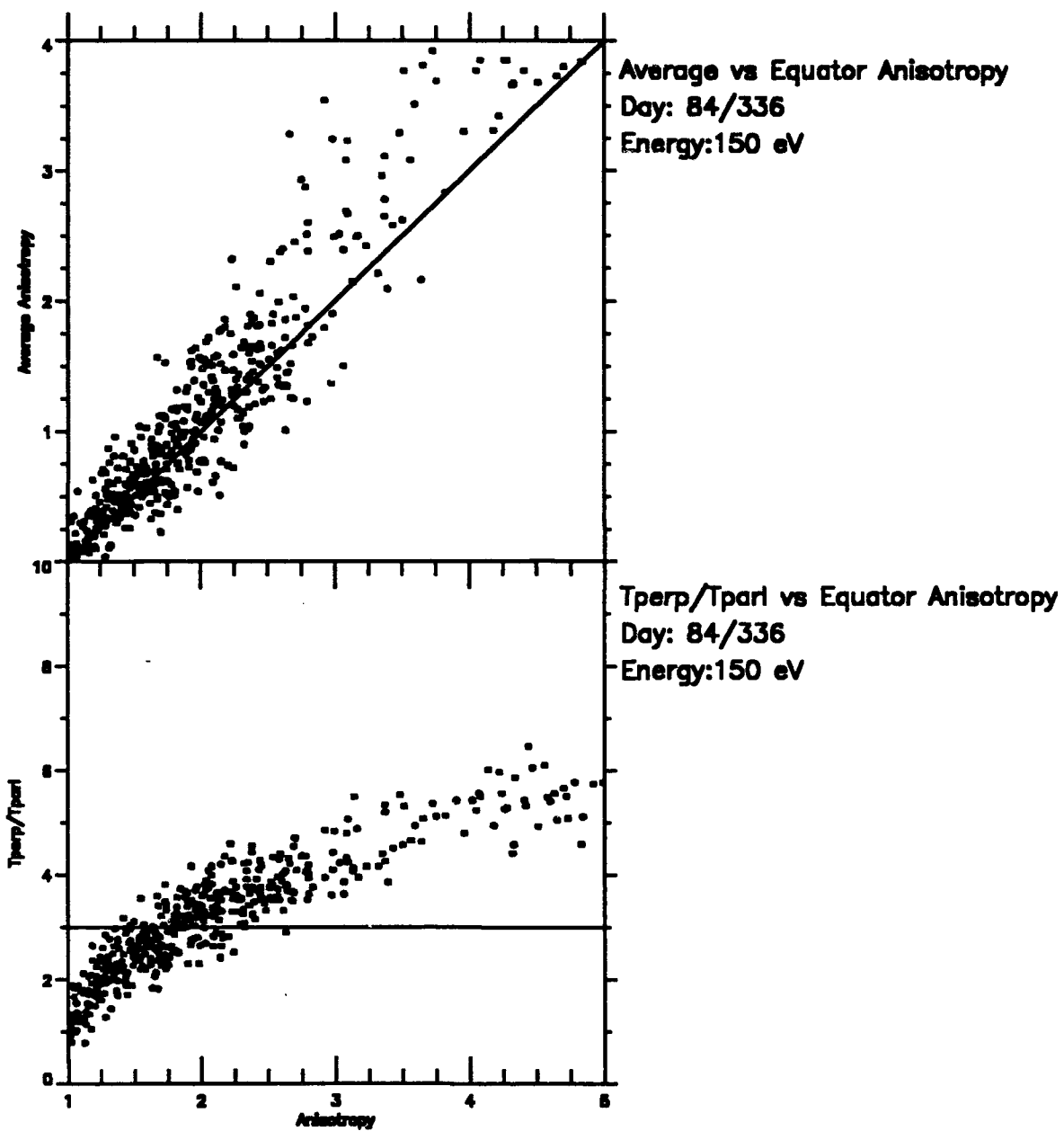


Figure 38. Average Anisotropy and Temperature Ratio verses Equator Anisotropy - Day 84/336, Energy 150 eV

average anisotropy of 2.0, a measurement within 10° of the magnetic equator, and the additional criterion for a ratio of T_{perp} vs T_{parl} to be greater than three an equatorially trapped plasma can be seen to start at around 0942 local time at a L value of 8.7 and at magnetic latitude of -2.4° . As L decrease with time all anisotropies increase to a peak at around 1050 local time and a L value of 6.9 and a temperature ratio of 6.0. All anisotropies decrease with time after that until the trapped distribution ends at around 1147, L of 5.30 and magnetic latitude of 2.4° .

b. 340 eV

Figure 39 shows the plots of the previously defined fluxes vs UT time at 340 eV. The solid horizontal line plotted with the fluxes in the bottom two plots is for the flux value of $5 \times 10^6 \text{ (cm}^2 \text{ s sr)}^{-1}$, the minimum threshold established in the previous chapter. Also, plotted on the x-axis are the local time, McIlwain L and the magnetic latitude.

Figure 40 shows the plots of the previously defined anisotropies versus time at 340 eV. The solid horizontal line plotted on each is the anisotropy threshold of 4.4, defined in the previous chapter as the minimum anisotropy allowed to characterize a trapped distribution. Also, shown in Figure 40 is the plots of T_{perp} vs time, T_{parl} vs time, and the ratio T_{perp} to T_{parl} vs time. The solid horizontal line plotted on the plots for temperature ratios vs time is the ratio threshold level of three defined in the last chapter. At the time the

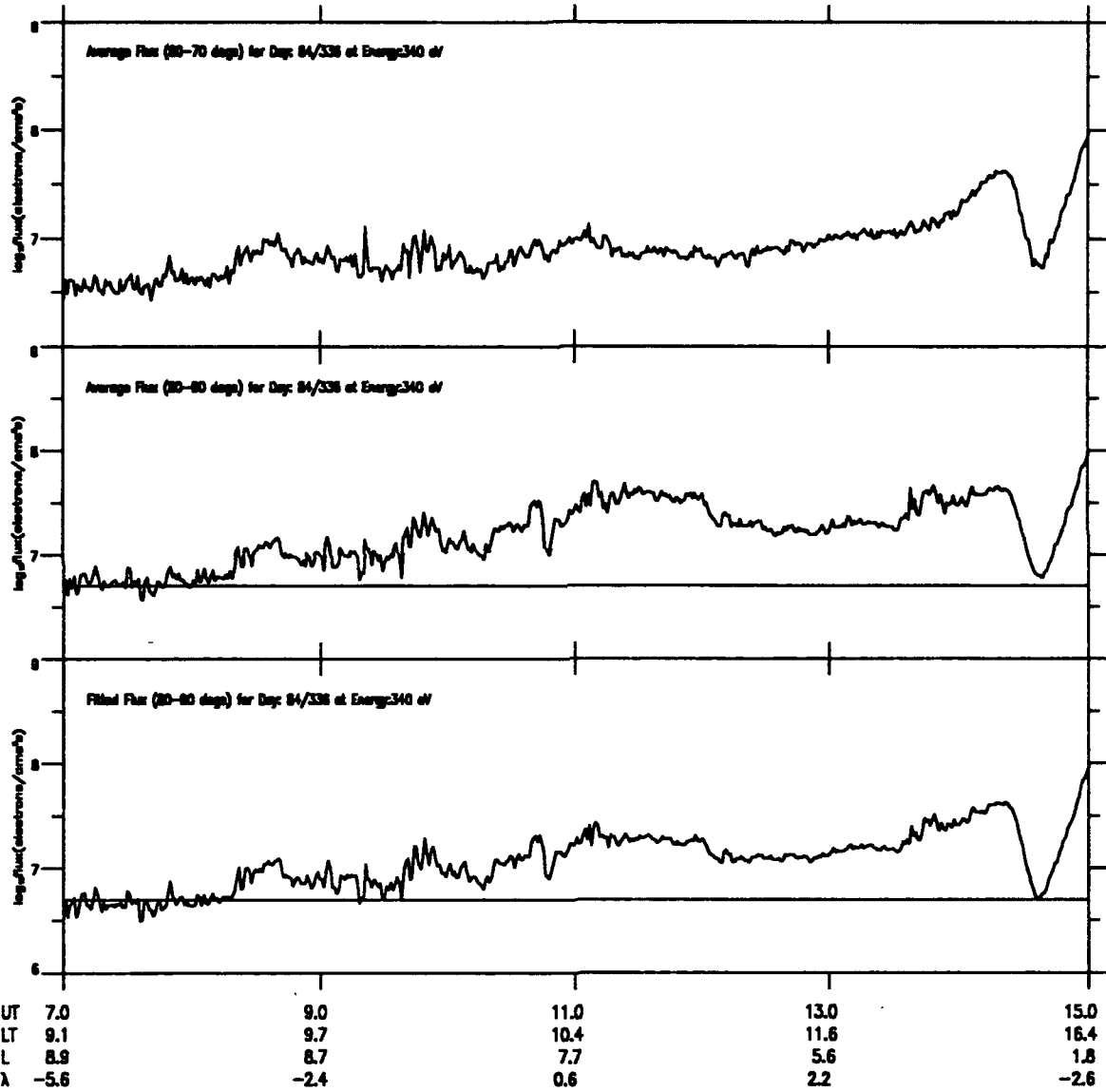


Figure 39. Fluxes versus Time - Day 84/336, Energy 340 eV

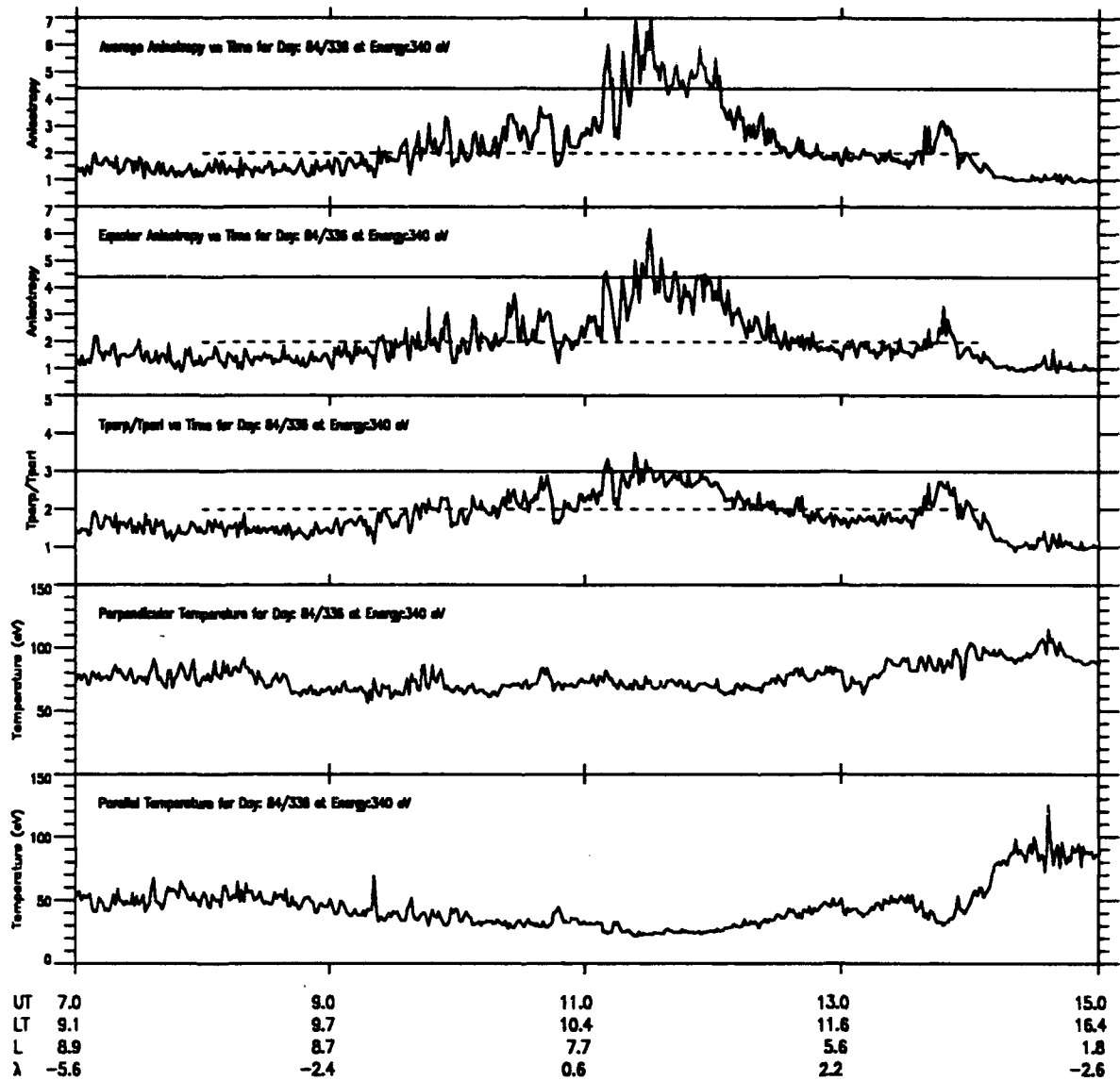


Figure 40. Anisotropies, Temperature Ratio and Temperatures versus Time - Day 84/336, Energy 340 eV

temperature ratio exceeds three perpendicular temperature is on average 70 eV while the parallel temperature drops to values of 23 eV. At this energy a trapped electron distribution appears to occur for a more limited McIlwain L range, at the higher end of the L range defined by the 150 eV data.

Using the criteria for trapped electron distributions defined in the previous chapter of a minimum flux for 340 eV electrons of 5×10^6 (cm² s sr)⁻¹, an average anisotropy of 4.4, a measurement within 10° of the magnetic equator, and the additional criterion for a ratio of T_{perp} vs T_{parl} to be greater than three an equatorially trapped plasma can be seen to start at around 1031 local time at a L value of 7.5 and at a magnetic latitude of 0.8°. The trapped distribution does not extend very far ending at 1041 at L equal to 7.2 and magnetic latitude of 1.2°. A more realistic anisotropy ratio of ~ 2 and a temperature ratio of 2, as shown by the dashed line in both plots of Figure 40 would give a latitude extent more in line with respect to the 150 eV results.

3. Day 85/002 Case Study Trapped Distributions

a. 150 eV

Figure 41 shows the plots of the 150 eV fluxes vs time for 85/002. The solid horizontal line plotted with the fluxes in the bottom two plots is for the flux value of 5×10^6 (cm² s sr)⁻¹. Also, plotted on the x-axis are the local time,

McIlwain L and the magnetic latitude. Comparison with the anisotropy suggests a flux level of 5×10^7 would be a more accurate indicator on this day, as shown by the dashed line in the plot.

Figure 42 shows the plots of the previously defined anisotropies versus time at 150 eV. The solid horizontal line plotted on each is the anisotropy threshold of 2.0, defined in the previous chapter as the minimum anisotropy allowed to characterize an equatorially trapped distribution. Note the periods that the anisotropies exceed the threshold corresponding to the periods of increased flux ($> 5 \times 10^7$). Also, shown in Figure 42 are the plots of T_{perp} vs time, T_{parl} vs time, and the ratio T_{perp} to T_{parl} vs time. The solid horizontal line plotted on the plots for temperature ratios vs time is the ratio threshold level of three. At the time the temperature ratio exceeds three perpendicular temperature is on average 80 eV while the parallel temperature drops to values of 20 eV. For this day a trapped electron distribution appears to occur for a McIlwain L value of about 5 to 7. Note the lower anisotropy ratio of 1.5 (the dashed line in Figure 42), used in the statistical survey would give a wider L extent, from $L = 5$ to 8. With this lower anisotropy and the corresponding L range as a boundary, for where equatorially trapped electron distributions exist, a flux value of 5×10^7 and a temperature ratio of two can be interpreted as new criterion thresholds for equatorially trapped electrons,

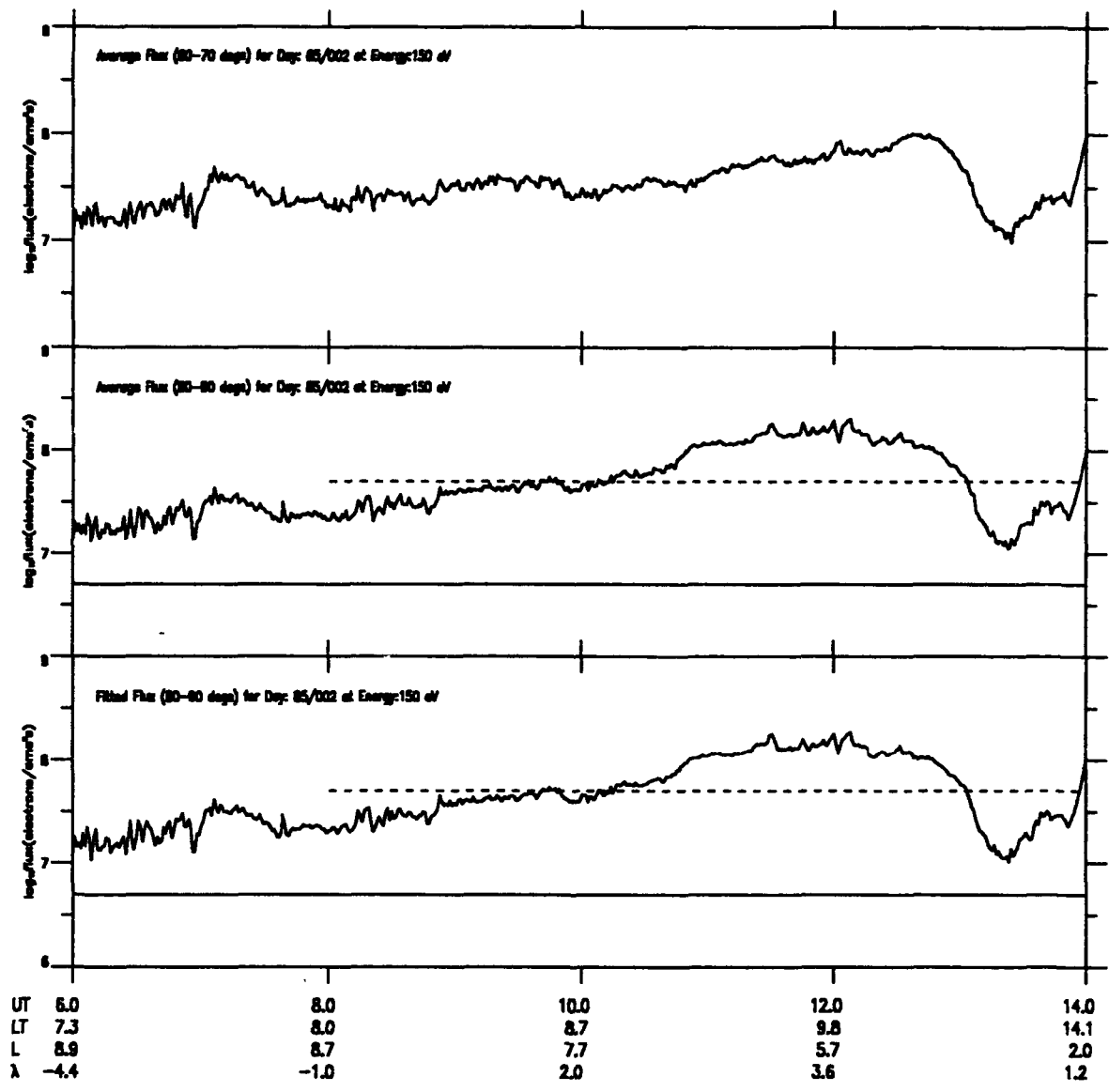


Figure 41. Fluxes verses Time - Day 85/002, Energy 150 eV

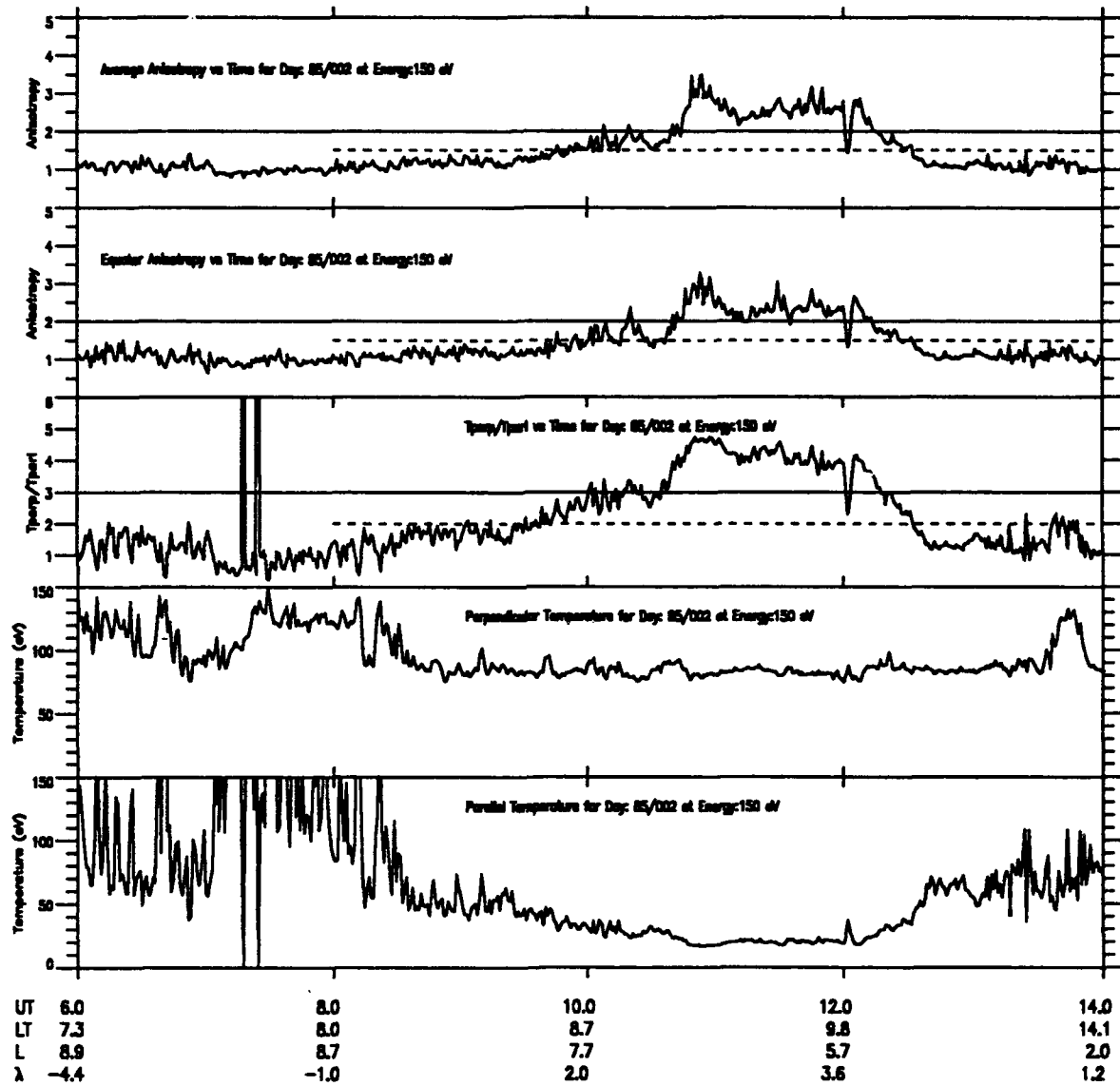


Figure 42. Anisotropies, Temperature Ratio and Temperatures versus Time - Day 85/002, Energy 150 eV

as seen by the dashed lines in the flux and temperature ratio plots of Figures 41 and 42.

Using the criteria for trapped electron distributions defined in the previous chapter of a minimum flux for 150 eV electrons of 5×10^6 ($\text{cm}^2 \text{ s sr}$)⁻¹, an average anisotropy of 2.0, a measurement within 10° of the magnetic equator, and the additional criterion for a ratio of T_{perp} vs T_{parl} to be greater than three a equatorially trapped plasma can be seen to start at around 0900 local time at a L value of 7.2 and at magnetic latitude of 2.6°. As L decreases with time the anisotropies increase to a peak at around 0909 local time and an L value of 6.9. The anisotropies decrease with time after that until the trapped distribution ends at around 1003, L of 5.30 and magnetic latitude of 3.6°.

b. 340 eV

Figure 43 shows the plots of the fluxes vs time at 340 eV. The solid horizontal line plotted with the fluxes in the bottom two plots is for the flux value of 5×10^6 ($\text{cm}^2 \text{ s sr}$)⁻¹. Also, plotted on the x-axis are the local time, McIlwain L and the magnetic latitude.

Figure 44 shows the plots of the anisotropies versus time at 340 eV. The solid horizontal line plotted on each is the anisotropy threshold of 4.4. Also, shown in Figure 44 are the plots of T_{perp} vs time, T_{parl} vs time, and the ratio T_{perp} to T_{parl} vs time. For the short interval where the temperature ratio exceeds three the perpendicular temperature

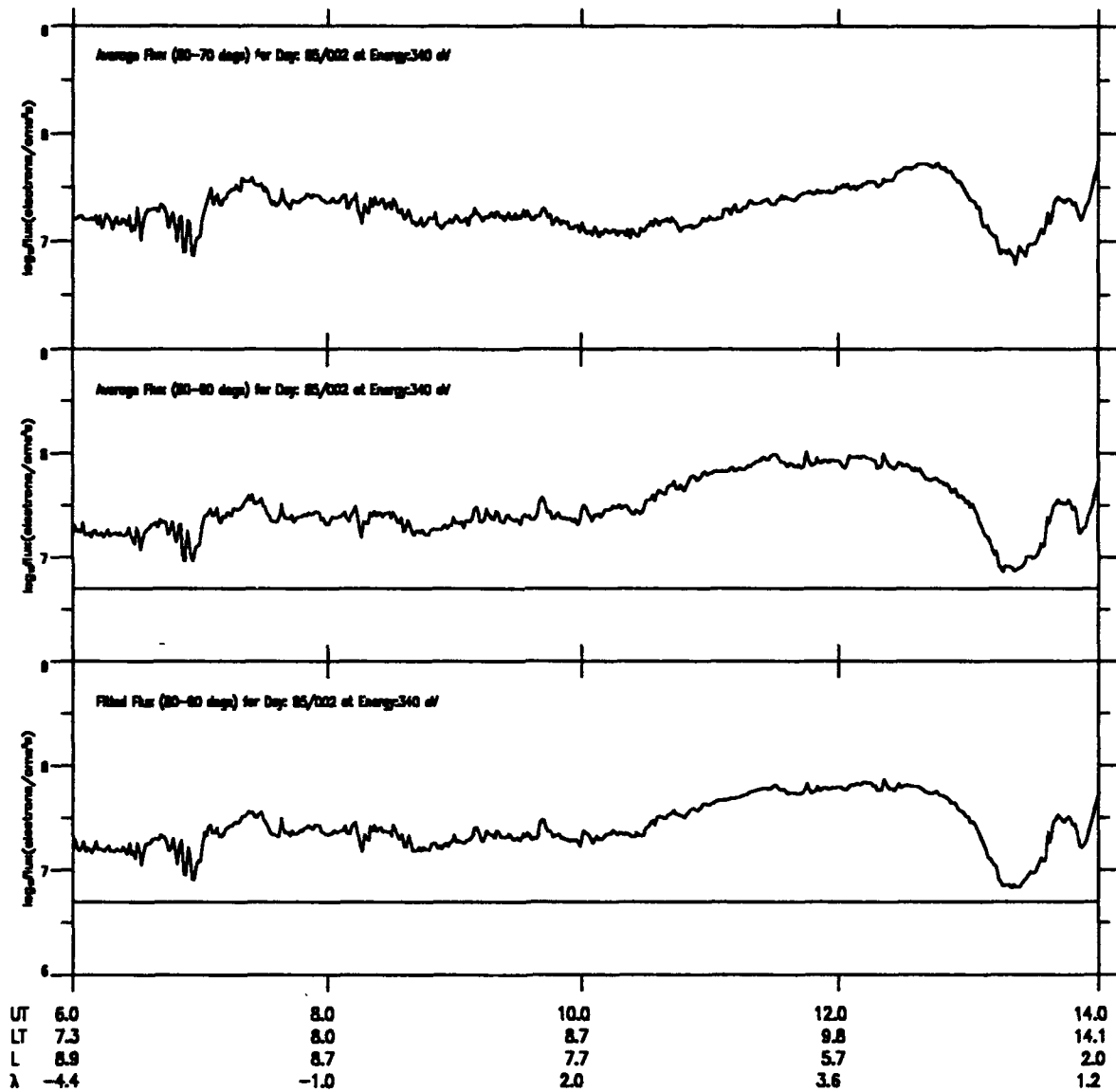


Figure 43. Fluxes verses Time - Day 85/002, Energy 340 eV

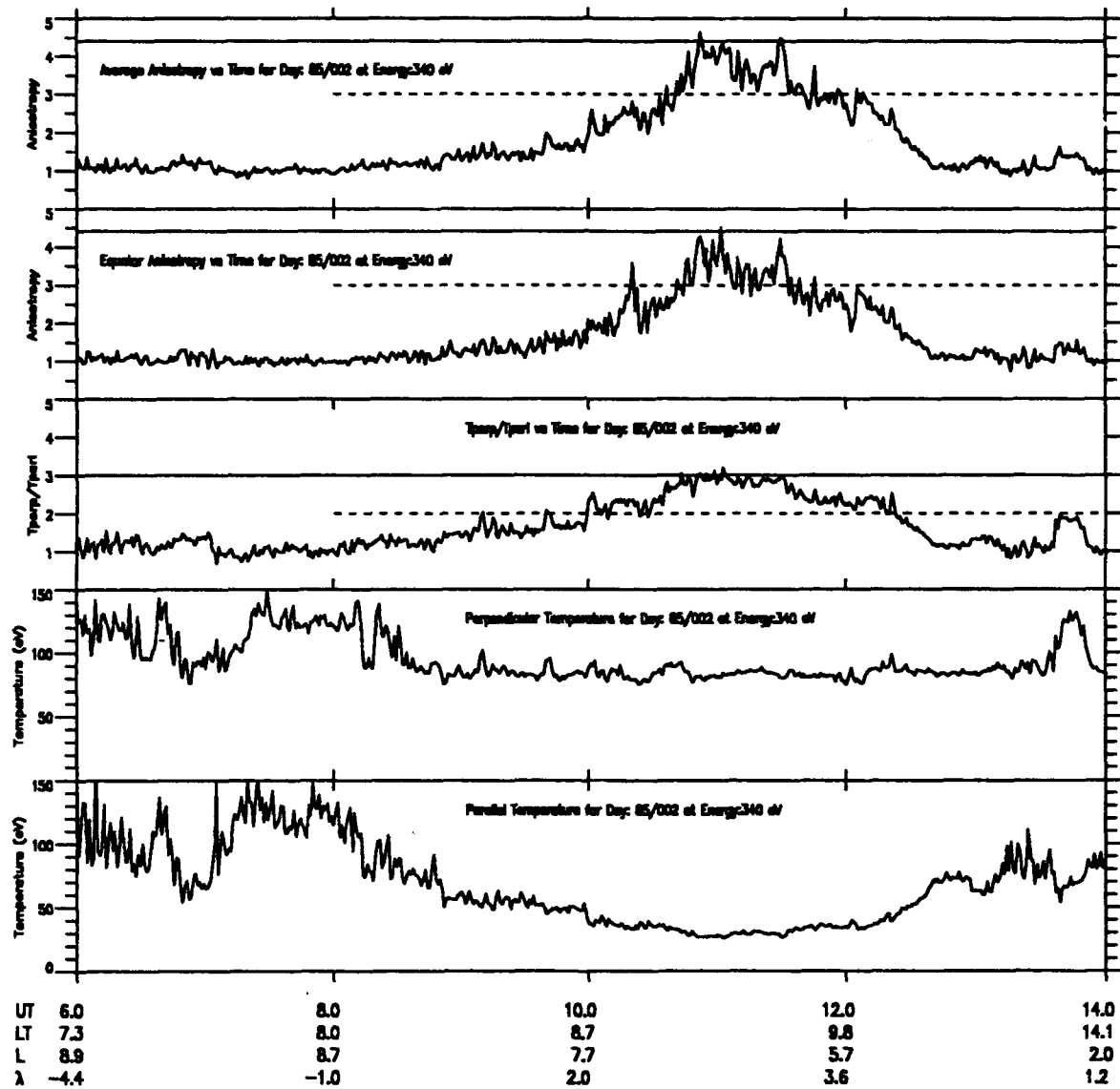


Figure 44. Anisotropies, Temperature Ratio and Temperatures versus Time - Day 85/002, Energy 340 eV

is on average 90 eV while the parallel temperature drops to values of 30 eV. Again, the equatorially trapped distribution is much more limited in its appearance at 340 eV. Indeed the criterion of a ratio of 4.4 is not met. However, if we lower the anisotropy criterion to 3.0 (the dashed line in the anisotropy plots of Figure 44) a trapped distribution would be defined to occur around a McIlwain L value range of 6 to 7.5 at around 0901 local time at a L value of 7.1 and at magnetic latitude of 2.8°. The trapped distribution does not extend very far ending at 0928 at L equal to 6.3 and magnetic latitude of 3.4°. This corresponds to a temperature ratio ~ 2 (the dashed line in the temperature ratio plot of Figure 44)

4. Detailed Analysis Trapped versus Non-Trapped Distributions

In Figure 34 there was evidence of two areas of trapped electron distributions for day 84/336. The first was presented using Figures 36 through 38, which was an equatorially trapped distribution as defined by our criteria. The other area that presents itself in Figure 34 is the time period between 0553 and 0700 local time. The broader distribution seen earlier in the day fail our criteria. Figure 45 and 46 show plots like previously of the fluxes, anisotropy, temperatures and temperature ratios, all verses time for the entire orbit on 84/336 at 150 eV. Though both

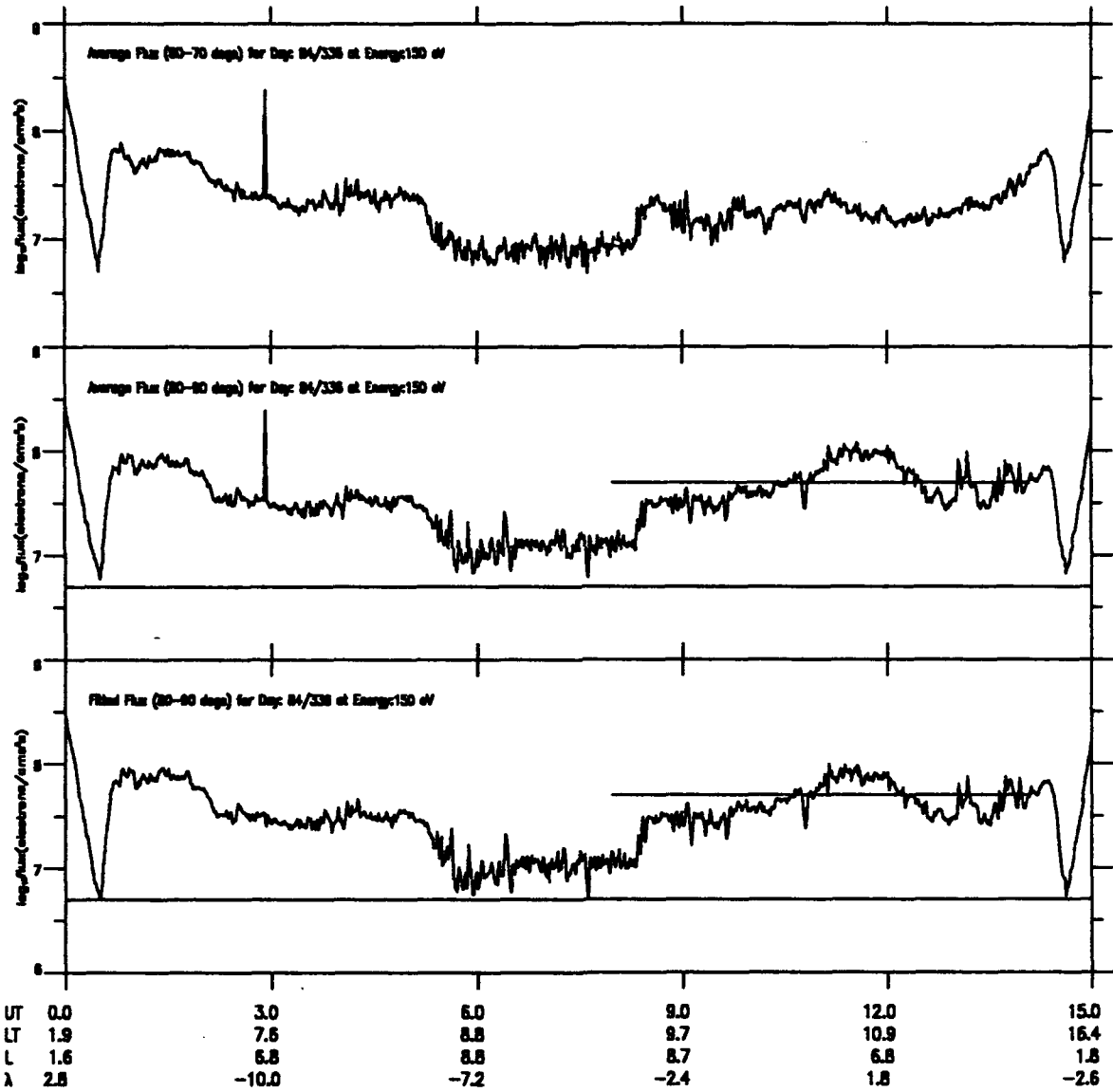


Figure 45. Fluxes versus Time - Day 84/336, Energy 150 eV
(Entire Orbit)

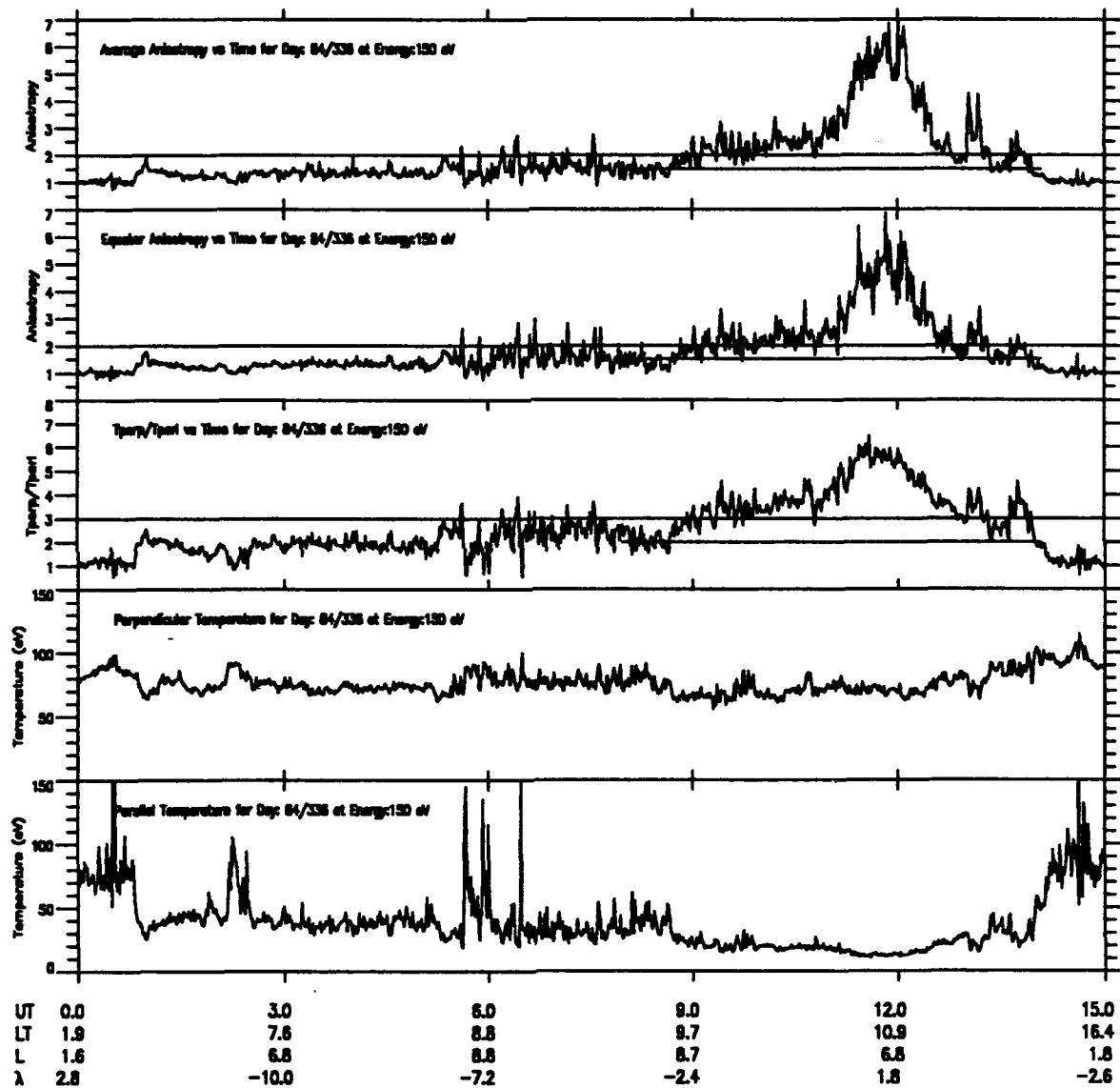


Figure 46. Anisotropies, Temperature Ratio and Temperatures versus Time - Day 84/336, Energy 150 eV (Entire Orbit)

time periods show similar increases in flux the anisotropies for the second time period barely exceeds 1.3 and the temperature ratio never rises above 2.0.

Figure 47 is a plot of the $\log_{10}f$ versus pitch angle for 150 eV electrons from different days and hours in the detailed analysis. The plot is organized from bottom to top to show a progression of non-trapped to trapped electron distributions. Plot a and b show the pitch angle distribution for periods when no trapped electron distribution is present. Plot c and d show the beginnings of trapped electron distributions. Plots e and f show the narrowest equatorially trapped electron distributions observed in the detailed analysis. Note that as the trapped distribution gets stronger the peak at 90° gets progressively more pronounced, indicating that the electrons are equatorially trapped. This characteristic suggests that the data may be fitted with a bi-Maxwellian distribution function as was done. This fit performed well and it was quite evident it did not fit well indicating that the distribution was not trapped. This criteria allows us to distinguish between (simply) trapped distributions (e.g., loss cones), versus equatorially trapped distributions.

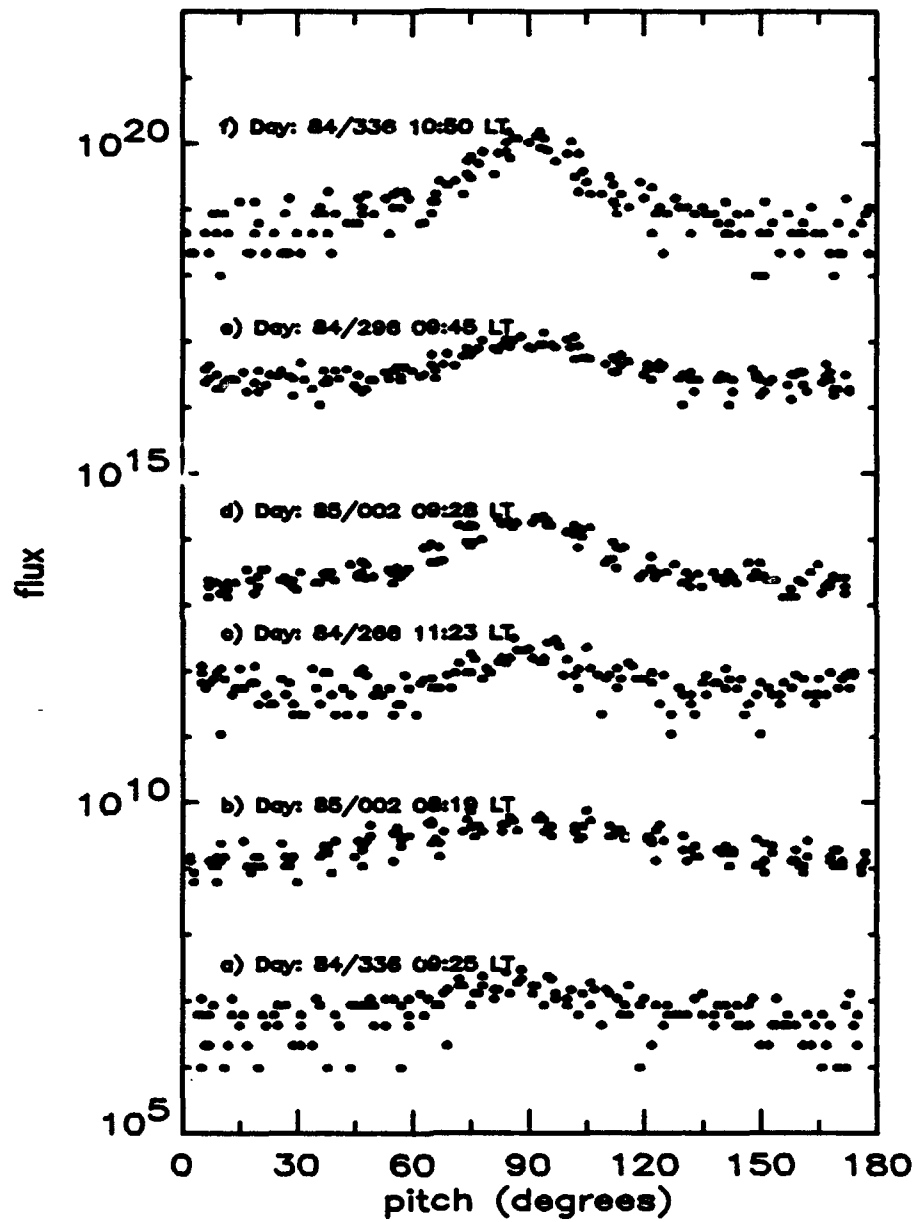


Figure 47. Flux verses Pitch Angle - Various Days

IV. DISCUSSION

A. STATISTICAL SURVEY

The probability distributions for equatorially trapped ions and electrons show clear localization for regions of high occurrence probability ($\geq 50\%$). This is particularly true of electrons. The electron distribution has a very localized peak at 1000 - 1100 local time, $L = 6.0 - 6.5$, and within 5 degrees of the magnetic equator. This is seen regardless of the selection criteria used in the surveys. This agrees with the results found by Braccio. The survey also showed the equatorially trapped electrons were primarily located outside the traditional plasmasphere, and were primarily confined to the dawn to noon sector. The peak in the electron distribution occurred near geosynchronous orbit.

The results for trapped ion distributions, also, agree closely with Braccio's results with the exception of his explanation for the decrease in probability between 1200 - 1400. He suggested that the decrease in probability is due to the average energy of the equatorially trapped ions going above the 150 eV energy he surveyed, in this local time region. Both the 240 eV and 442 eV ions surveyed showed the same decrease in ion probability distribution for this local time region. It maybe possible that Braccio's hypothesis is correct. Sagawa et al (1987) did not show a decrease in

probability for the region from 1200 to 1500 local time. However, Sagawa et al. used summary results from approximately 10 eV to 1 keV, whereas Braccio's survey and this survey covered 50 to 442 eV. To accurately determine if higher energy ions inhabit this region of decreased probability the additional energy channels of 657, 885 and 1127 eV ought to be surveyed. The ion survey reinforces Braccios' and other previous work with ISEE-1 and DE-1, with peak ion flux inside the plasmopause.

B. DETAILED ANALYSIS CASE STUDIES

In the analysis only 13 days were looked at, therefore a statistical analysis isn't appropriate. However, the orbital coverage, Figure 48, of the days analyzed was widespread enough to see patterns or tendencies emerge in the data.

Figure 49 is a plot of where the 150 eV data from the 13 days that met the criteria to be considered a trapped electron distribution occurred; namely a flux greater than 5.0×10^6 (cm² s sr)⁻¹, an anisotropy greater than 2.0, a temperature ratio greater than 3.0 and within 10° of the magnetic equator. The data is plotted in the x-y plane of the AMPTE satellite orbit. The trapped distributions start at dawn at a mean L value of about 3.8 and increase in orbital density and L to a maximum between 0900 and 1100 local time and an average L of 7.0. The distributions then drop off rather rapidly with only smaller occurrences of equatorially trapped distributions in

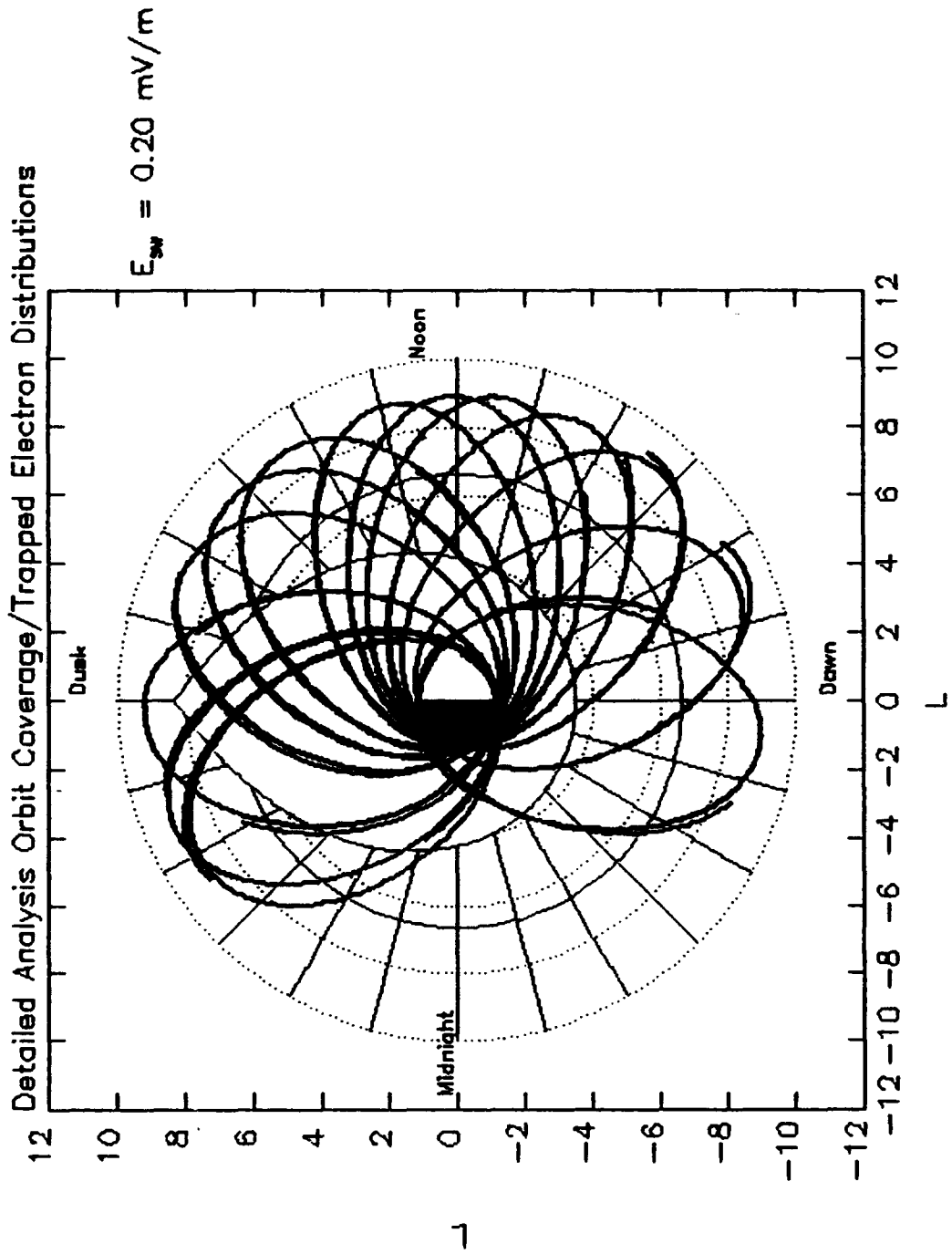


Figure 48. Detailed Analysis Orbital Coverage

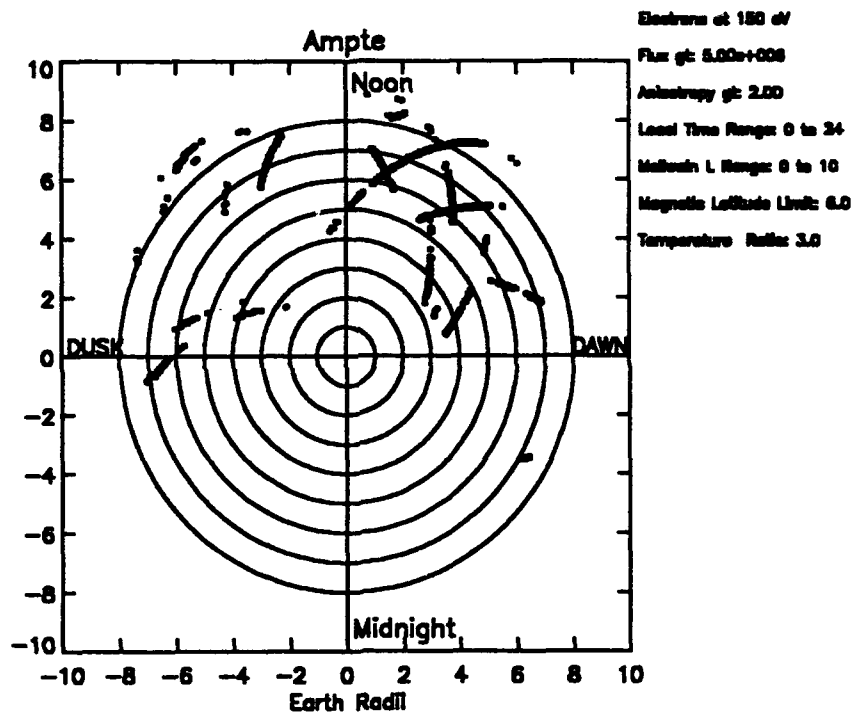


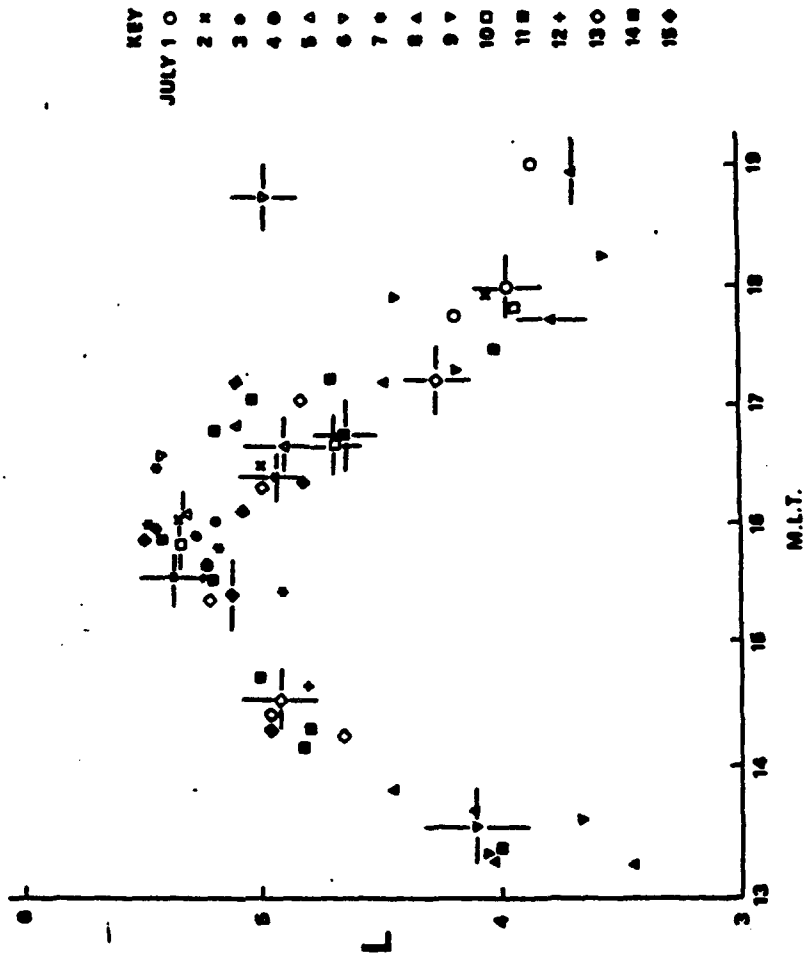
Figure 49. Equatorially Trapped Electron Distributions -
 Energy 150 eV

mid-afternoon at L values in excess of 7.0 and at dusk when the distributions move back into the smaller L values of 5.0 to 6.5.

Braccio (1991) in his statistical survey found a similar general pattern to exist for trapped electron distributions at the 150 eV energy range. He found that the electron distribution had a very localized peak at 0900 local time, $L = 6$, and within 5° of the magnetic equator. The difference in the results can be attributed to his survey considering all days of operation the AMPTE satellite while this thesis only considered a small portion of the operational life.

The tendency for the trapped electron distributions to move out further in L value starting at dawn until late afternoon and then move back in near dusk can be explained in terms of plasmopause location. Figure 50 is taken from Williams *et al.* (1981). It shows the location of the plasmopause as a function of local time. The shape of this plot mimics the behavior of the trapped electron distributions in the case studies. Then as the plasmopause moves out during the day so does the location of the trapped electrons.

Braccio (1991) found that trapped electrons seem to be excluded from regions of high trapped ion probabilities and vice versa. He, also, found that the trapped electron



L-value of plasmopause, on different days in July 1972, derived from Explorer 45 (S₁-A) data and plotted against magnetic local time.

Figure 50. Plasmopause Location

distributions probabilities drop off by local noon at the beginning of the peak of the trapped ion probabilities, which he found to peak between 1400 and 1500 local time at $L = 8$. Horowitz *et al.* (1981) observed that trapped ion distributions tended to occur along the plasmopause boundary in the dawn to dusk region with the majority just inside the boundary. Therefore Braccio postulated that if trapped ions occur at the plasmopause, then as the altitude of the plasmopause rises, in the course of a day, the region where trapped electron distributions usually occur is saturated with trapped ions. This ion saturation seems to, in turn, lead to a disruption in the process by which the trapped electrons are produced. This approach could be used to explain the gap in trapped electron distributions found in the case studies, Figure 49, between 1200 and 1700 local time inside of $L = 7$.

Figure 51 is a plot of the occurrence of 340 eV data in the 13 days that met the criteria to be considered a trapped electron distribution; namely a flux greater than 5.0×10^6 ($\text{cm}^3 \text{ s sr})^{-1}$, an anisotropy greater than 4.4, a temperature ratio greater than 3.0 and within 10° of the magnetic equator. The data is plotted in the x-y plane of the AMPTE satellite orbit. There appears to be no major grouping of trapped electron distributions at this energy level. This is probably the result of the higher anisotropy requirement of 4.4. The trapped distributions are localized to 0900 to 1100 local time at L of 7.0 and at dusk from 1700 to 1800 local time at $L=5.0$.

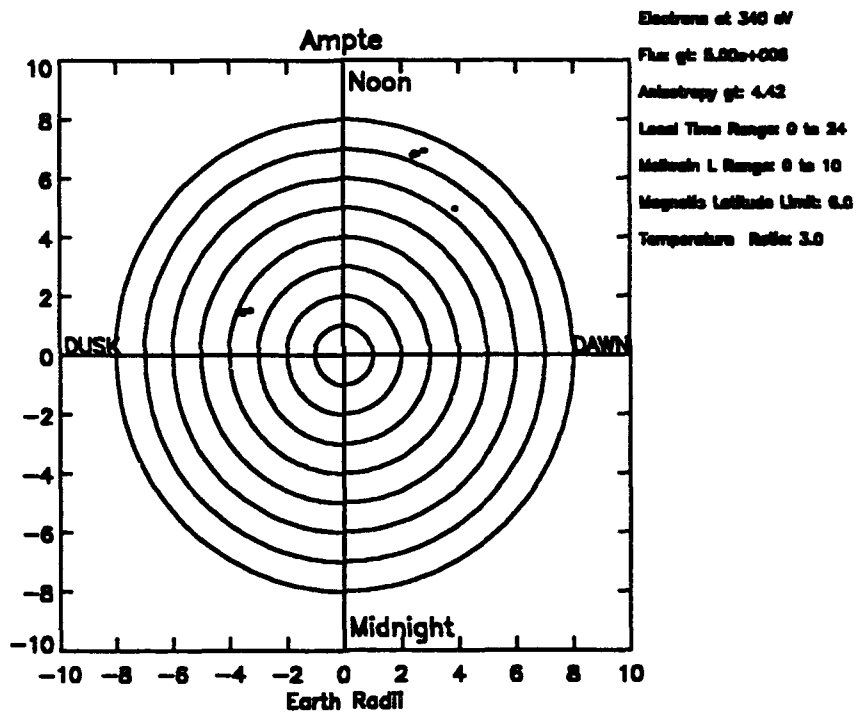


Figure 51. Equatorially Trapped Electron Distributions -
 Energy 340 eV

A comparison of the two different anisotropies used to characterize the data found that they tracked reasonably well with the equator anisotropy being on average 1.075 times the equator anisotropy in the dawn to noon region and only 0.59 times the equator anisotropy in the noon to post dusk region. The difference in anisotropy ratios for the equator anisotropy between the morning and the afternoon local time could be due to a lack of samples taken in the afternoon region that were characterized as trapped.

Over 28,000 samples taken in 13 orbits are summarized in Figure 52, the plot of $T_{\text{perp}}/T_{\text{parl}}$ vs Equator Anisotropy for 150 eV electrons. This figure shows a different technique for defining anisotropy of a equatorially trapped electron distribution and suggests that there is a monotonic relationship between a temperature ratio greater than 3 and an anisotropy of 2.0 for 150 eV and 4.42 for 340 eV. For all days the threshold of 3 for a temperature ratio begins to be exceeded at the anisotropies of about 2.0 for 150 eV and about 4.42 for 340 eV.

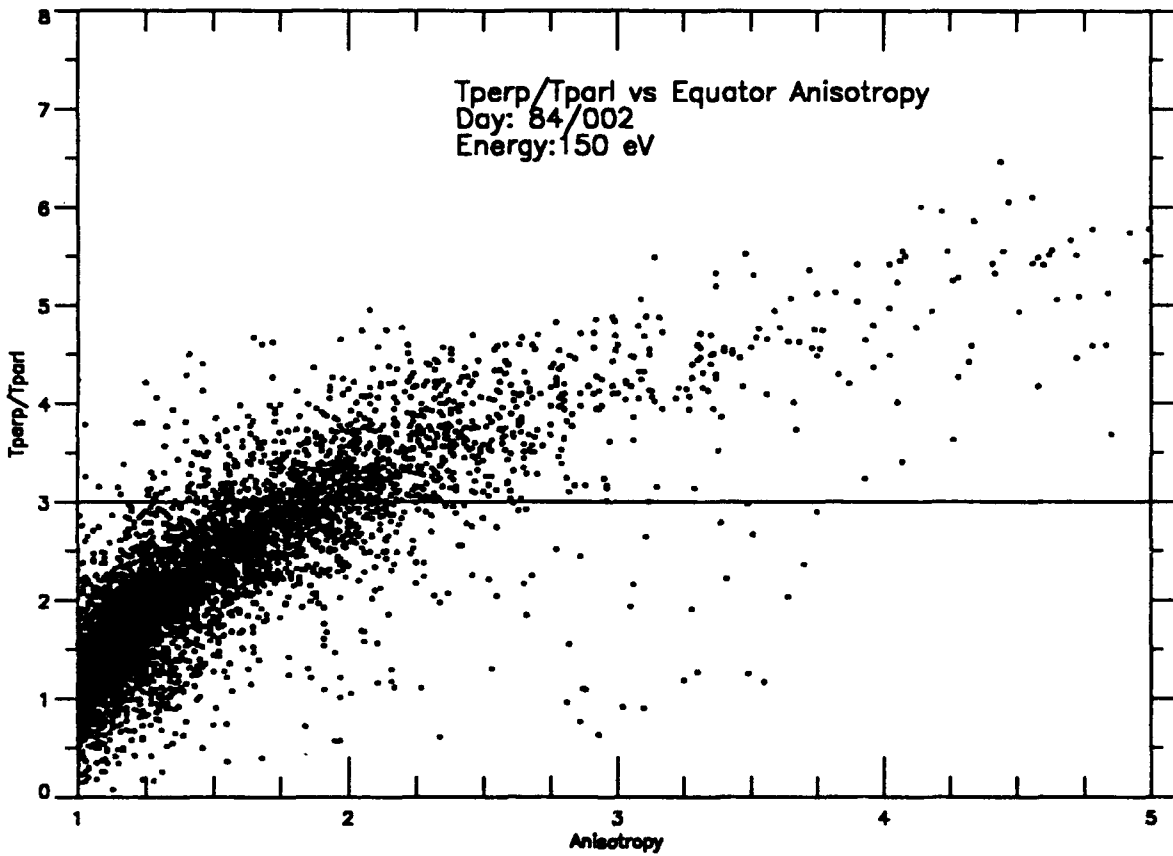


Figure 52. Temperature Ratio verses Equator Anisotropy - All 13 Detailed Analysis Case Study Days, Energy 150 eV

V. CONCLUSIONS

A. STATISTICAL ANALYSIS

The location of the equatorially trapped plasmas are species dependent. The ions and electrons show a different local time dependence in the location of their occurrence probability peak. Electrons show a uniform high probability distribution centered at 0900 local time and an L value of 6. The fact that trapped electrons begin to be seen at local dawn lead to speculation that their existence is dependent on photoelectron emission from the Earth's ionosphere. The shape of this distribution is basically conical, however, it drops off more rapidly than it increases, with respect to local time.

Ions, meanwhile, have a probability distribution that shows a strong L dependence on local time. The high trapped probability region begins at local dawn, for L approximately 4, and rises to a maximum at between 1400 and 1500 local time with an L value of 8. The distribution then drops quickly in altitude as local time increases. Additionally, there is a region of decreased probability in the afternoon sector for this data that was speculated by Braccio (1991) to be inhabited by higher energy ions, but still is present for the higher energies surveyed.

The overall shape of the high trapped ion probability

region mirrors that of the location of the plasmopause. This suggests that the trapped ion distribution is linked to the plasmopause. This would confirm Horwitz et al.'s (1981) observations that 'pancake' distributions often occur in the vicinity of the plasmopause.

Additionally, it has been observed that trapped electrons seem to be excluded from regions of high trapped ion probabilities and vice versa. If the trapped ions actually do occur at the plasmopause, then as the altitude of the plasmopause rises, in the course of a day, this exclusion would effectively create a barrier that restricts the trapped electron distribution to the dawn to noon sector.

B. DETAILED ANALYSIS CASE STUDIES

The results of the detailed analysis case studies in general agree with the above results found by Braccio (1991). Trapped electron distributions are concentrated in the dawn to noon region with a peak around 1000 at an L value of 7. What trapped distributions occur in the afternoon are generally at higher L values until late afternoon when they move back into L values around 5 to 6 at 1800. This follows with the results found by Braccio (1991) who found that large trapped electron distributions are excluded from areas of high trapped ion distributions that peak in the 1400 to 1500 local time region. This also suggests a connection between the plasmopause and trapped electron distributions.

The threshold flux level used in the statistical survey was too low for 150 eV electrons. A higher flux level of 5×10^7 $(\text{cm}^2 \text{ s sr})^{-1}$ could be used for this energy level. The use of an anisotropy of 1.5 and a temperature ratio of 2.0 produced results more in keeping with the results of the statistical survey. The threshold flux level for 340 eV appeared to be correct.

The use of an average anisotropy at a latitude within 6° of the magnetic equator vice a calculated equator anisotropy in defining trapped electron distributions is generally pretty accurate. The average difference is only 7.5% between the two.

It has been shown that equatorially trapped plasmas can be described by a bi-Maxwellian distribution function. With such a description the values of the perpendicular and parallel temperatures can be calculated and their ratio used along with an anisotropy ratio between the flux in the 80° to 90° pitch angle range with the flux in the 60° to 70° pitch angle range to define a electron distribution as equatorially trapped or not. It was found that a temperature ratio of three along with anisotropies of 2.0 for 150 eV electrons and 4.4 for 340 eV electrons could be used to define a trapped electron distribution along with the required flux and magnetic latitude requirements.

However, the 340 eV anisotropy of 4.4 produce less reliable results than the 150 eV anisotropy with the theoretical anisotropy and temperature ratios for 340 eV being

too high. In this study T_{perp} is calculated from the bi-Maxwellian distribution function and this results in the same T_{perp} for both 150 eV and 340 eV. This was the only method available. However, the method produces a T_{perp} that is an underestimate of the perpendicular temperature for 340 eV particles. This suggests that the trapped electron distributions at this energy are not true bi-Maxwellians, but are more like a kappa function.

APPENDIX (DETAILED ANALYSIS SPECTROGRAMS)

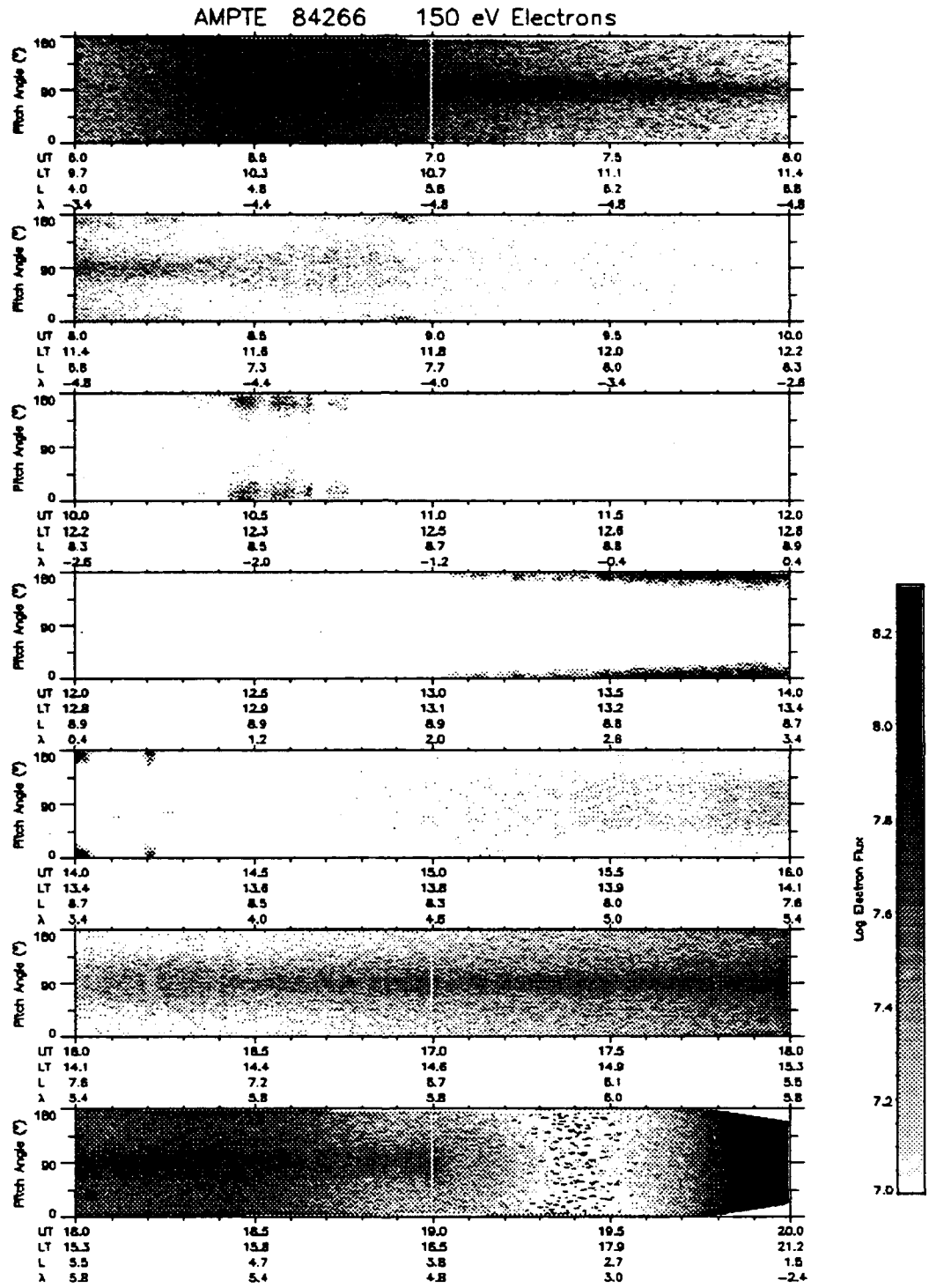


Figure 53. Pitch Angle verses Time Spectrogram - Day 84/266, Energy 150 eV

AMPTe 84283 150 eV Electrons

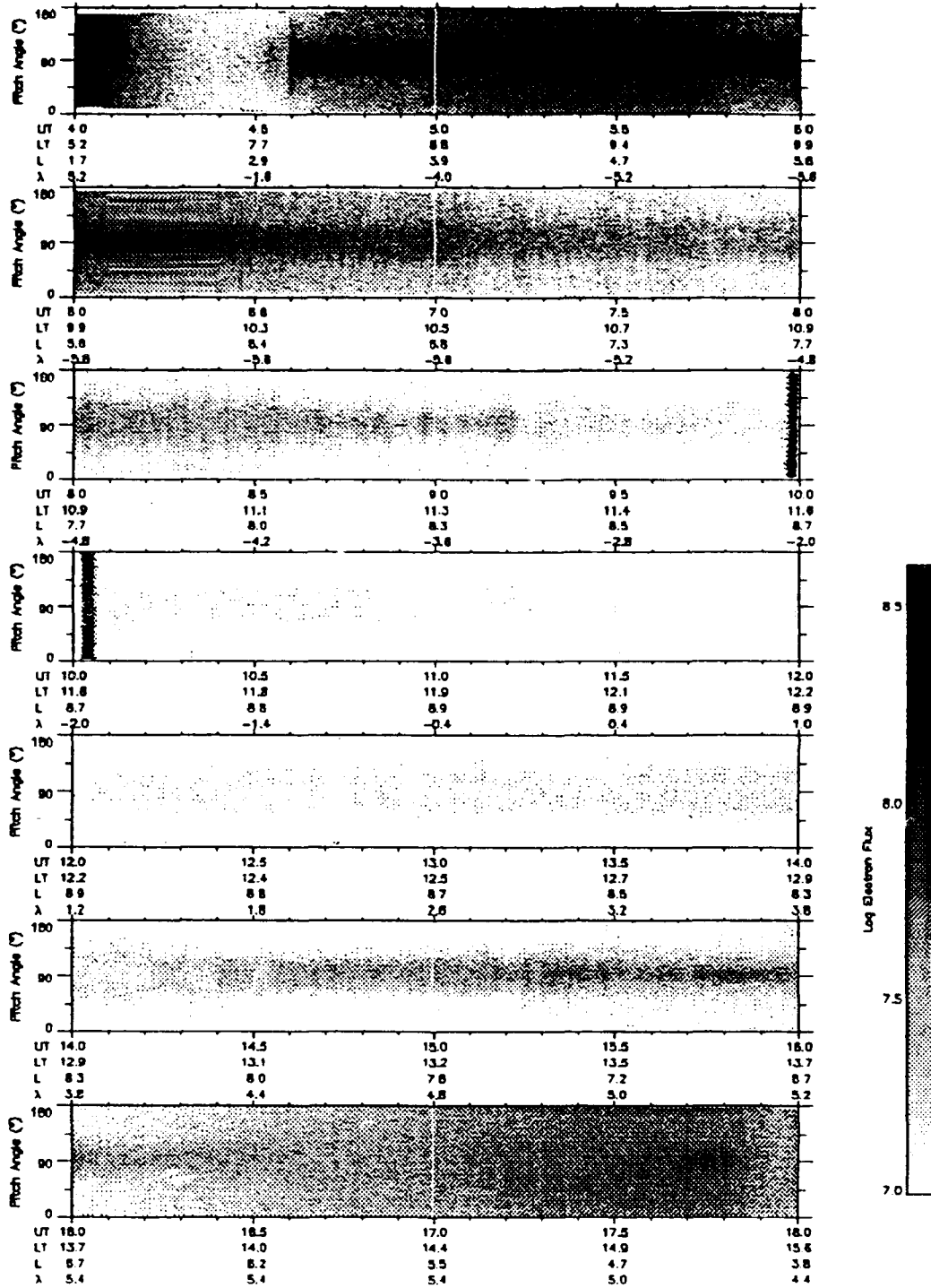


Figure 54. Pitch Angle versus Time Spectrogram - Day 84/283, Energy 150 eV

AMPTE 84296 150 eV Electrons

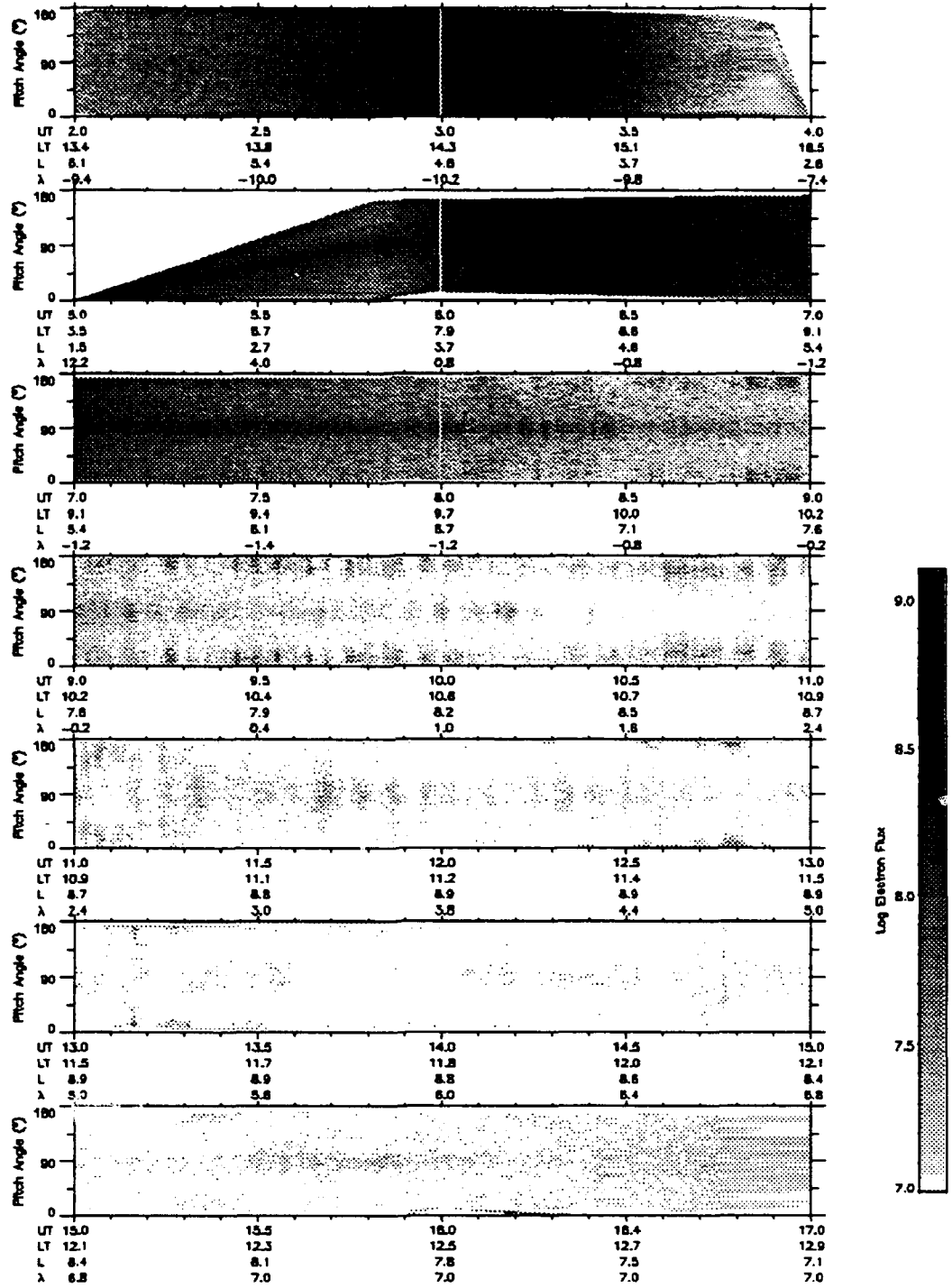


Figure 55. Pitch Angle versus Time Spectrogram - Day 84/296, Energy 150 eV

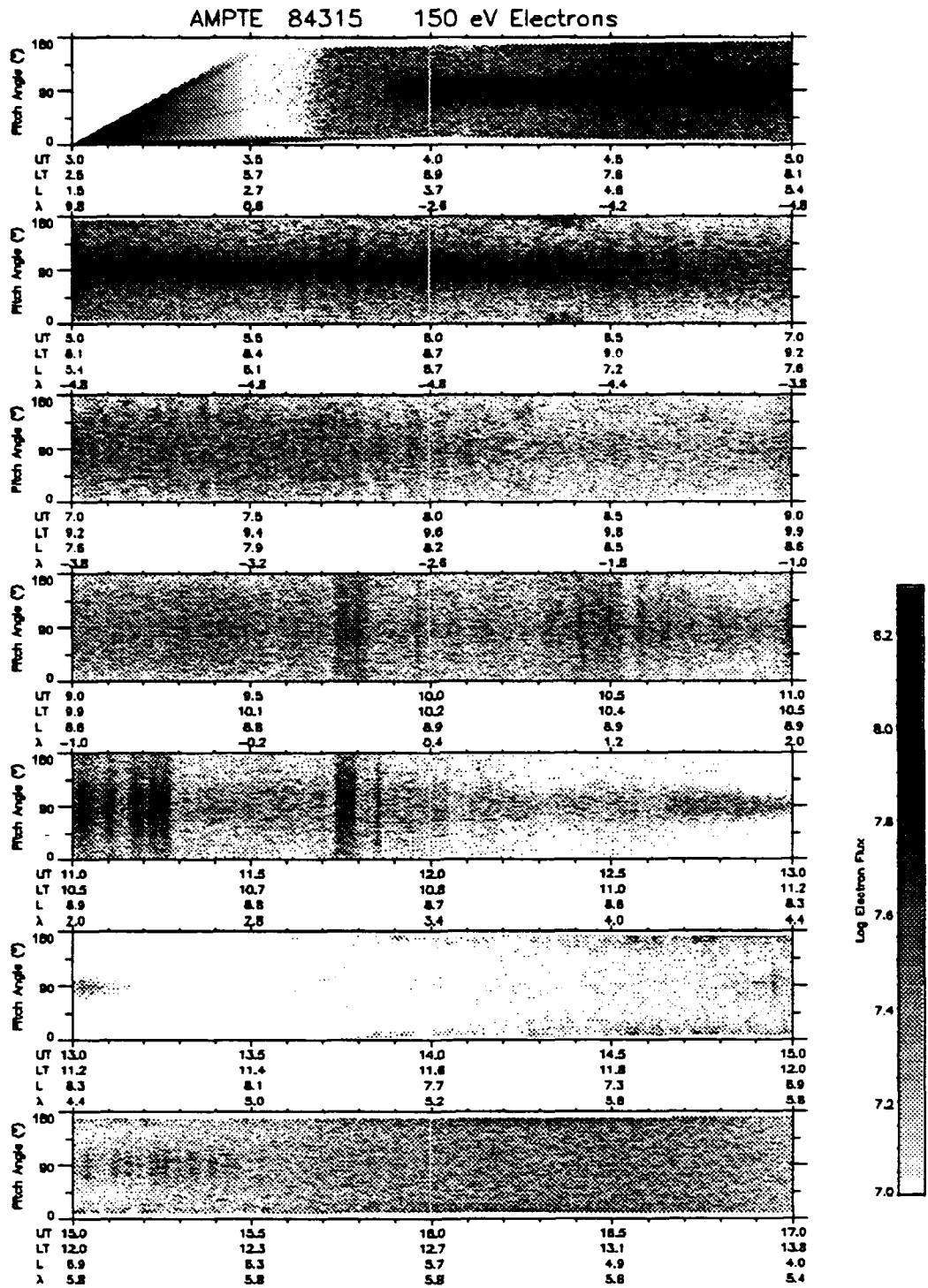


Figure 56. Pitch Angle versus Time Spectrogram - Day 84/315, Energy 150 eV

AMPTe 85002 150 eV Electrons

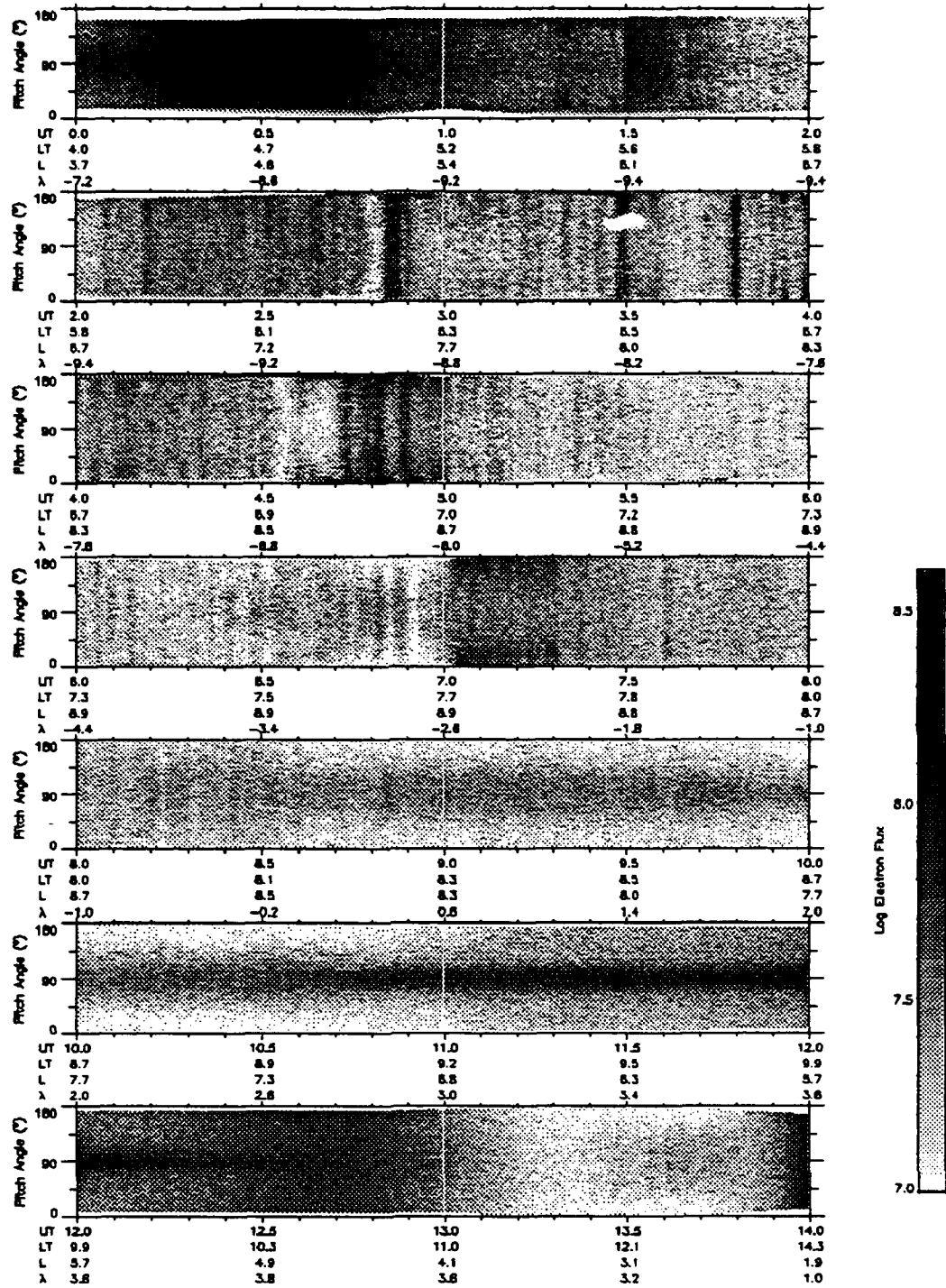


Figure 57. Pitch Angle versus Time Spectrogram - Day 85/002, Energy 150 eV

AMPTe 85039 150 eV Electrons

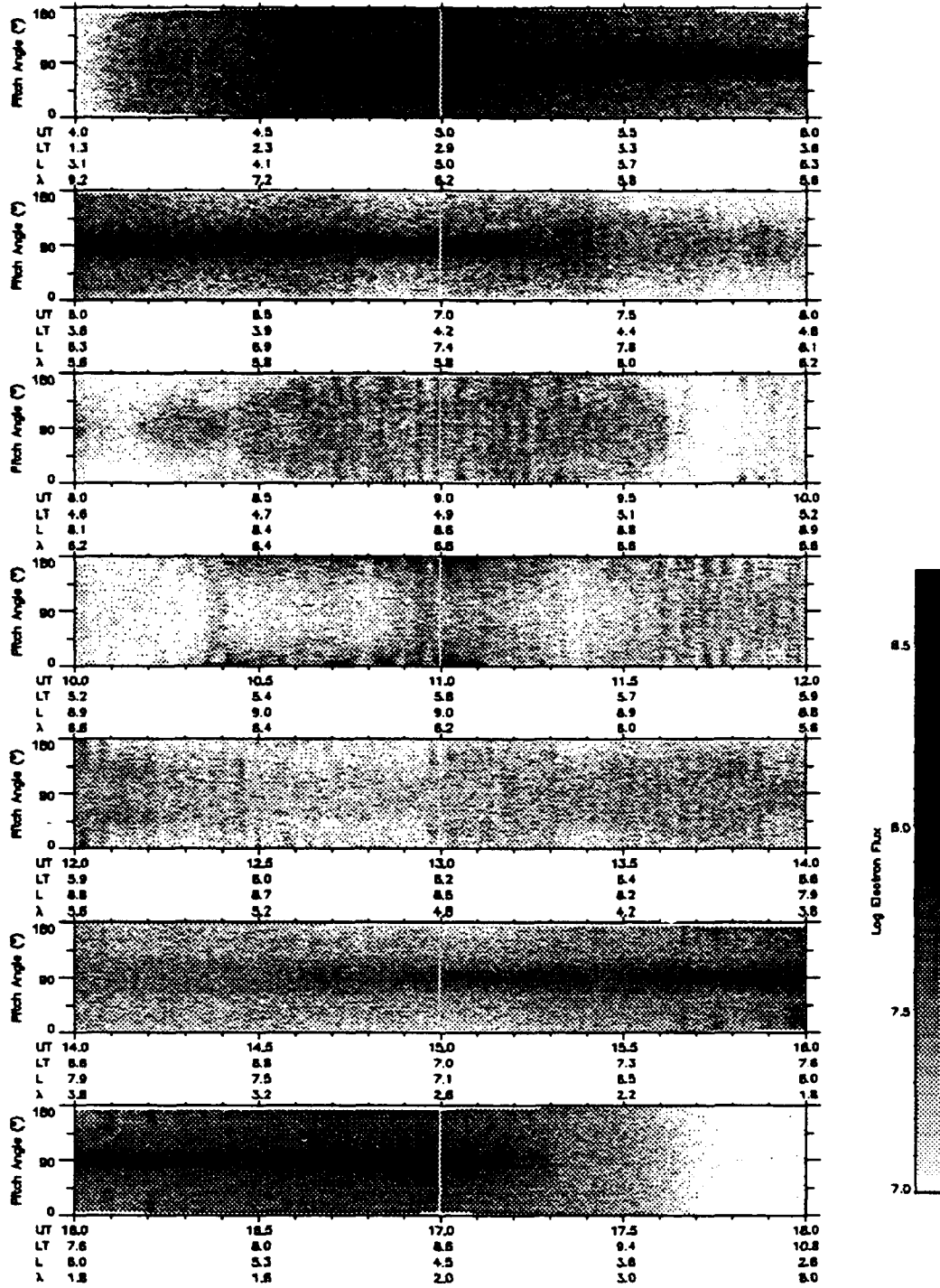


Figure 58. Pitch Angle versus Time Spectrogram - Day 85/039, Energy 150 eV

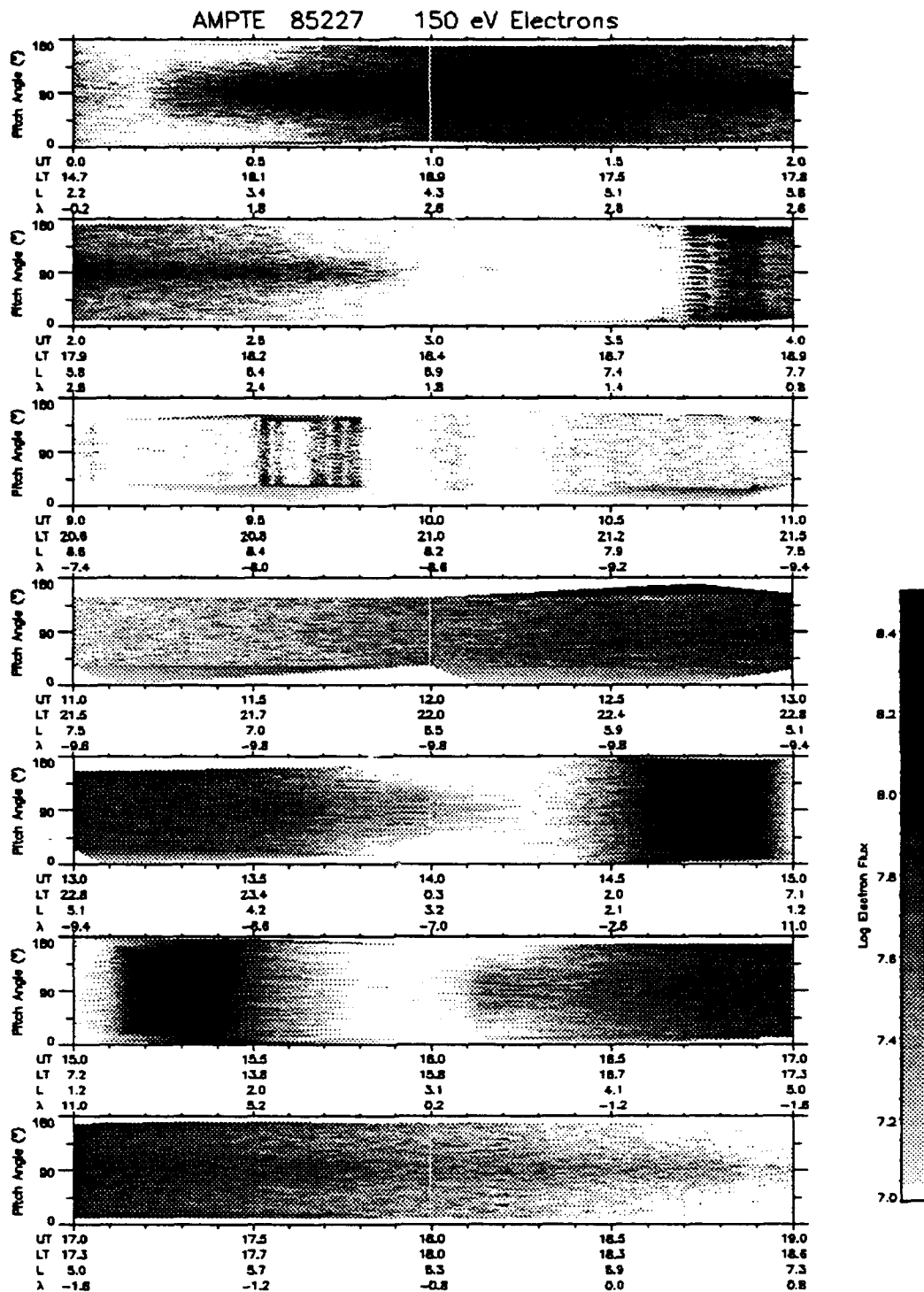


Figure 59. Pitch Angle versus Time Spectrogram - Day 85/227, Energy 150 eV

AMPTE 85238 150 eV Electrons

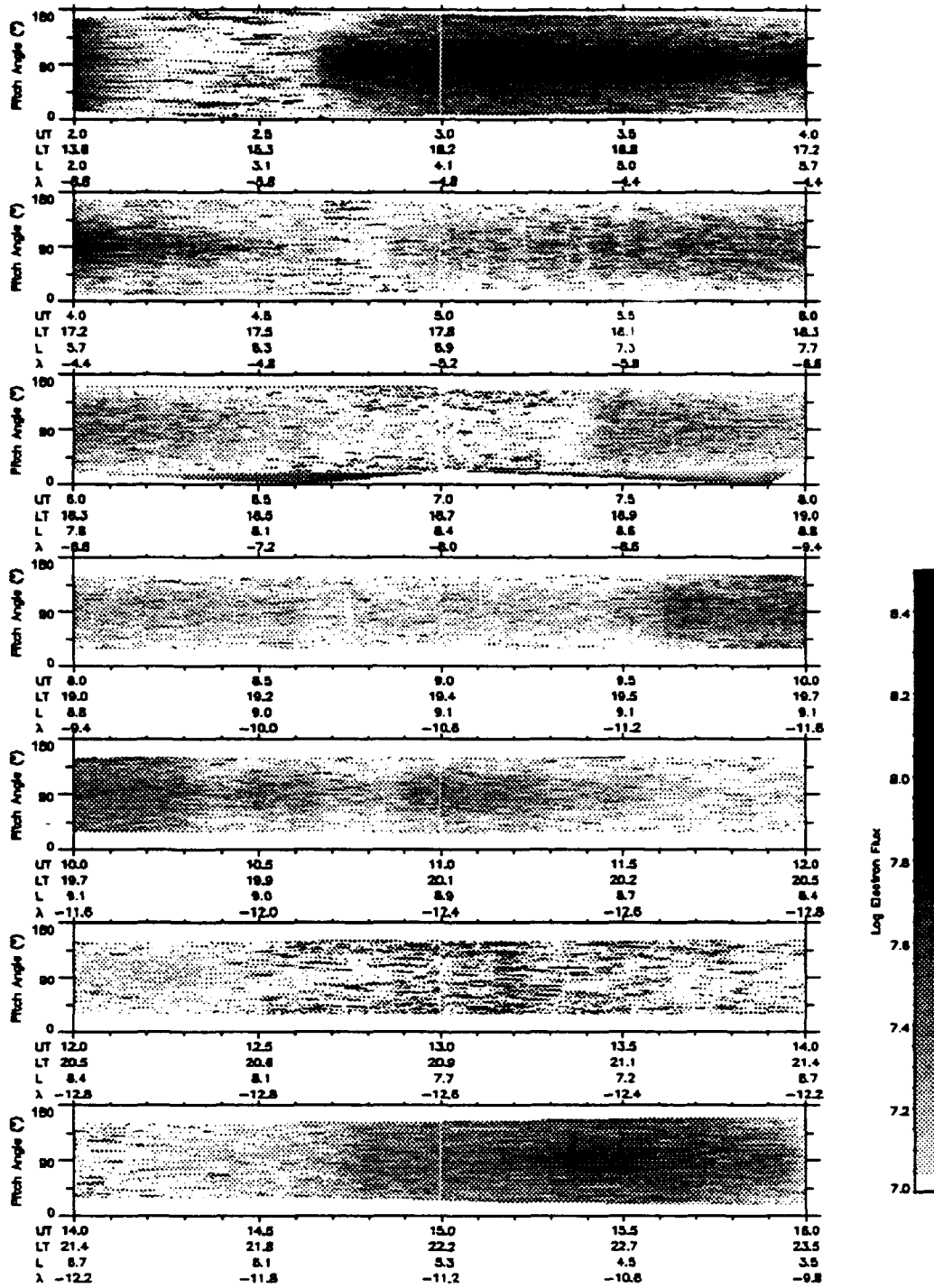


Figure 60. Pitch Angle versus Time Spectrogram - Day 85/238, Energy 150 eV

AMPT 85264 150 eV Electrons

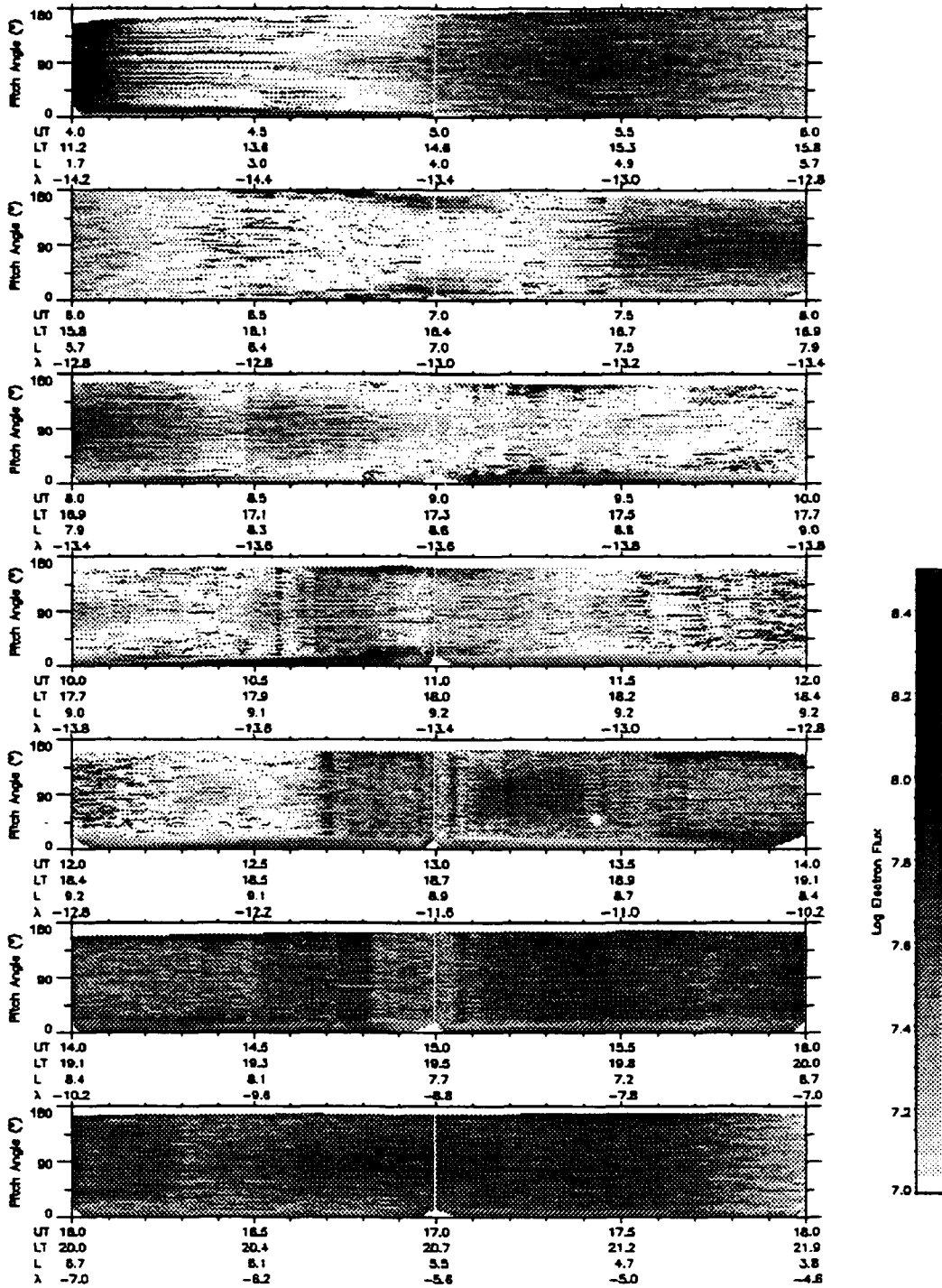


Figure 61. Pitch Angle versus Time Spectrogram - Day 85/264, Energy 150 eV

AMPTE 85301 150 eV Electrons

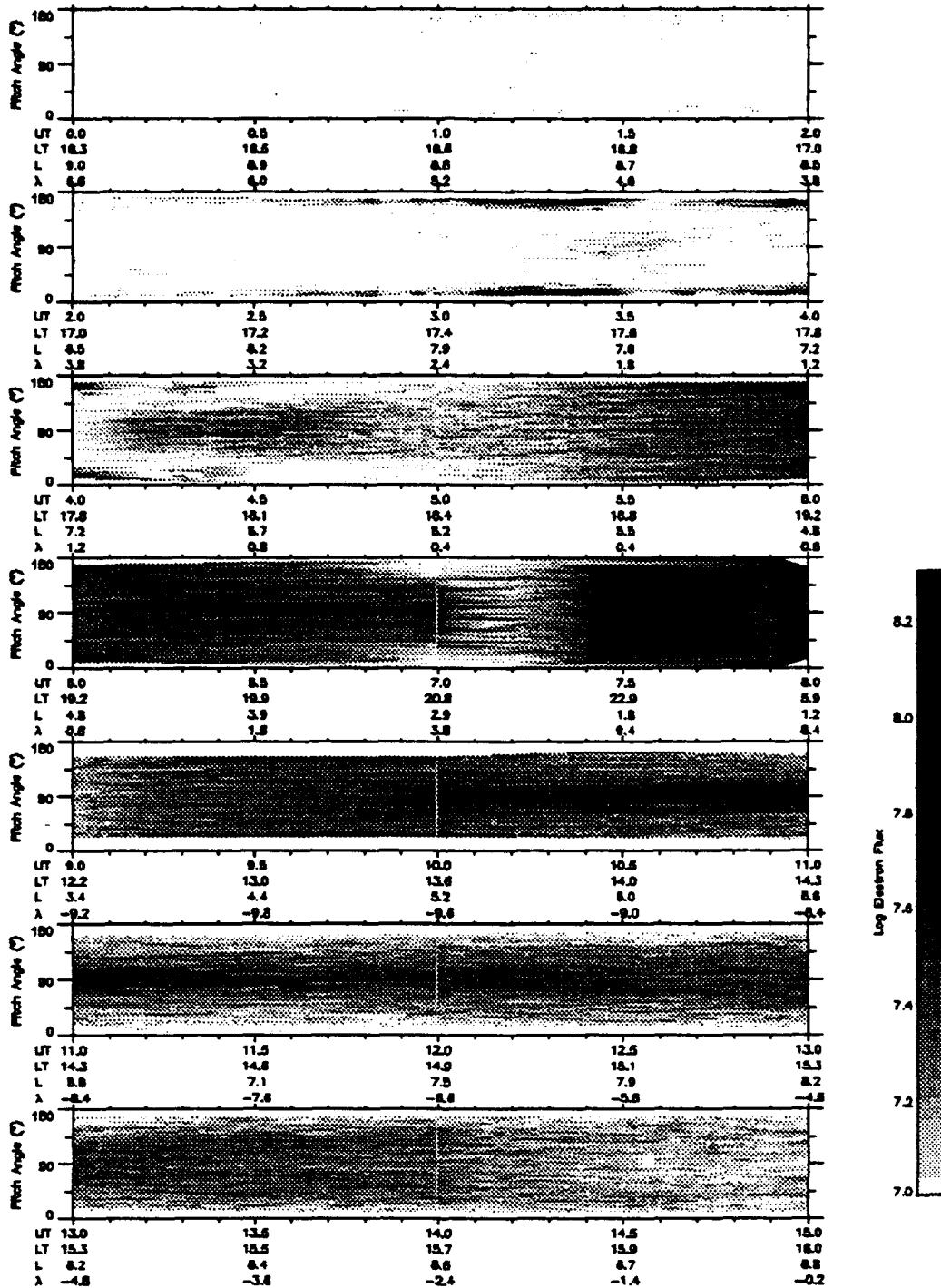


Figure 62. Pitch Angle versus Time Spectrogram - Day 85/301, Energy 150 eV

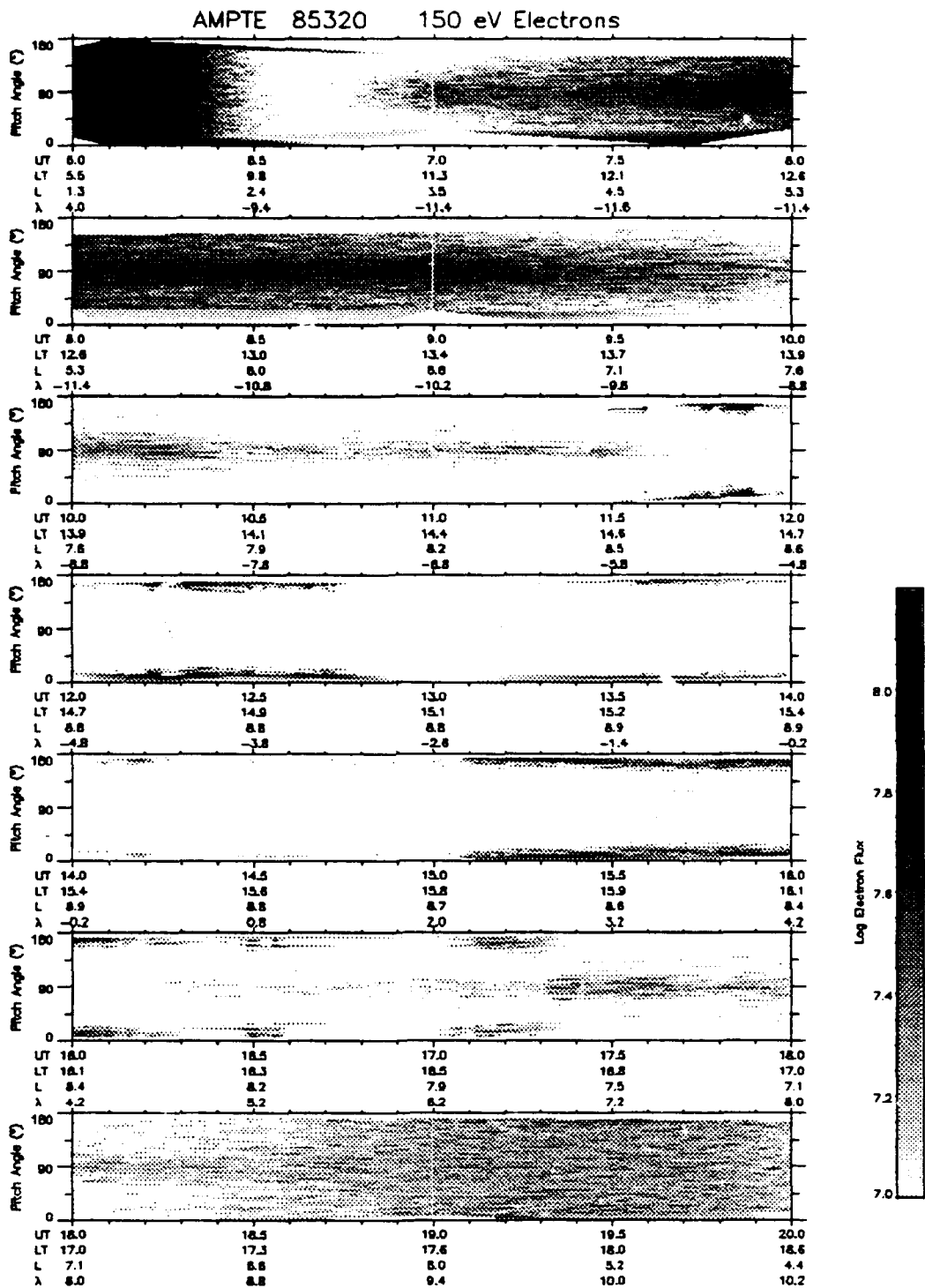


Figure 63. Pitch Angle versus Time Spectrogram - Day 85/320, Energy 150 eV

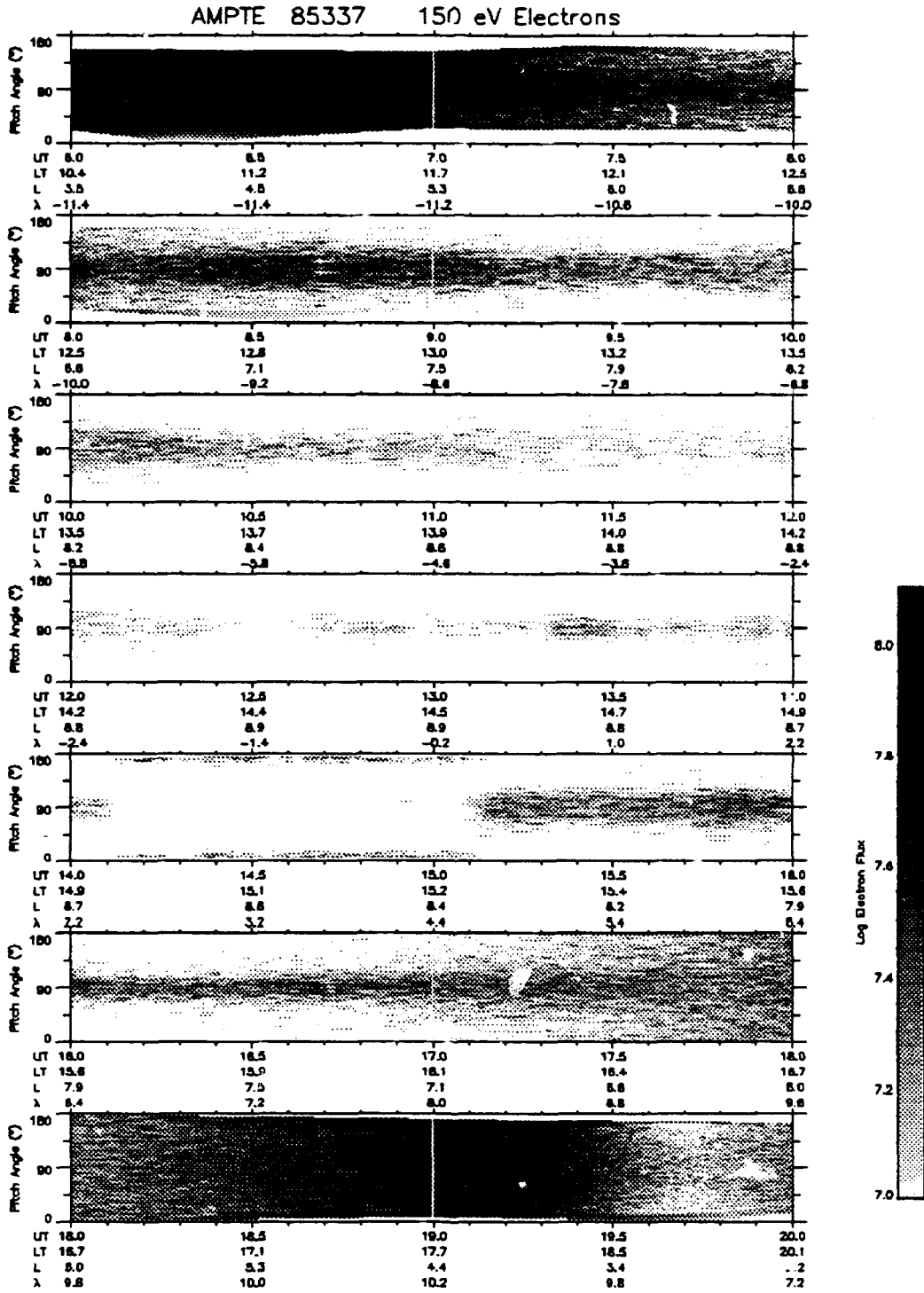


Figure 64. Pitch Angle versus Time Spectrogram - Day 85/337, Energy 150 eV

AMPT 84266 340 eV Electrons

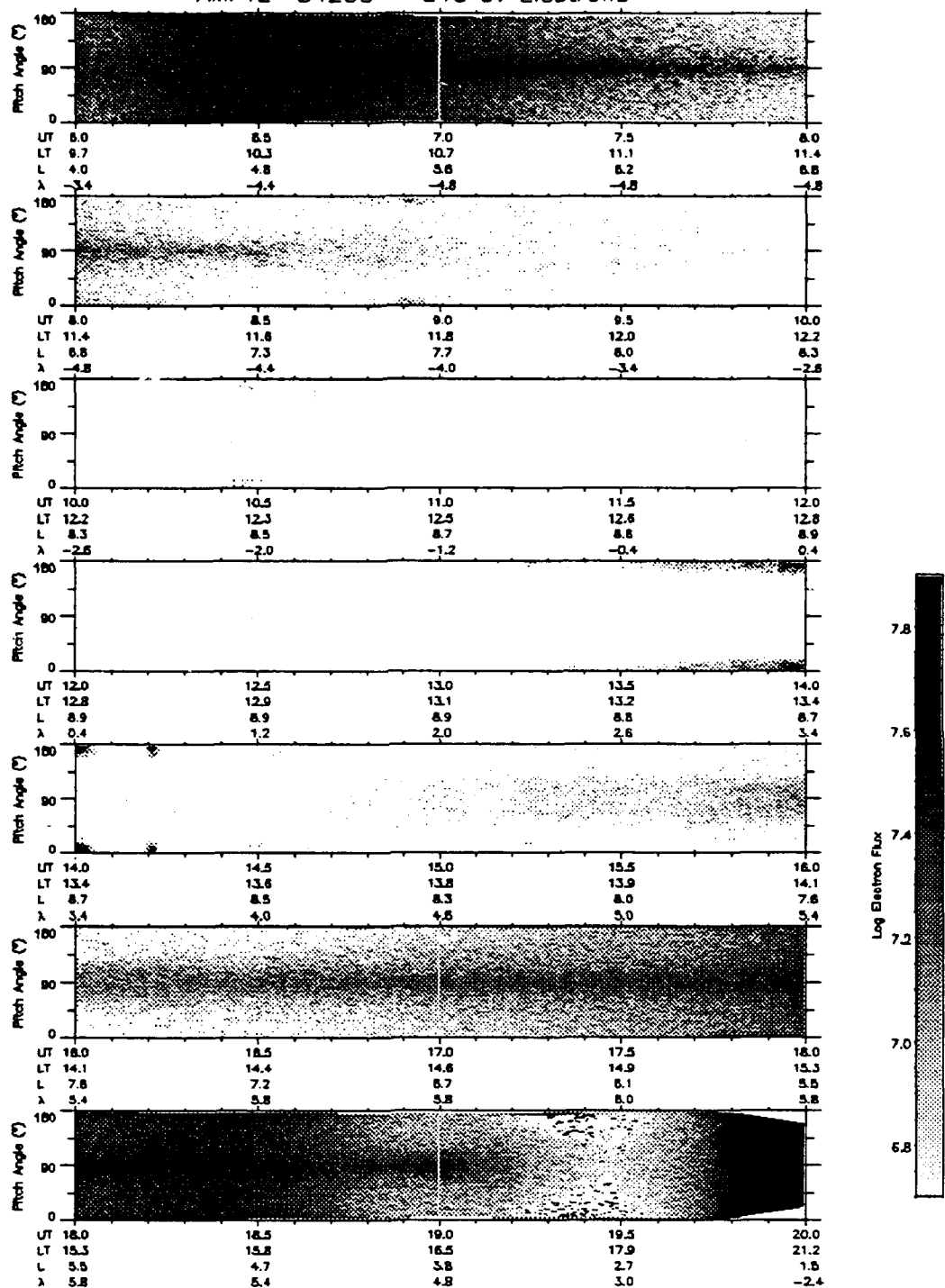


Figure 65. Pitch Angle versus Time Spectrogram - Day 84/266, Energy 340 eV

AMPTE 84283 340 eV Electrons

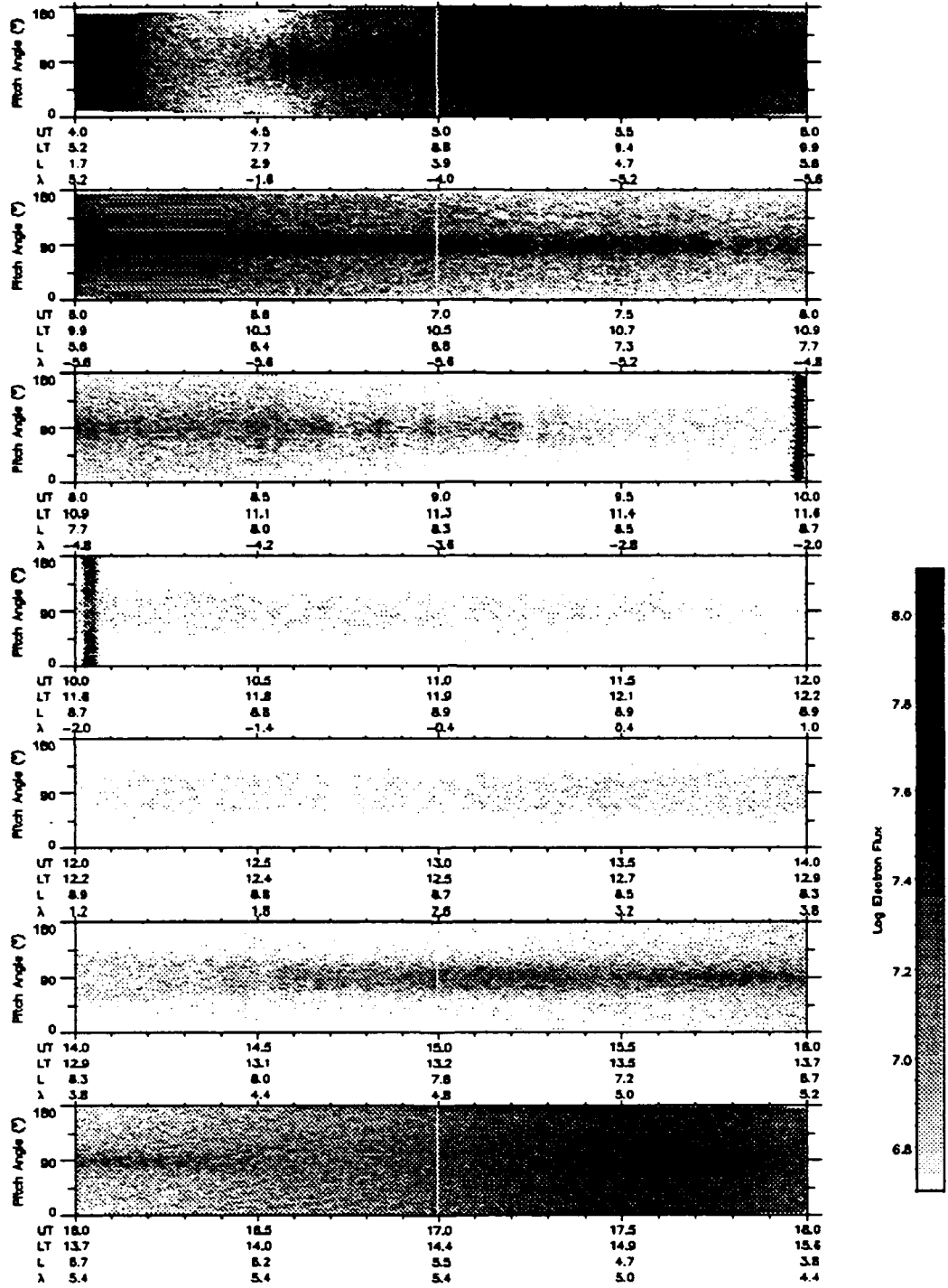


Figure 66. Pitch Angle verses Time Spectrogram - Day 84/283, Energy 340 eV

AMPTE 84296 340 eV Electrons

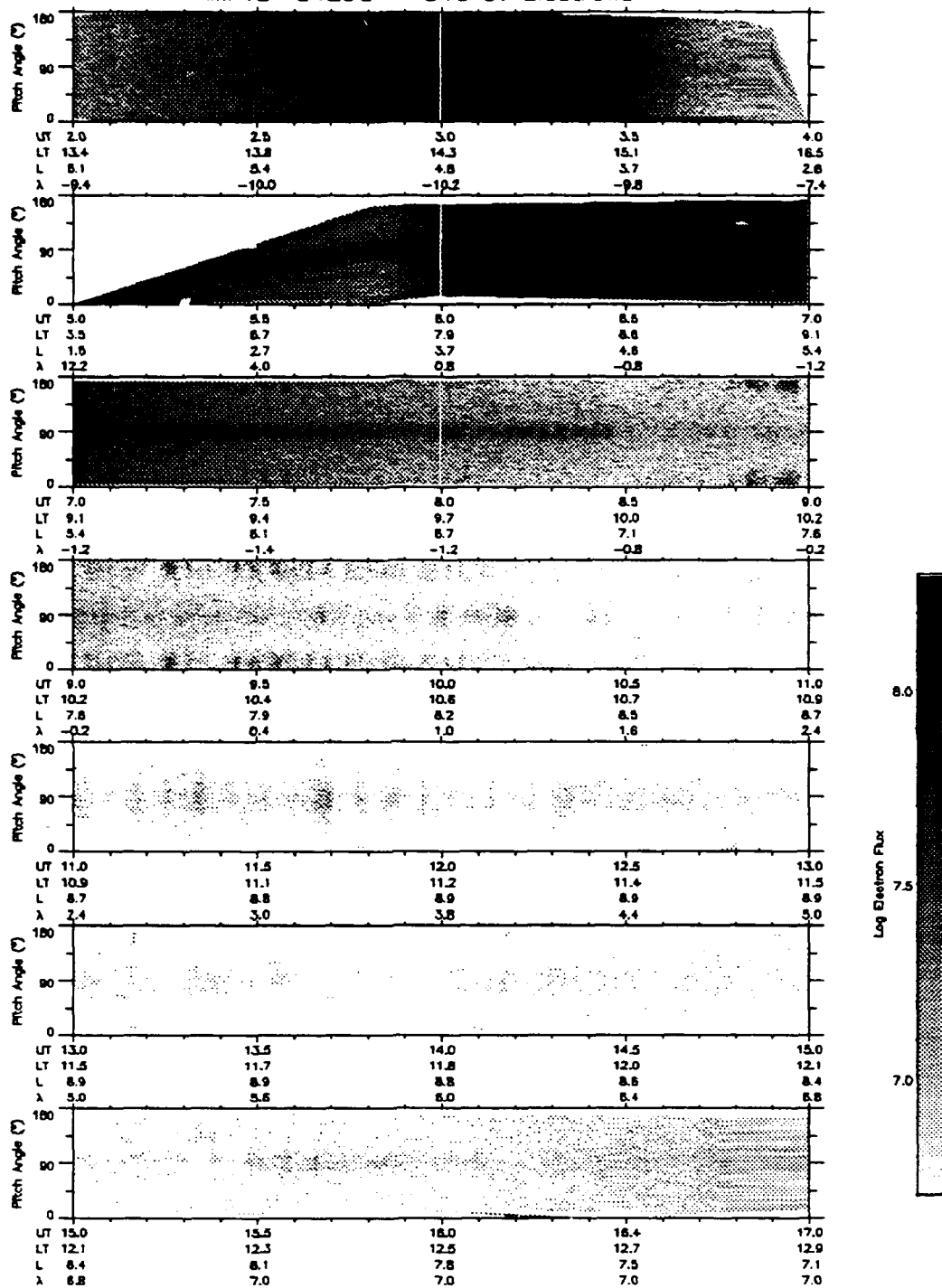


Figure 67. Pitch Angle versus Time Spectrogram - Day 84/296, Energy 340 eV

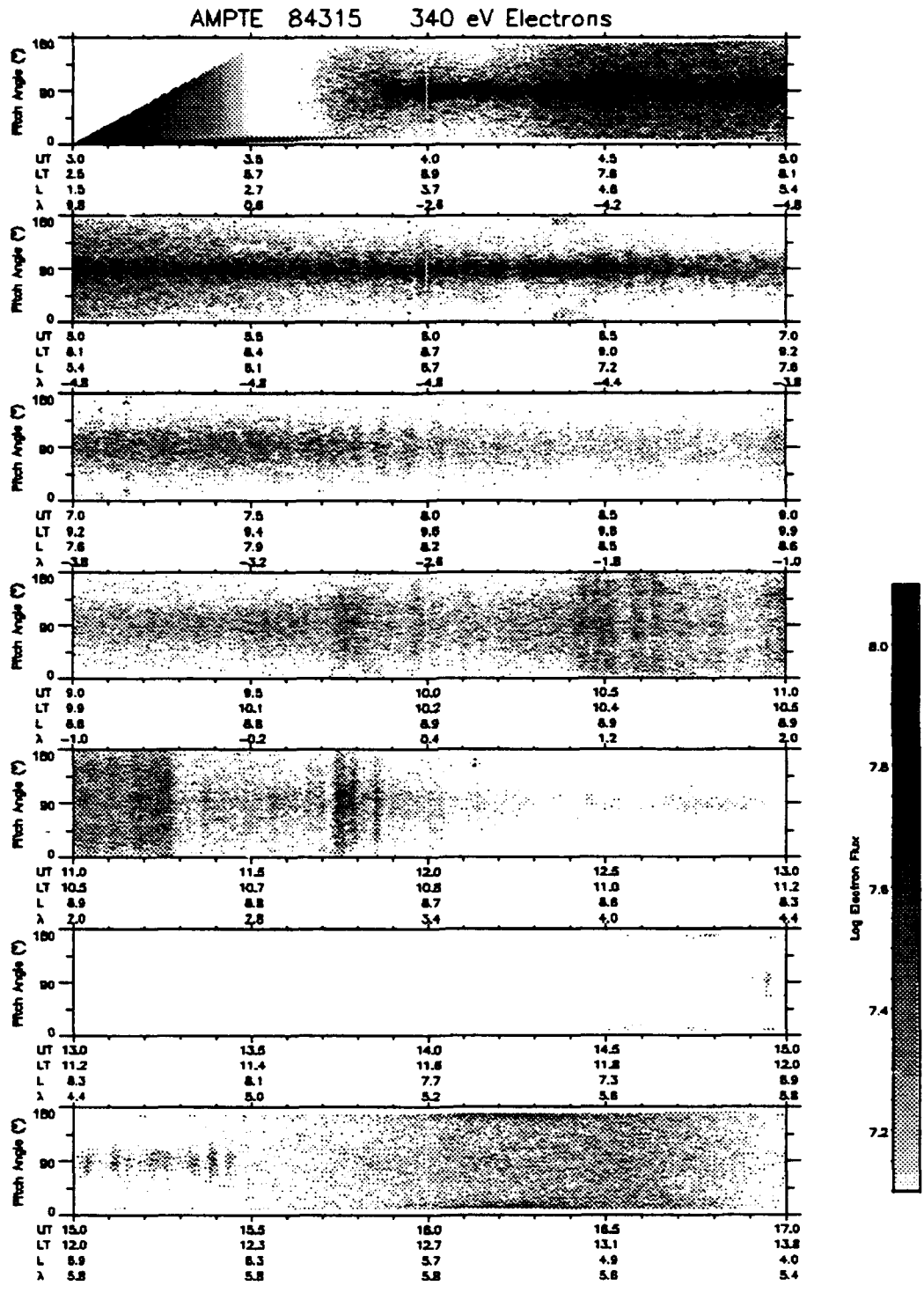


Figure 68. Pitch Angle versus Time Spectrogram - Day 84/315, Energy 340 eV

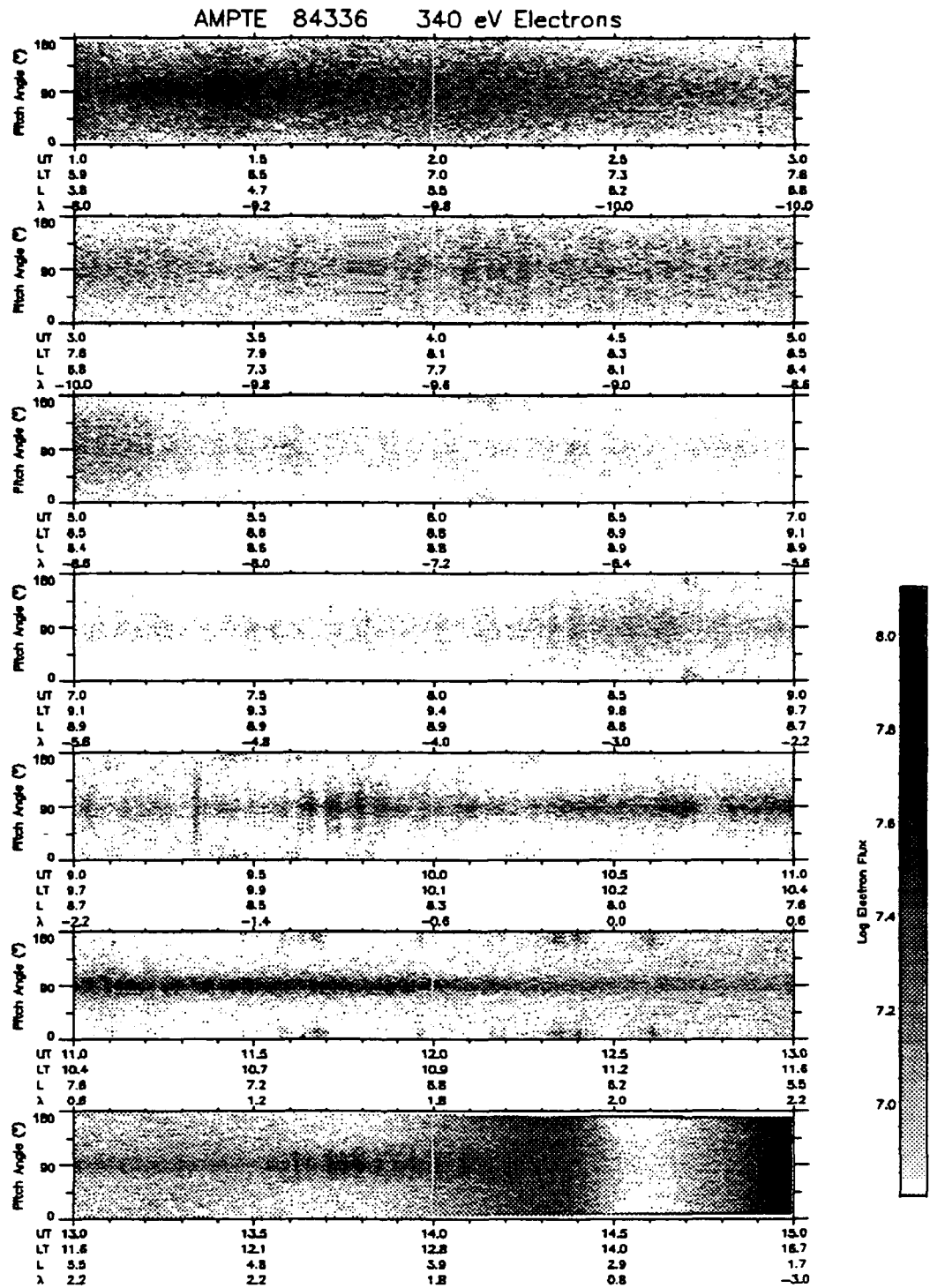


Figure 69. Pitch Angle versus Time Spectrogram - Day 84/336, Energy 340 eV

AMPT 85002 340 eV Electrons

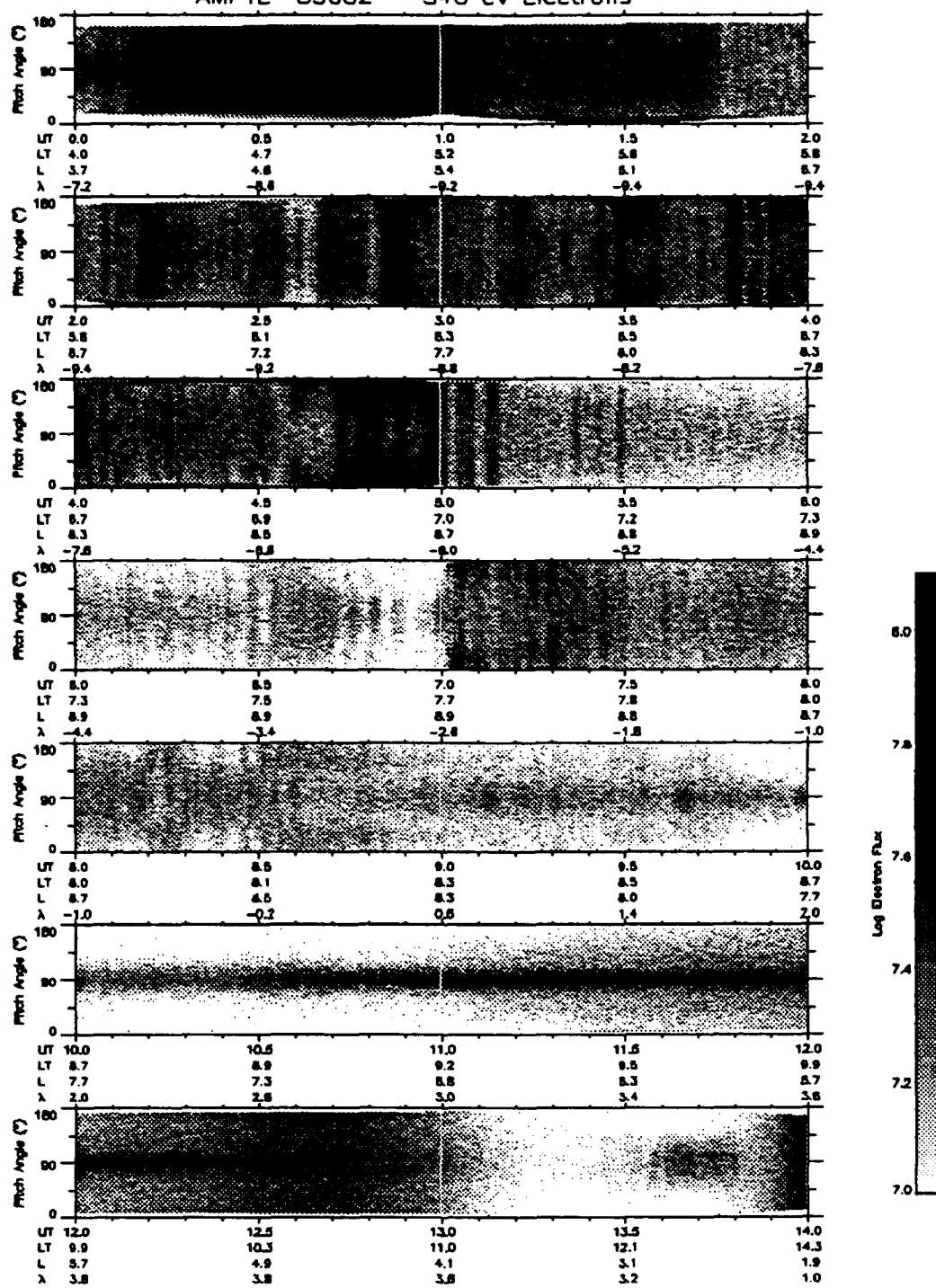


Figure 70. Pitch Angle versus Time Spectrogram - Day 85/002, Energy 340 eV

AMPTE 85039 340 eV Electrons

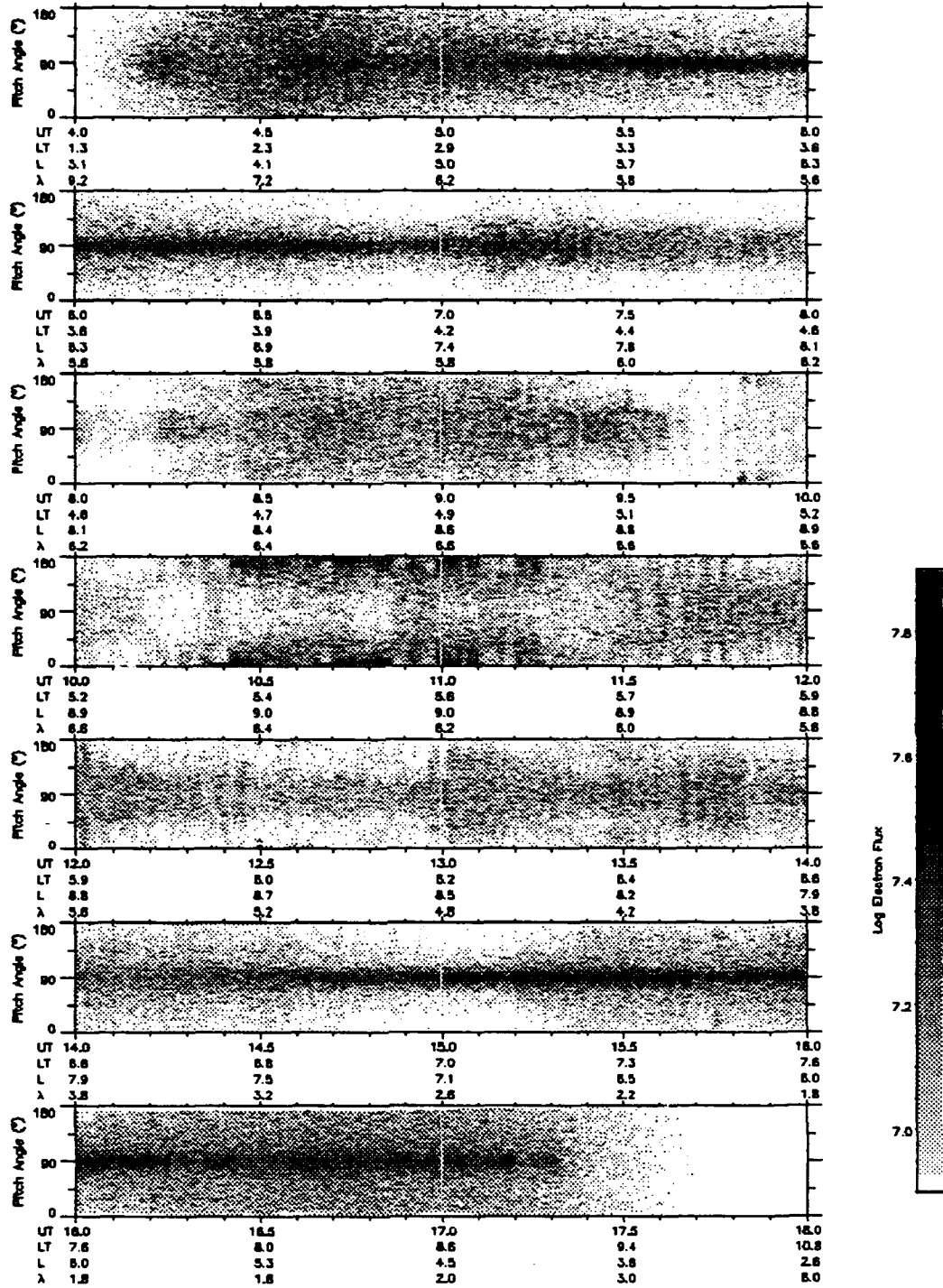


Figure 71. Pitch Angle versus Time Spectrogram - Day 85/039, Energy 340 eV

AMPT 85227 340 eV Electrons

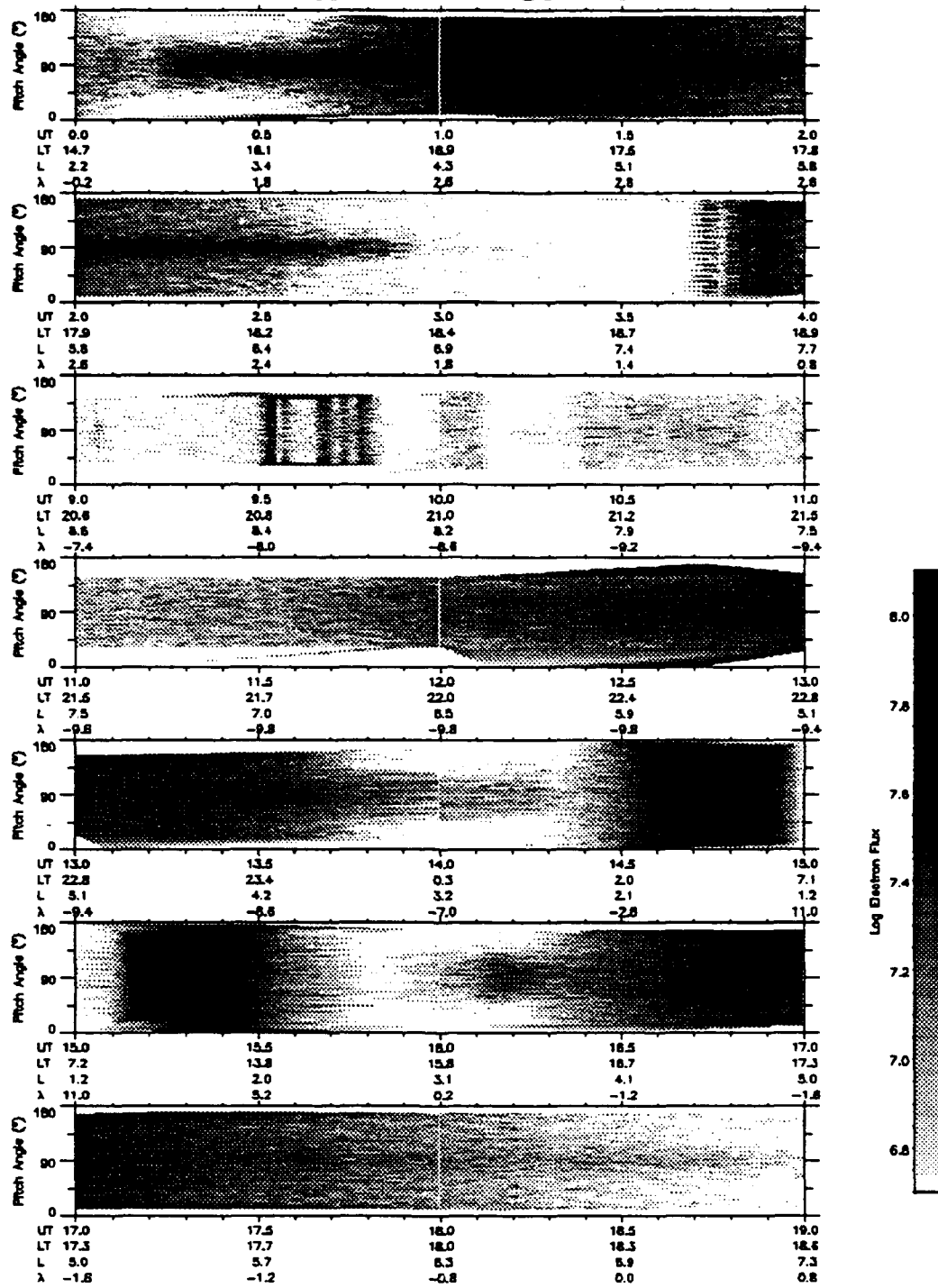


Figure 72. Pitch Angle versus Time Spectrogram - Day 85/227, Energy 340 eV

AMPTE 85238 340 eV Electrons

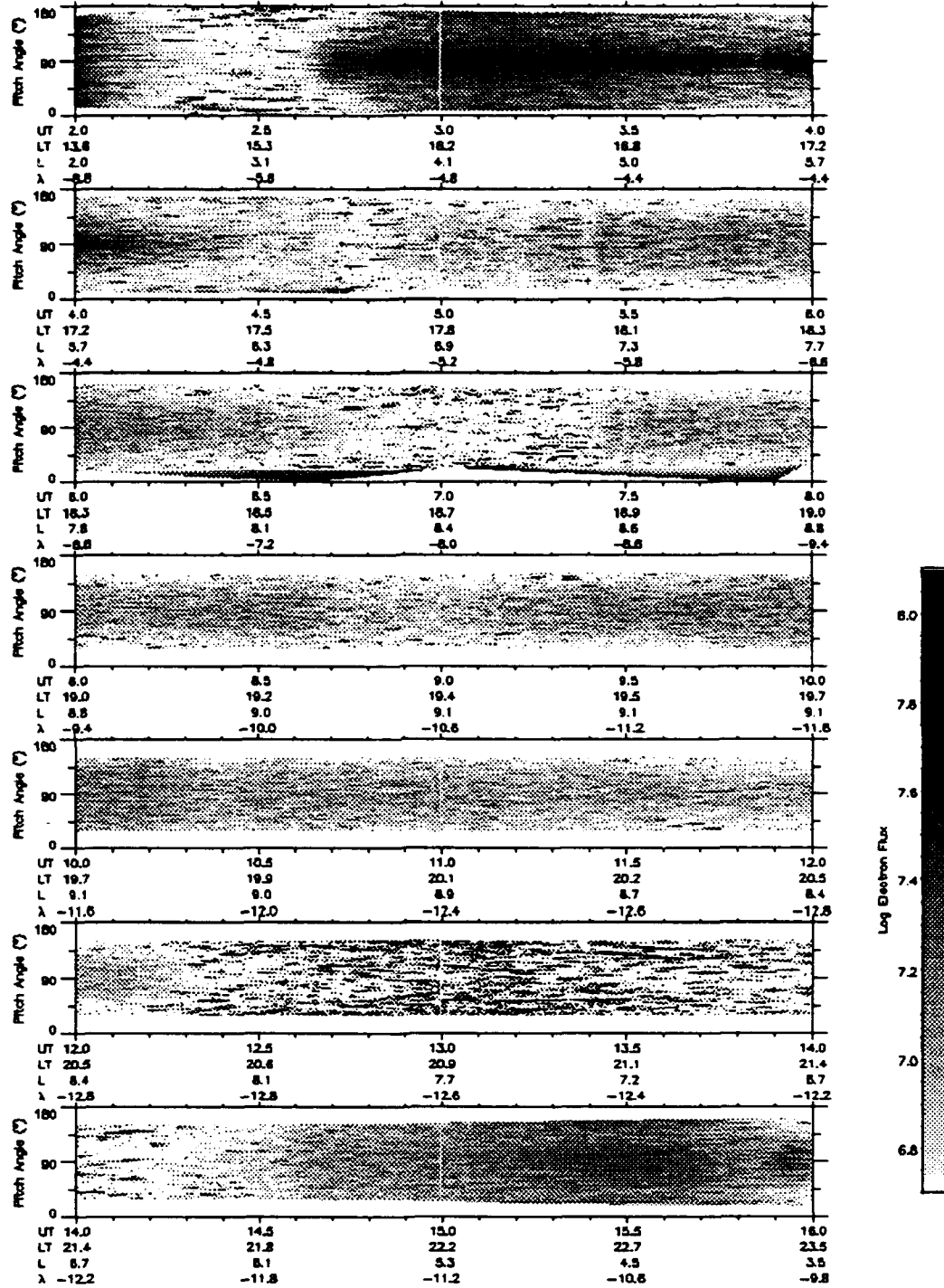


Figure 73. Pitch Angle versus Time Spectrogram - Day 85/238, Energy 340 eV

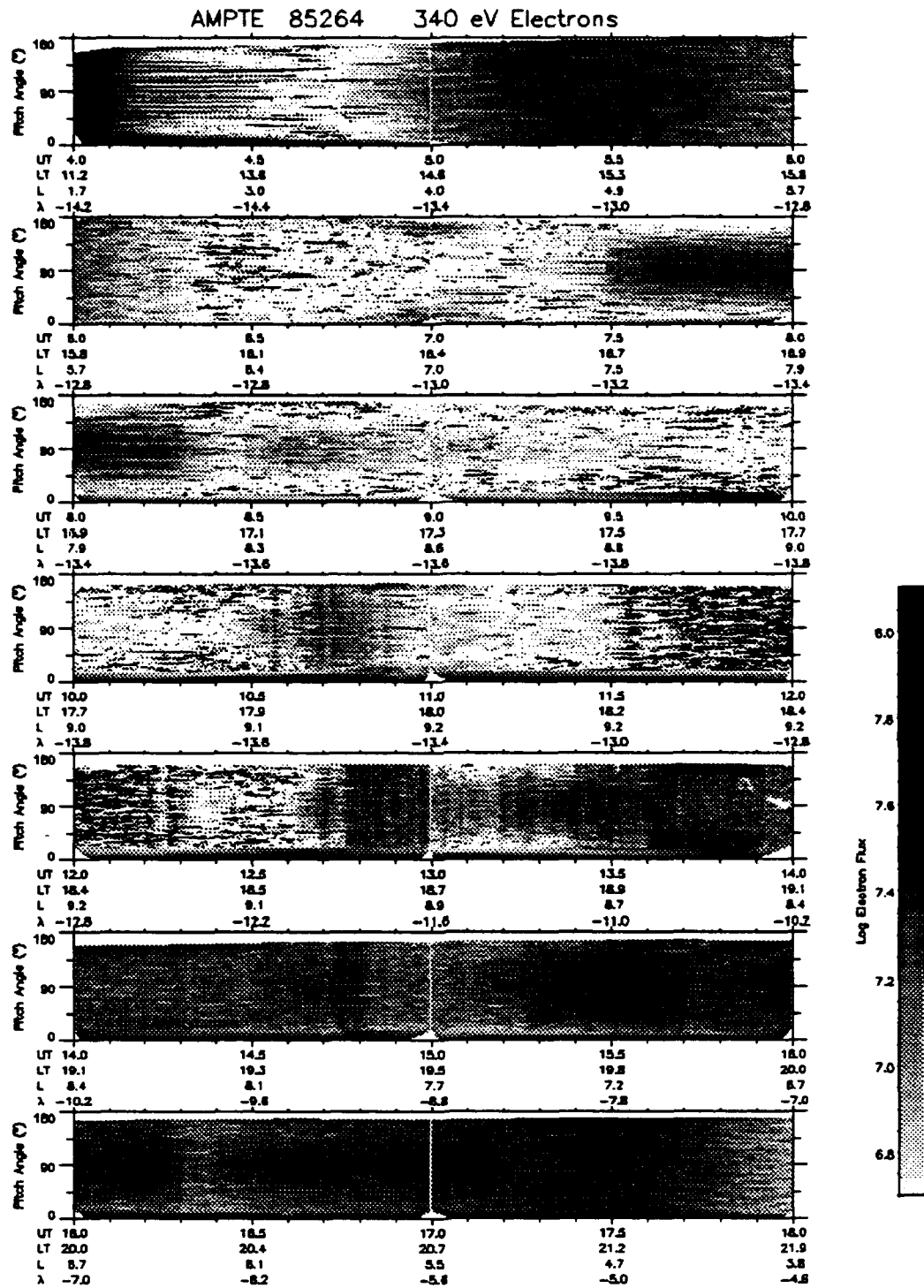


Figure 74. Pitch Angle versus Time Spectrogram - Day 85/264, Energy 340 eV

AMPT 85301 340 eV Electrons

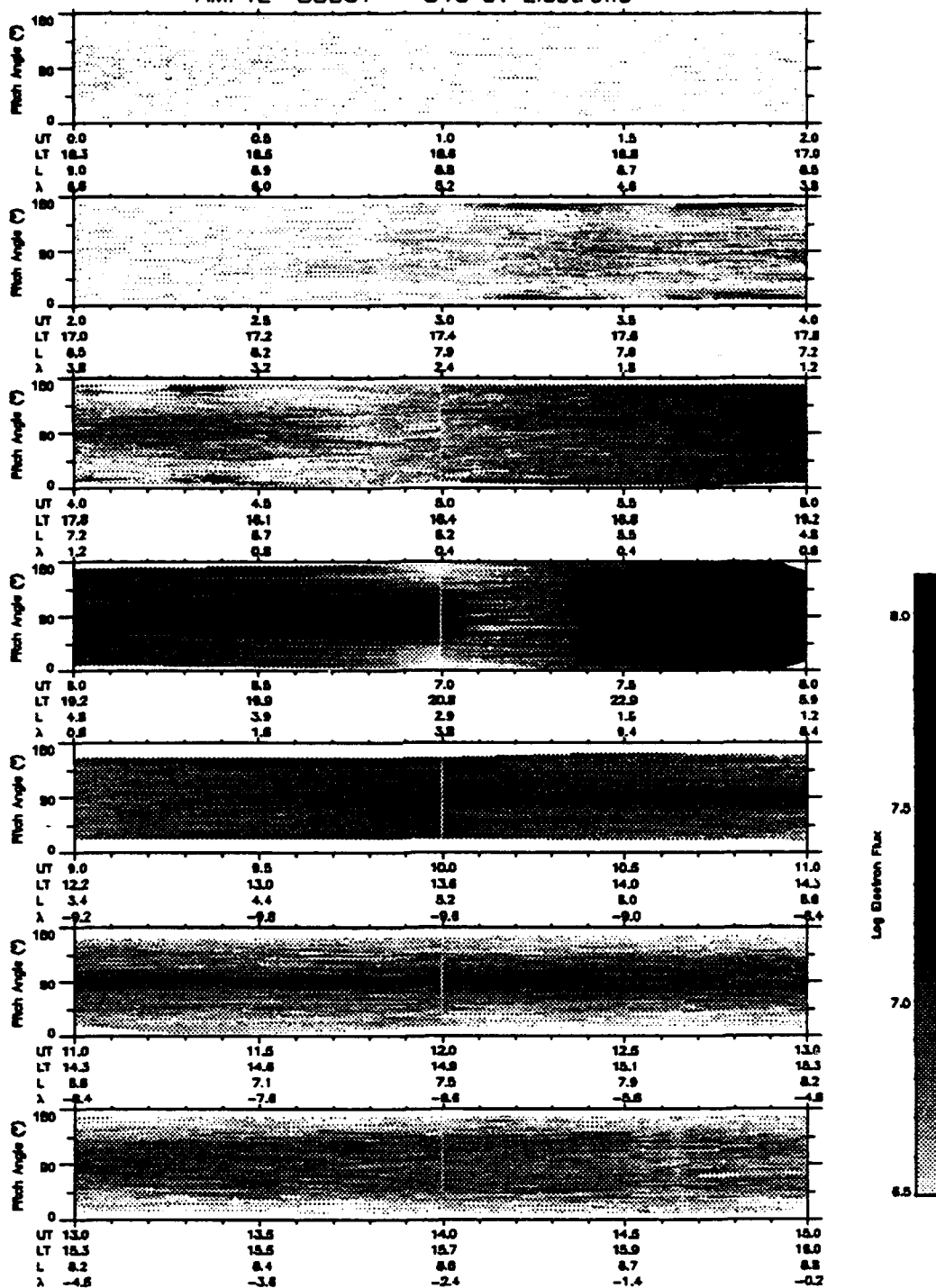


Figure 75. Pitch Angle versus Time Spectrogram - Day 85/301, Energy 340 eV

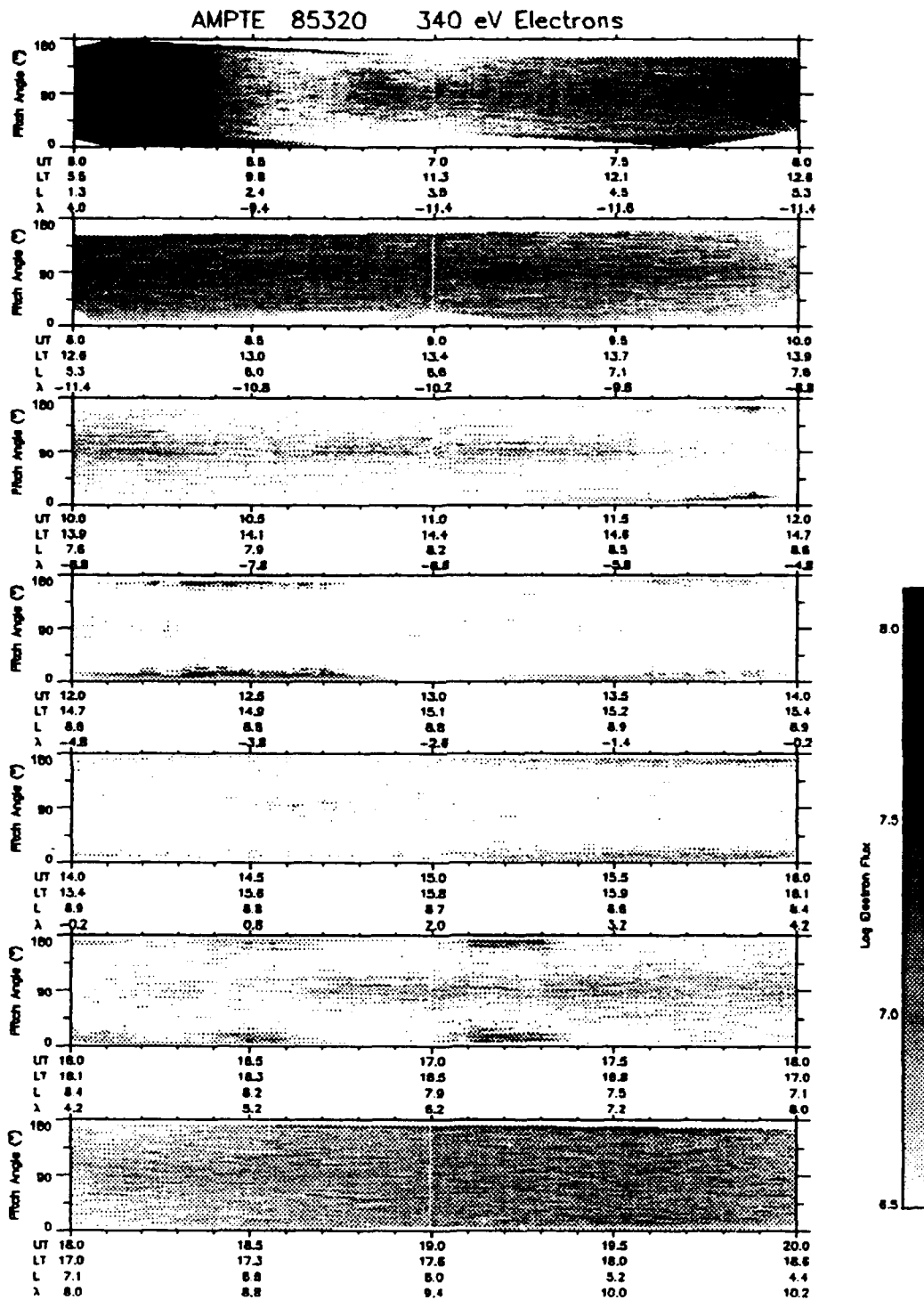


Figure 76. Pitch Angle versus Time Spectrogram - Day 85/320, Energy 340 eV

AMPTE 85337 340 eV Electrons

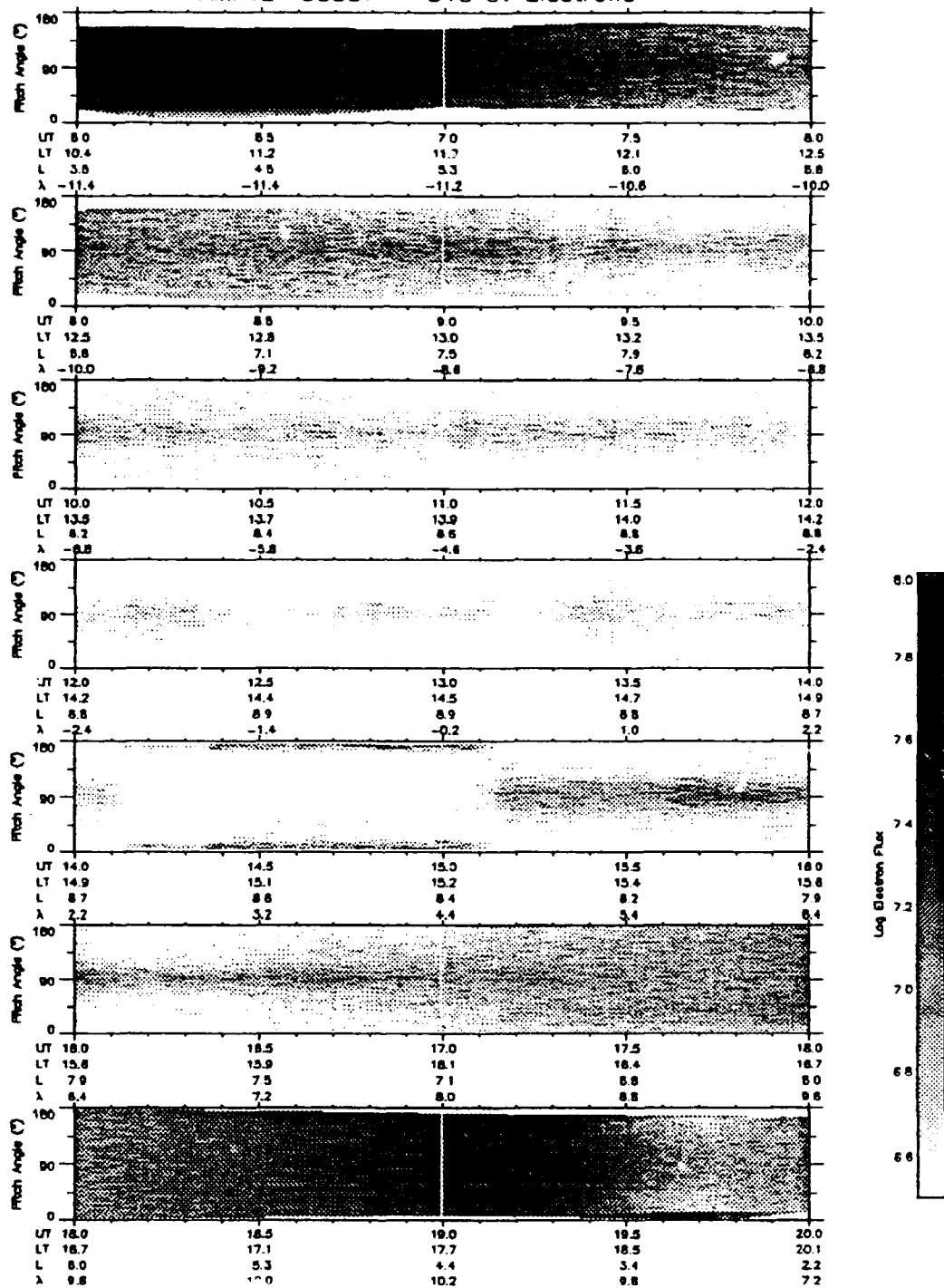


Figure 77. Pitch Angle versus Time Spectrogram - Day 85/337, Energy 340 eV

LIST OF REFERENCES

- Acuna, M. H., Ousley, G. W., McEntire, R. W., Bryant, D. A., and Paschmann, G., "Editorial: AMPTE-Mission Overview," *IEEE Transactions on Geoscience and Remote Sensing*, vol GE-23, no. 3, pp. 175-176, May 1985
- Banks, P. M. and Holzer, T. E., "The Polar Wind," *Journal of Geophysical Research*, vol. 73 , no. 21, pp. 6846-6854, 1 November 1968
- Braccio, P. G., *Survey of Trapped Plasmas at the Earth's Magnetic Equator*, Master's Thesis, Naval Postgraduate School, Monterey, California, December 1991
- Chappell, C. R., Harris, K. K., and Sharp, G. W., "The Morphology of the Bulge Region on the Plasmashpere," *Journal of Geophysical Research*, vol. 75, no. 19, pp. 3848-3861, 1 July 1970
- Chen, F. F., *Introduction to Plasma Physics and Controlled Fusion*, 2nd ed., vol. 1, Plenum Press, 1983
- Comfort, R. H. and Horowitz, J. L., "Low Energy Ion Pitch Angle Distributions Observed on the Dayside at Geosynchronous Altitudes," *Journal of Geophysical Research*, vol. 86, no. A3, pp.1621-1627, 1 March 1981
- Dassoulas, J., Margolies, D. L., and Peterson, M. R., "The AMPTE CCE Spacecraft," *IEEE Transactions on Geoscience and Remote Sensing*, vol. GE-23, no. 3, pp. 182-191, May 1985
- Glasstone, S., *Sourcebook on the Space Sciences*, D. van Nostrand Company, Inc., 1967
- Gurnett, D. A., "Plasma Wave Interactions With Energetic Ions Near the Magnetic Equator," *Journal of Geophysical Research*, vol. 81, no.16, pp.2765-2770, 1 June 1976
- Harris, K. K., Sharp, G. W., and Chappell, C. R., "Observations of the Plasmopause from OGO 5," *Journal of Geophysical Research*, vol 75, no. 1, pp. 219-224, 1 January 1970
- Horowitz, J. L., " Major Questions on the Interchange of Thermal Plasmas Between the Ionosphere and Plasmopause," *Journal of Atmospheric and Terrestrial Physics*, vol 45, no. 11, pp. 765-775, 1983

Horowitz, J. L., Baugher, C. R., Chappell, C. R., Shelly, E. G., and Young, D. T., "Pancake Pitch Angle Distributions in Warm Ions Observed With ISEE 1," *Journal of Geophysical Research*, vol 86, no. A5, pp. 3311-3320, 1 May 1981

Horowitz, J. L. and Chappell, C. R., "Observations of Warm Plasma in the Dayside Plasma Trough at Geosynchronous Orbit," *Journal of Geophysical Research*, vol 84, no. A12, pp. 7075-7090, 1 December 1979

Klumpar, D. M. and Shelley, E. G., "Equatorially Trapped Light Ions at the Plasmapause/Ring Current Interface," *EOS*, vol 67, p.1154, 1986

Kurth, W. S., Craven, J. D., Frank, L. A., and Gurnett, D. A., "Intense Electrostatic Waves Near the Upper Hybrid resonance Frequency," *Journal of Geophysical Research*, vol. 84, no. A8, pp. 4145-4164, 1 August 1979

Parks, G. K., *Physics of Space Plasmas*, Addison-Wesley Publishing Company, 1991

Olsen, R. C., "Equatorially Trapped Plasma Populations," *Journal of Geophysical Research*, vol. 86 no. A13, pp. 11,235-11,245, 1 December 1981

Olsen, R. C., "The Density Minimum at the Earth's Magnetic Equator," *Journal of Geophysical Research*, in press 1992

Olsen, R. C., Shawhan, S. D., Gallagher, D. L., Green, J. I., Chappell, C. R., and Anderson, R. R., "Plasma Observations at the Earth's Magnetic Equator," *Journal of Geophysical Research*, vol. 92, no. A1, pp. 2385-2407, 1 March 1987

Sagawa, E., Yau, A. W., and Whalen, B. A., "Pitch Angle Distributions of Low Energy Ions in the Near-Earth Magnetosphere," *Journal of Geophysical Research*, vol. 92, no. A11, pp. 12,241-12,254, 1 November 1987

Scott, L. J., *On the Consequences of Bi-Maxwellian Distributions On Parallel Electric Fields*, Master's Thesis, Naval Postgraduate School, Monterey, California, December 1991

Shelly, E. G., Ghielmetti, A., Hertzburg, E., Battel, S. J., Altwegg-von Burg, K., and Balsiger., "The AMPTE/CCE Hot Plasma Composition Experiment (HPCE)," *IEEE Transactions on Geoscience and Remote Sensing*, vol. GE23, no. 3, pp. 241-245, May 1985

Williams, D. V., Rycroft, M. J., Smith, A. J., Bezrukikh, V. V., Gringauz, K. I., Maynard, N. C., Morgan, M. G., and Thomas,

T. W., "Intercomparison of Various Measurements of Thermal Plasma Densities At and Near the Plasmopause," *Advances in Space Research*, vol. 1, pp. 235-238, 1981

INITIAL DISTRIBUTION LIST

	No. Copies
1. Defense Technical Information Center Cameron Station Alexandria VA 22304-6145	2
2. Library, Code 052 Naval Postgraduate School Monterey CA 93943-5002	2
3. Department Chairman, Code Ph Department of Physics Naval Postgraduate School Monterey, CA 93943-5000	2
4. Dr. R. C. Olsen, Code Ph/Os Department Of Physics Naval Postgraduate School Monterey, CA 93943-5000	3
5. Dr. D. M. Klumpar Dept 91-20 Bldg. 255 Lockheed Palo Alto Research Laboratory 3251 Hanover St. Palo Alto, CA 94304	1
6. Dr. T. E. Moore NASA/MSFC/ES53 Huntsville, AL 35812	1
7. Dr. J. L. Horowitz CSPAR University of Alabama Huntsville, AL 35899	1
8. Dr. N. Singh Department of Electrical Engineering University of Alabama Huntsville, AL 35899	1
9. Mr. F. Joiner Code 1114SP Office of Naval Research 800 N. Quincy St. Arlington, VA 22217	1